DEVELOPMENT AND BIOLOGICAL EVALUATION OF NOVEL RADIOPHARMACEUTICALS FOR CANCER

By
SURESH SUBRAMANIAN
LIFE01200804003

BHABHA ATOMIC RESEARCH CENTRE
MUMBAI 400084

A thesis submitted to the
Board of Studies in Life Sciences
In partial fulfillment of requirements
For the Degree of
DOCTOR OF PHILOSOPHY
of
HOMI BHABHA NATIONAL INSTITUTE

November, 2013

Homi Bhabha National Institute

Recommendations of the Viva Voce Board

As members of the Viva Voce Board, we certify that we have read the dissertation prepared by Suresh Subramanian entitled "Development and Biological Evaluation of Novel Radiopharmaceuticals for Cancer" and recommend that it may be accepted as fulfilling the dissertation requirement for the Degree of Doctor of Philosophy.

____ **Date:**

Chairman - Dr. M.G.R. Rajan

____ **Date:**

Convenor - Dr. (Mrs.) M. Venkatesh (Guide)

____ **Date:**

Member - Dr. S. Gupta (Co-Guide)

____ **Date:**

External Examiner - Dr. A. Malhotra

____ **Date:**

Member - Dr. B.N. Pandey

____ **Date:**

Member - Dr. (Mrs.) B. Shankar

Final approval and acceptance of this dissertation is contingent upon the candidate's submission of the final copies of the dissertation to HBNI.

I hereby certify that I have read this dissertation prepared under my direction and recommend that it may be accepted as fulfilling the dissertation requirement.

Date:

Place: **(Guide)** **(Co-Guide)**

STATEMENT BY AUTHOR

This dissertation has been submitted in partial fulfillment of requirements for an advanced degree at Homi Bhabha National Institute (HBNI) and is deposited in the Library to be made available to borrowers under rules of the HBNI.

Brief quotations from this dissertation are allowable without special permission, provided that accurate acknowledgement of source is made. Requests for permission for extended quotation from or reproduction of this manuscript in whole or in part may be granted by the Competent Authority of HBNI when in his or her judgment the proposed use of the material is in the interests of scholarship. In all other instances, however, permission must be obtained from the author.

Suresh Subramanian

PUBLICATIONS FROM THE THESIS

Journal Articles

1. Technetium-99m-labeled poly(DL-lactide-co-glycolide) nanoparticles as an alternative for sentinel lymph node imaging. **Subramanian S**, Dandekar P, Jain R, Pandey U, Samuel G, Hassan PA, Patravale V, Venkatesh M. Cancer Biother Radiopharm 2010; 25: 637-44.
2. Mannosylated dextran derivatives labeled with fac-[M(CO)3]+ (M = (99m)Tc, Re) for specific targeting of sentinel lymph node. Morais M, **Subramanian S**, Pandey U, Samuel G, Venkatesh M, Martins M, Pereira S, Correia, JDG, Santos I. Mol Pharmaceutics 2011; 8: 609-20.
3. Studies Toward the Biological Efficacy of 99mTc-Labeled Dextran-Cysteine-Mannose ([99mTc(CO)3] DCM20) for Sentinel Lymph Node Detection. **Subramanian S**, Pandey U, Papadopoulos M, Pirmettis I, Venkatesh M, Samuel G. Cancer Biother Radiopharm 2012; 27: 365-70.
4. Modification of PLGA Nanoparticles for Improved Properties as a 99mTc-Labeled Agent in Sentinel Lymph Node Detection. **Subramanian S**, Pandey U, Gugulothu D, Patravale V, Samuel G. Cancer Biother Radiopharm 2013; 28: 598-606.
5. Comparative biological evaluation of two [99mTc(CO)3]-dextran pyrazolyl mannose conjugates developed for use in sentinel lymph node detection. **Subramanian S**, Pandey U, Morais M, Correia JD, Santos I, Samuel G. Q J Nucl Med Mol Imaging 2014; 58: 216-23.

Conference / Symposium Presentations

1. Preparation and preliminary bioevaluation studies of 90Y-oxine in lipiodol for liver cancer therapy. **S Subramanian**, U Pandey, HD Sarma, G Samuel, M Venkatesh. J Labelled Comp Radiopharm. 2009; 52(S1): S518 Poster presentation at 18th International Symposium on Radiopharmaceutical Sciences (ISRS-18) held in Edmonton, Canada Jul 13-17, 2009.
2. Development of a mannose-based radioligand for receptor-targeted imaging of sentinel lymph nodes to detect metastasis in the clinic. **S Subramanian**, U Pandey, G Samuel, M Venkatesh. J Adv Biotech 2010; 10(5): 100. Oral presentation at the International Conference on Radiation Biology – Nanotechnology, Imaging and Stem Cell Research in Radiation Oncology (ICRB-NISRRO) held at Sri Ramachandra University, Chennai Nov 15-17, 2010.
3. Yttrium-90 labeled Biorex 70 microspheres for liver cancer. **S Subramanian**, U Pandey, G Samuel, PR Chaudhari, S Gupta. Oral Presentation at SISNM 2013, Chennai, Aug 16-18, 2013.

Suresh Subramanian

DECLARATION

I, hereby declare that the investigation presented in the thesis has been carried out by me. The work is original and has not been submitted earlier as a whole or in part for a degree / diploma at this or any other Institution / University.

Suresh Subramanian

DEDICATION

For what it's worth, I dedicate this thesis to my mother **Saroja Subramanian**, who by her selfless approach to home-making and tireless spirit of sacrifice is entirely responsible for any good qualities I might possess, and to my father **TP Subramanian** who did his utmost to provide for and encourage his children to avail of all avenues open to them.

Acknowledgments

It is with the greatest pleasure that I express my indebtedness to my Guide **Dr. Meera Venkatesh**, Director, Physical and Chemical Sciences, Department of Nuclear Sciences and Applications, International Atomic Energy Agency (IAEA), Vienna and former Head, Radiopharmaceuticals Division (RPhD). Apart from her own experience and broad understanding of the radiopharmaceuticals field, Dr. Meera's ability to inspire her students to face the challenges they undertake and proactive stance towards forging meaningful collaborations with suitable research partners have been invaluable for the completion of the objectives described in this thesis. Despite her deputation to the IAEA in the midst of the work and the manifold responsibilities of her position there, she ensured that I received a similar level of guidance and support as before. Her kind countenance and morale-boosting words have on various occasions assauged arising self-doubts. She is the beacon that has lighted the path of my thesis from its nascence to its logical conclusion.

My Co-Guide **Dr. Sanjay Gupta**, Tata Memorial Centre - Advanced Centre for Treatment, Research, Education in Cancer (TMC-ACTREC), Navi Mumbai has been a towering pillar of support and inspiration for me. While his immense expertise in liver cancer and ready accessibility for discussion gave me the guidance towards developing the necessary animal model and doing the various biological efficacy studies for the section devoted to therapeutic radiopharmaceuticals for hepatocellular carcinoma (HCC), I equally acknowledge his enthusiastic hands-on approach, ability to quickly devise alternative solutions and infectious positive attitude, which have at critical junctures lifted my spirits and galvanized me into prioritizing and executing my tasks within the stipulated time.

I heartily acknowledge the support of my superior **Dr. Grace Samuel**, Head, Radiopharmaceuticals Evaluation Section (RPES). As principal investigator (India) for the IAEA coordinated research project (CRP) from which a fair portion of the work related to sentinel lymph node (SLN) detection in this thesis is taken, and as immediate overseer of my day-to-day activities pertaining to the Ph.D work on behalf of my Guide during the period of deputation, she has been always there for me, doing her best to ensure that I was able to pursue my thesis in the midst of routine departmental responsibilities. By shouldering the administrative tasks pertaining to the official collaborations involved, she has smoothed my path considerably, allowing me to focus on the science.

Dr. Ashutosh Dash, Head, Isotope Production & Applications Division (IP&AD) kindly arranged for me to have regular availability of Yttrium-90 (90Y) radioisotope from the in-house electrochemical generator developed in the Radiochemicals and Radiation Sources Section (RC&RSS). The RC&RSS group is also involved in the regular production of Molybdenum-99 radioisotope, used for preparing generator to obtain Technetium-99m radioisotope. As part of a Division with a dedicated production component, one sometimes takes certain facilities for granted, but a herculean effort in production, maintenance and troubleshooting is called for to provide these amenities on a regular basis for clinical and research use. I hereby express my deepest respect for Dr. Dash and his wonderful team of both seasoned and young professionals for their continued achievements in this regard.

Dr. M.R.A. Pillai, former Head, RPhD's most direct contribution to this thesis is his initiative in nurturing the CRP on 'Development of 99mTc radiopharmaceuticals for sentinel node detection and cancer diagnosis' during his tenure at the IAEA, which gave me direct exposure to the international work in this field. That apart, his ability to devise scientific programs, focus the resources at hand to their timely fulfilment and exhort others to deliver their best effort through his own example have given me lessons in professional outlook, for which I am grateful and hope to emulate to the best of my ability in my own work.

Dr. Isabel Santos of the Unit of Chemical and Radiopharmaceutical Sciences, Institute of Nuclear Technology (ITN), Technical University of Lisbon, Sacavém, Portugal, **Dr. Ioannis Pirmettis** of the Institute of Radioisotopes and Radiodiagnostic Products, National Centre for Scientific Research Demokritos, Athens, Greece and **Dr. Vandana Patravale** of the Department of Pharmaceutical Sciences and Technology, Institute of Chemical Technology (ICT), Mumbai have been wonderful collaborators in the work pertaining to development of various tracers for SLN detection and I express my gratitude to them and their respective groups for sharing their knowledge and resources to achieve a common goal.

Dr. Pradip Choudhari, TMC-ACTREC has extended exceptional collaboration towards the animal studies done for HCC therapy radiopharmaceuticals. His own technical expertise apart, he has a pivotal logistical contribution towards the project. Managing the funds provided herein by BARC to ACTREC, he was instrumental in procuring the cell lines, arranging the necessary facilities at ACTREC towards maintenance of animals and preparation of histolgical blocks and slides, and in recruitment of a JRF responsible for necessary tissue culture work and assisting in the animal studies. Without his active cooperation and accommodating nature these studies would never have been accomplished as they were.

I also take the opportunity to thank **Dr. Haladhar Sarma**, Head, Animal House Facility & Radioisotope Laboratory, Radiation Biology & Health Science Division. My interest in SLN detection and HCC therapy began with studies performed with his active participation. He has guided me in the necessary techniques for performing the in vivo activity distribution studies used in the SLN detection and HCC therapy sections of my thesis, and also provided invaluable technical guidance in various aspects of animal studies. As in-charge of the BARC Animal House, he has forever extended superlative logistical support to the radiopharmaceuticals research program, which has benefited my work tremendously.

Dr. Usha Pandey with her expertise in conjugation and radiolabeling chemistry has been an active colleague and adviser to me for the work done in both SLN detection and liver cancer therapy radiopharmaceuticals, as reflected in her position as co-author in all the publications related to this thesis. I express my sincere thanks for this rewarding working relationship.

I am grateful for the fruitful interaction I had with **Mr. Mauricio Morais** (ITN), **Dr. Prajakta Dandekar** (ICT), and **Mr. Dalapathi Gugulothu** (ICT) for the development and evaluation of the various nanoparticles for SLN detection. I would like to acknowledge **Ms. Monica Tyagi** (TMC-ACTREC) for her participation and unstinting help in histological studies required for the HCC work, and **Dr. Kiran Bendale** (TMC-ACTREC) whose experience in veterinary surgery provided me guidance in performing the orthotopic induction studies for development of the animal model for HCC. **Ms. Geetanjali** (TMC-ACTREC), who was recruited to assist in tissue culture and animal studies in the work on HCC radiopharmaceuticals, proved herself a reliable support with her resourcefulness and hard work.

I thank my colleagues **Dr. Aruna Korde, Dr. Mythili Kameswaran, Dr. Tapas Das, Dr. Sudipta Chakraborty, Dr. Madhava Mallia, Dr. Rubel Chakravarty, Mr. Viju Chirayil** and others for the useful scientific dialog and other help in regard to the work and writing of the thesis. It would be gravely amiss to not mention the help given me by the technical staff. **Mr. ND Gandhle** provided exceptional support throughout all the animal studies at BARC for which I am extremely grateful. I also thank **Mr. AD Kadam** and **Mr. EG Mohite** for providing valuable assistance to my work in far too diverse ways to describe.

Contents

SYNOPSIS

Preamble

While the progress made by mankind in the field of medical applications has allowed it to conquer or effectively control several diseases, cancer is a condition that, despite gargantuan efforts made on a global scale over several decades, cannot be said to have been defeated. The nature of the disease, its unpredictability, complex etiology, difficulty in early identification and in effective administration of treatment while minimizing hazardous effects to the rest of the body are all factors that have allowed cancer to persist as a formidable opponent to modern medicine. Of course, the specific strategies followed and the extent of their success depend a lot on the origin and cellular / tissue-level properties of the particular malignancy, but at an empirical level, the effective control of any cancer will have the following components:

1. Early diagnosis to identify the disease in an individual and initiate necessary treatment before significant metastasis has occurred.
2. Effective therapy regimen that will eliminate or limit to the maximum extent

all apparent malignancy, while avoiding gratuitous damage to surrounding normal tissue.

3. Sensitive and accurate prognostic evaluation before and after treatment to assess the possibility of relapse and need for supplementary treatment.

In addressing the above issues, radioisotopes play a vital role both in diagnosis and treatment. Nuclear medicine, a specialty that employs radiolabeled molecules or radiopharmaceuticals as tracers for diagnostic purpose or as tools of radiation for therapeutic purpose, has a unique role to play in cancer management. The work reported in this thesis is related to development of radiopharmaceuticals for use in cancer management.

The thesis is divided into four chapters, the contents of which are described below in brief.

Chapter 1: Introduction

Nuclear medicine, succinctly described as a “multidisciplinary field that develops and uses instrumentation and tracers (radiopharmaceuticals) to study physiological processes and non-invasively diagnose, stage and treat diseases” [1], has been applied to address clinical problems of several origins, including various organ function studies (heart, lungs, liver, kidney, brain), detection of infection / inflammatory disorder, or treatment of joint diseases and thyroid disorders, but it has always had a major thrust in the detection and treatment of cancer. Radiopharmaceuticals, defined as radionuclide incorporating pharmaceutical preparations administered in vivo for clinical purposes, in a formulation of adequate purity and pharmaceutical safety suitable for administration to humans / animals [2], are a prime component of in vivo nuclear medicine. Several such formulations are actively employed in the clinic for isolating and tackling malignancies, and many more are in various stages of development with the eventual aim of adding to the arsenal of strategies to keep at bay this scourge of contemporary human life.

This thesis deals with the development and biological evaluation of some novel radiopharmaceutical preparations that could be useful towards the fight against cancer. Under the title of “Development and Biological Evaluation of Novel Radiopharmaceuticals for Cancer” the work done as a part of this thesis is focused on two major objectives:

Objective 1 The development and biological evaluation of novel tracers for detection of sentinel lymph nodes (SLN).

Objective 2 The development and biological evaluation of novel complexes for therapy of liver cancer.

For the first objective, using the gamma-emitting diagnostic radioisotope technetium-99m (99mTc) [3], tracers of different classes have been developed for the detection of sentinel lymph nodes, an important component of prognosis in cancers of several origins. For the second objective, using the beta-emitting therapeutic radioisotope yttrium-90 (90Y) [4], various preparations have been attempted towards the treatment of liver cancer. In both, suitable animal models have been employed for the testing of these novel preparations. The studies performed herein are ultimately dedicated towards the development of new tools for nuclear medicine clinicians in their ongoing battle against cancer and thereby benefit society at large.

Chapter 2: PLGA Based SLN Detection Tracers

2.1 Background

Identification of the SLN followed by excision for detailed biopsy is an important factor in the prognosis and staging of cancers of several origins (breast, head & neck, skin) [5, 6, 7, 8]. Major lymphoscintigraphy agents previously reported in the literature include colloidal Gold-198 (198Au) [9] to 99mTc-labeled forms of colloidal antimony trisulfide [10], sulfur colloid [11], human serum albumin (soluble) [12] and colloidal human serum albumin [13]. But as none of these are ideal, there is a scope for developing new nanoparticle SLN tracers with improved properties. Poly [lactide (co-glycolide)] (PLGA) is a bio-compatible polymer [14] that may be employed in development of nanoparticles for SLN detection with the advantages of uniform desired particle size range and reduced chance of handling potentially hazardous biological material or allergic reactions. It was hence proposed to develop and evaluate various PLGA derivatives towards use as 99mTc-labeled SLN detection tracers.

2.2 Materials and Methods

Three types of poly PLGA based nanoparticles were developed for use in SLN detection: a) Plain / Unmodified PLGA b) Mebrofenin-loaded PLGA (Mebrofenin-PLGA) c) Ditheylenetriamine pentaacetate (DTPA) conjugated PLGA (DTPA-PLGA). The PLGA nanoparticles were prepared by the method of emulsion solvent evaporation and physico-chemically characterized by dynamic light scattering (DLS) analysis with regards to parameters like particle size and Polydispersity Index (PI). Using these parameters the formulations were optimized with respect to the choice and concentration of emulsifying agent. The nanoparticles were then subjected to lyophilization for long-term storage. Post-lyophilization reconstitution was assessed and the choice and concentration of cryoprotectant was optimized based on DLS measurements conducted on reconstituted nanoparticle suspensions.

99mTc-labeling of the various PLGA derivatives was performed using Tin (II) chloride as the reducing agent and reaction conditions were optimized.

In vivo biological evaluation of the PLGA based derivatives was performed using Wistar rat animal strain by the footpad injection model. In this model, the preparation was administered subcutaneously in the footpad, and transport of the tracer from the site of injection (footpad) to the nearest node (popliteal) and beyond was taken as an index of its biological behavior. In vivo radioactivity distribution measurement studies and scintigraphic imaging studies were performed. Activity retained in relevant organs / tissues was expressed as a percentage of total injected activity (%ID). Popliteal Extraction (PE) was calculated as a quantitative expression of the specific retention of a sentinel lymph node tracer in the footpad model [15].

The toxicity of relevant ligands was evaluated, using the reported protocol for single-dose acute toxicity studies. Evaluation studies included relevant hematological parameters – RBC, hemoglobin, WBC, platelets – and biochemical parameters – Serum albumin, bilirubin, glutamate oxaloacetate transferase / aspartate transaminase (SGOT/AST), glutamate pyruvate transferase / alanine transaminase (SGPT/ALT). Hemocytometry and relevant biochemical assays were performed for the above. Histological slides were prepared by taking tissue samples, processing them to obtain paraffin blocks, then sectioning by microtomy and hematoxylin-eosin staining.

2.3 Results

Optimization studies performed for preparation of PLGA nanoparticles showed that Vitamin E was the most suitable emulsifier and dextrose with poloxamer, the most suitable cryoprotectant. The particle diameters for the various PLGA derivatives in final optimized form are as follows: Plain PLGA 189.3±22.4 nm (PI of 0.17±0.01), Mebrofenin-PLGA 224±6.15 nm (PI 0.26±0.027), DTPA-PLGA 212±9.66 nm (PI 0.21±0.04). Additionally, for mebrofenin-PLGA, the efficiency of mebrofenin incorporation in PLGA nanoparticles was found using UV spectrophotometry to be 51±2.3 %. For DTPA-PLGA, the conjugation of DTPA residues onto the surface of PLGA was confirmed with a combination of FT-IR spectroscopy, elemental analysis by energy dispersive spectroscopy (EDS) and zeta potential measurement.

Under the tested conditions for 99mTc labeling, plain PLGA showed ~70 % 99mTc-labeling after reaction at 37 °C, 60 min with 250 µg tin chloride. Mebrofenin-PLGA under similar conditions showed ~65 % labeling, indicating the lack of any advantage offered by mebrofenin-loading towards yield and ease of 99mTc-labeling. DTPA-PLGA showed much improved labeling characteristics, giving >90 % 99mTc-labeling under significantly more moderate reaction conditions (RT, 30 min with 75 µg tin chloride) highlighting the significant role of DTPA residues on the surface of PLGA nanoparticles in formation of complex with 99mTc.

In the in vivo evaluation studies, plain PLGA nanoparticles showed uptake in the SLN, but the low uptake percentage (1.75±0.65 %ID at 180 min p.i. with 65.77 %PE) and lack of in vivo stability makes them unsuitable in the clinical scenario. The in vivo behavior of 99mTc-labeled mebrofenin-PLGA was similar (1.35±0.14 %ID SLN uptake at 180 min p.i.), though it showed greater SLN retention (86.89±0.37 %PE) and in vivo stability. In the case of DTPA-PLGA, there was an increase in SLN uptake (3.47±0.11 %ID at 180 min p.i.), good retention (82.89±3.22 %PE) and good in vivo stability with respect to 99mTc activity as per the negligible accumulation in gastrointestinal region. DTPA-PLGA in toxicology tests did not show any appreciable symptoms of toxic / inflammatory reaction.

Summary: Of the various PLGA derivatives developed and tested as potential 99mTc-labeled tracers for SLN detection, DTPA-PLGA offers the best properties, in terms of both tracer preparation and biological efficacy, and can be a good substitute with improved properties to existing conventional nanoparticle tracers for SLN.

Chapter 3: Mannose Based SLN Detection Tracers

3.1 Background

This work may be regarded as a follow-up to the previous one on development of PLGA based SLN detection tracers, whose biological behavior is mainly a function of the particle size. In this case, mannose residues present on the ligands are expected to interact with mannose receptors expressed on the cell surface of lymph node macrophages and allow for a significantly smaller in size class of 99mTc-labeled SLN tracers that may be expected to have improved clearance and sensitivity in vivo [15, 16, 17]. The work described here was done as part of an International Atomic Energy Agency (IAEA) coordinated research project (CRP) on the "Development of 99mTc radiopharmaceuticals for sentinel node detection and cancer diagnosis".

3.2 Materials and Methodologies

The ligands used for the studies carried out here – one Dextran-Cysteine-Mannose ligand (DCM20) and two Dextran-Pyrazolyl-Mannose ligands (DAPM4 and DAPM8) – were supplied after synthesis and physico-chemical characterization by the various international research groups participating in this project. Labeling with 99mTc for all the ligands was performed via a 99mTc-tricarbonyl intermediate [18]. Characterization was performed by HPLC. In vitro evaluation studies were performed with mannose receptor bearing RAW 264.7 macrophage precursor cells. Saturation binding curves were obtained and binding affinity (Kd) was calculated. In vivo evaluation studies for all the 99mTc-labeled tracer preparations were performed with different ligand concentrations using the footpad injection model in Wistar rat as described previously [Section 2.2].

3.3 Results

For all the tested ligands (DCM20, DAPM4 and DAPM8) 99mTc-labeling yield and stability of labeled complex at 180 min post-preparation were >90 %. In the in vitro uptake studies, DCM20 was observed to have significantly higher receptor binding affinity (19.41 nM) than DAPM4 (116.05 nM) or DAPM8 (111.27 nM). However, these results were not proportionally reflected in the animal studies. All the dextran-mannose ligands tested herein showed appreciable SLN uptake and excellent popliteal extraction at their optimal concentrations at 180 min p.i. - DCM20 3.35±0.72 %ID with 98.02±3.06 %PE, DAPM4 5.02±0.61 %ID with 92.92±3.38 %PE, DAPM8 6.02±1.94 %ID with 91.8±3.85 %PE. None of the ligands in toxicology studies showed any alarming signs of toxicity, suggesting their safety at pharmaceutical concentrations.

Summary: Of the ligands tested, 99mTc-labeled DCM20 showed the highest clearance and popliteal extraction and may be considered to have the best potential as a mannose receptor targeting SLN detection tracer.

4 Radiopharmaceuticals for Liver Cancer Therapy

4.1 Background

The work reported here deals with the preparation, characterization and preliminary biological evaluation of novel embolic radiopharmaceuticals bearing therapeutic radionuclides. Liver cancer is an important disease to be addressed in the Asian context with high associated clinical morbidity [19, 20]. Localized treatment with beta-emitting radiopharmaceuticals in an embolizing preparation is an attractive approach for combating the disease and extending / improving the life of the patient. 90Y with its suitable emission properties (Half-life = 64 h, Energy of βmax = 2.3 MeV) is ideally suited for therapy of liver cancer. But the currently available products are very expensive and must be imported. To meet the needs of the Indian population, it is essential to develop indigenous radio-embolic therapy alternatives. With this in mind two 90Y-bearing vehicles were proposed to be developed and tested in suitable in vivo model: a) Polymeric microspheres of suitable diameter labeled with 90Y that will be trapped in liver capillaries b) Suitable complexing ligand that may be labeled with 90Y and dispersed in lipiodol, a viscous fluid that can embolize liver capillaries and is used as an MRI contrast agent.

4.2 Materials and Methodologies

Two 90Y-labeled preparations were developed for evaluation as therapeutic radiopharmaceuticals for liver cancer: a) 90Y-labeled oxine in lipiodol - prepared by reaction of oxine with 90Y, separation of the labeled product by chloroform extraction, and finally dispersal in lipiodol b) 90Y-labeled Biorex 70 microspheres - prepared by simple exposure of resin microspheres to 90Y activity followed by centrifugation.

The animal model for testing of liver cancer therapy radiopharmaceuticals was generated by orthotopic induction of known hepatocellular carcinoma cell line N1S1 into Sprague-Dawley rat. Development of the model was followed by measurement of various hematological parameters - RBC, Hemoglobin, WBC, Platelets - and biochemical parameters - serum bilirubin, AST/SGOT, ALT/SGPT, alpha-fetoprotein. For animal studies, the 90Y-labeled preparations were administered via hepatic vein (blood flow from intestine to liver) in a survival surgery protocol under anesthesia. The animals were allowed to recover from surgery, and kept under normal conditions for various time points (1-2-5-7 days). At the end of the respective time points they were sacrificed and in vivo distribution of 90Y-activity from the administered preparations was assessed. Biological efficacy parameters like tumor regression and effect on relevant biochemical parameters (as specified above) were studied.

4.3 Results

90Y-labeling of oxine (8-hydroxyquinoline) was optimized with respect to reaction conditions (>90 % labeling yield at 80 ºC, 60 min, pH 8.5). The stability of the 90Y-oxine was studied and found to be >85 % after 3 days at 37 ºC. 90Y-oxine showed good dispersal (>90 %) in lipiodol, the embolizing carrier in which it would be administered in vivo. Biorex 70 microspheres (45-70 µm wet diameter) were labeled with 90Y with >95 % yield (Room temperature, 15 min, pH 5.0). The labeled preparation was observed to retain > 95 % stability even at 7 days post-preparation and incubation at 37 ºC.

The protocol for generating tumor was optimized, giving single tumor lesion of appreciable size (~20-25 mm diameter) in 3 weeks period. The major relevant parameter in development of tumor model was serum alpha-fetoprotein, whose level increased proportionally with tumor diameter.

The two 90Y-labeled products were then compared for their in vivo biological parameters. In the case of 90Y-oxine in lipiodol, significant leakage of the preparation from the liver was observed (only 23.8±2.61 %ID retained in liver at 7 days), with significant (34.22±5.39 %ID) bone accumulation in the same period. The size of tumor in animals treated with 90Y-labeled oxine in lipiodol was 23.6±3.2 mm at 7 days p.i. while animals administered with unlabeled “cold” lipiodol in oxine showed tumors of marginally higher size (25.2±4.7 mm). In contrast, 90Y-labeled Biorex 70 microspheres exhibited 87.72±1.56 %ID liver accumulation even at 7 days with minimal release into bone (0.56±0.97 %ID, 7 days). Thus, In terms of in vivo distribution and pharmacokinetics, Biorex 70 microspheres show excellent properties for use as a vehicle of therapy in liver cancer. The 90Y-labeled Biorex 70 microspheres also appeared to have appreciable tumor-treatment properties. Animals receiving cold Biorex 70 microspheres showed tumors with diameter of 27.4±5.9 mm at 7 days, but in the case of 90Y-labeled Biorex 70 microspheres, the tumor size was reduced to 16.3±3.8 mm. In the studies of biochemical parameters, again the consistent parameter was serum alpha-fetoprotein which dipped to 19.49±3.72 ng/ml in the case 90Y-Biorex 70 microspheres and 37.49±4.65 ng/ml with 90Y-oxine in lipiodol, as compared to 51.44±11.97 ng/ml in untreated controls. Histological studies showed significant damage to liver cancer tissue from 90Y-Biorex 70 microspheres at 7 days p.i.

Summary: Of the two 90Y-labeled preparations developed and evaluated, Biorex 70 microspheres in terms of in vivo retention and apparent efficacy shows the better potential for use as an agent of liver cancer therapy.

Bibliography

[1] Kramer-Marek G, Capala J. The role of nuclear medicine in modern therapy of cancer. Tumor Biol (2012) 33: 629-40.

[2] Sood DD, Reddy AVR, Ramamoorthy N. Applications of radioisotopes in healthcare. In: Fundamentals of Radiochemistry, 1st Edition, Indian Association of Nuclear Chemists and Allied Scientists, Mumbai (2000) 301-26.

[3] Hamoudeh M, Kamleh MA, Diab R, Fessi H. Radionuclides delivery systems for nuclear imaging and radiotherapy of cancer. Adv Drug Deliver Rev (2008) 60: 1329–46.

[4] Liu S. Bifunctional coupling agents for radiolabeling of biomolecules and target-specific delivery of metallic radionuclides. Adv Drug Deliver Rev (2008) 60: 1347-70.

[5] Morton DL, Chan AD. The Concept of Sentinel Node Localization: How It Started. Semin Nucl Med (2000) 30: 04-10

[6] Tobler NE, Detmar M. Tumor and lymph node lymphangiogenesis — impact on cancer metastasis. J Leukocyte Biol (2006) 80:691–96.

[7] Fisher B, Fisher E. Barrier function of lymph node to tumor cells and erythrocytes. I. Normal nodes. Cancer (1967) 20: 1907-13.

[8] Harish K. Sentinel node biopsy: Concepts and current status. Front Biosci (2005) 10: 2618-44.

[9] Hultborn KA, Larsonn LG, Ragnhult I. The lymph drainage from the breast to the axillary and parasternal lymph nodes studied with the aid of colloidal Au 198. Acta Radiol (1955) 43: 52-63.

[10] Bergqvist L, Strand SE, Persson B, Hafström L, Jönsson PE. Dosimetry in lymphoscintigraphy of Tc-99m antimony sulfide colloid. J Nucl Med (1982) 23: 698-705.

[11] Eshima D, Fauconnier T, Eshima L, Thornback JR. Radiopharmaceuticals for Lymphoscintigraphy: Including Dosimetry and Radiation Considerations. Semin Nucl Med (2000) 30: 25-32.

[12] Bergqvist L, Strand SE, Persson BR. Particle sizing and biokinetics of interstitial lymphoscintigraphic agents. Semin Nucl Med (1983) 13: 9-19.

[13] Wilhelm AJ, Mijnhout GS, Franssen EJF. Radiopharmaceuticals in sentinel lymph-node detection – an overview. Eur J Nucl Med (1999) 26 (Suppl): S36–S42.

[14] Danhier F, Ansorena E, Silva JM, Coco R, Breton AL, Préat V. PLGA-based nanoparticles: An overview of biomedical applications. J Control Release (2012) 161: 505-22.

[15] Vera DR, Wallace AM, Hoh CK, Mattrey RF. A synthetic macromolecule for sentinel node detection: 99mTc-DTPA-Mannosyl-Dextran. J Nucl Med (2001) 42: 951-59.

[16] Vera DR, Wallace AM, Hoh CK. [99mTc]–MAG3-Mannosyl-Dextran: a receptor-binding radiopharmaceutical for sentinel node detection. J Nucl Med (2001) 28: 493-98.

[17] Takagi K, Uehara T, Kaneko E, Nakayama M, Koizumi M, Endo K, Arano Y. 99mTc-labeled mannosyl-neoglycoalbumin for sentinel lymph node identification. Nucl Med Biol (2004) 31: 893-900.

[18] Alberto R, Schibli R, Egli A, Schubiger AP, Abram U, Kaden TA. A novel organometallic aqua complex of technetium for the labelling of biomolecules: Synthesis of [99mTc(OH2)3(CO)3]+ from [99mTcO4]– in aqueous solution and its reaction with a bifunctional ligand, J Am Chem Soc (1998) 120: 7987–8.

[19] Poon RT, Fan ST, Tsang, FH, Wong J. Locoregional therapies for hepatocellular carcinoma: A critical review from the surgeon's perspective. Ann Surg (2002) 235: 466-86.

[20] Blum HE. Hepatocellular carcinoma: Therapy and prevention. World J Gastroentero (2005) 11: 7391-400.

List of Figures

List of Tables

1. INTRODUCTION

1.1. NUCLEAR MEDICINE - A PRIMER

If the 1909 report of FH Williams describing the use of pure radium salts for treatment of some epitheliomas [1] may be regarded as one the early applications of nuclear medicine techniques, then today the nuclear medicine field is more than a century old. With the discovery of artificial production of radioisotopes in the 1930s, and the significant strides in the technologies of nuclear fission reactors and charged particle accelerators, radioisotopes began to be used in the treatment of cancers from the early 1940s and this practice has continuously grown over the decades [2]. However, official recognition for nuclear medicine came in 1971 when it was listed as a medical specialty by the American Medical Association. Summarizing the definition provided by the World Health Organization [3], nuclear medicine refers to the in vivo application of radioisotopes (apart from external sealed radioisotope sources for therapy) through ingestion, inhalation or injection for relevant ends in clinical diagnosis and therapy. It has been succinctly described as a “multidisciplinary field that develops and uses instrumentation and tracers (radiopharmaceuticals) to study physiological processes and non-invasively diagnose, stage and treat diseases” [4]. Nuclear medicine is regarded as non-invasive and providing minimal distress to patients compared to some of the other techniques employed in the clinic. At least so far as diagnostic applications go, the radiation received by patients for typical nuclear medicine procedures is of the same order as that occurring naturally on an annual scale, and appreciably lower than for equivalent X-ray techniques [5].

In diagnostic nuclear medicine, a “trace” amount of radioisotope tagged to a suitable carrier is administered into the body and then tracked using a nuclear medicine imaging system. As lucidly laid out by Green and Seidel [6], a nuclear medicine imaging system functions in the following order of steps: i) Photon detection ii) Data acquisition iii) Data processing iv) Image processing and v) Display and analysis. Following this sequence, the radiations emitted by the tracer depending on its in vivo pharmacokinetics are collected and recorded as data by the instrument, and then processed to provide an “image” of the radiopharmaceutical within the body. Depending on the emission characteristics of the tagged radioisotope, the imaging technique employed may be either Single Photon Emission Computed Tomography (SPECT) or Positron Emission Tomography (PET). Diagnostic nuclear medicine has the potential to provide sensitive functional imaging, allowing for the detection of disease conditions far before other imaging techniques like Computed Tomography (CT) or structural Magnetic Resonance Imaging (MRI) that depend on gross anatomical changes. While newer modalities like functional MRI have alleviated such differences, the comparative simplicity of the instrumentation coupled with economic advantages have given nuclear medicine continued validity as a premier clinical investigation tool [7].

In therapeutic nuclear medicine the patient is administered radiation in the form of in vivo administered radioisotope tagged to an appropriate carrier, at a dose sufficient for therapy. In most cases, a function of cell killing is performed by the emitted radiation to achieve the desired therapeutic effect. For example, tumor-targeted therapy aims to kill malignant cells, while in the case of radiation synovectomy, a palliative treatment for rheumatoid arthritis, therapeutic radiation is targeted towards the cells responsible for symptoms of acute inflammation. This cell killing occurs in accordance with the principles of the interaction of radiation with matter, namely ionization and generation of free radicals in the surrounding tissue, which lead to the dysfunction or degradation of critical cellular macromolecules like DNA with ensuing fatal consequences for the cell. The nature and form of the carrier vary according to the intended application. The use of in vivo administered therapeutic radiation offers the possibility of more specific localization of treatment as compared to external beam radiation therapy (Teletherapy), reducing the overall requirement of radiation dose and thereby lowering the undesirable effects of non-specific radiation damage. In many cases, therapeutic nuclear medicine is prescribed as an adjunct to conventional therapy measures including drugs and/or surgery.

Before delving into further details of this subject some of the terms related to radioactivity and radiation are defined.

Radioactivity: Radioactivity or radioactive decay has been described as the process whereby a nucleus that contains an excess of energy undergoes a transformation to a more stable state by emitting energy in the form of elementary particles or electromagnetic radiation [8]. Radioactivity in elements may be natural or artificially induced by a process of bombarding stable precursor targets with various projectiles. The majority of radioisotopes used in nuclear medicine are artificially produced, either in reactors by neutron bombardment or in cyclotrons by bombardment with charged particles such as protons, deuterons or alpha particles that have been accelerated to high energies by passage through electric and magnetic fields. The choice of mode of production depends on the suitability of the product radioisotope for the desired application, taking into consideration its half-life, decay mode, energy, specific activity, radionuclidic purity, processing time etc. [9]

Alpha (α) decay: Alpha radiation/decay refers to the emission of an α-particle, which consists of two protons and two neutrons (identical to a Helium nucleus). Here the mass number and atomic number of the product nucleus are reduced by 4 and 2 units respectively as compared to the starting nucleus.

Beta (β) decay: Beta radiation/decay refers to the emission of a β-particle. This may comprise of one of the following three processes i) negatron decay (β^-) ii) positron decay (β^+) iii) Electron Capture (EC). In all three processes, atomic number of the product nucleus differs from starting nucleus by one unit, without any change in mass number. However, EC is a special class of beta decay that need not result in particulate emission. Further reference to beta decay in this thesis refers essentially to the emission of negatrons or positrons.

Gamma (γ) radiation: In the process of de-excitation of a product nucleus, following α or β decay by the starting nucleus, it may emit high frequency electromagnetic radiations. These are known as γ-photons or γ-rays. Unlike α or β emissions, γ-emissions do not involve the release of any particulates.

Linear Energy Transfer (LET): This refers to the energy transferred per unit length traveled by the emitted particle/photon in the surrounding medium. LET depends upon the nature of the radiation, kinetic energy of the emission and the stopping power of the medium, which in turn is dependent upon the mass number and atomic number of the medium. Typically, charged particle emissions have greater LET than gamma emissions. This implies that they cause a greater number of ionizations in the surrounding medium per unit distance traveled, but lower penetration range through the medium consequent to the loss of kinetic energy. Therefore by convention, gamma emitting radioisotopes are used in diagnostic applications and charged particle emitting radioisotopes are used in therapeutic applications.

1.2. RADIOPHARMACEUTICALS

When a radionuclide incorporating pharmaceutical preparation is administered in vivo for clinical purposes, in a formulation of adequate purity and pharmaceutical safety suitable for administration to humans/animals, the resulting preparation is called a Radiopharmaceutical [10]. Typically a radiopharmaceutical is made up of two main components:

- **Radionuclide:** The radionuclide/radioisotope is responsible for the radioactive effects of the preparation. The choice of radionuclide is governed by whether the radiopharmaceutical is intended for diagnostic/therapeutic end-use.
- **Carrier:** The carrier is responsible for the in vivo transport and localization of the radiopharmaceutical preparation. The purpose of the carrier could either be to bind/chelate the radioisotope or for biologically selective accumulation in the target region or a combination of these two aspects. The carrier could be a simple ligand with desirable physico-chemical properties or have structural analogy to a bio-molecule or have a supra-molecular structure that defines its in vivo behavior. It may or may not have pharmacological activity on its own.

Based on their chemical nature radiopharmaceuticals may be categorized as follows:

1. **Simple Radiopharmaceuticals** - These are simple inorganic molecules eg. [131I]-Sodium Iodide (thyroid therapy), [201Tl]-Thallium chloride (myocardial imaging).

2. **Labeled compounds** - Here the radioisotope is covalently linked to the carrier. It may function as a true label, where the radiolabel is an isotope of a natural element eg. [11C]-Methionine (tumor imaging), or a foreign label, where it replaces another element eg. [18F]-Fluorodeoxyglucose (tumor imaging).
3. **Coordinate complexes** - Most commonly available radiopharmaceuticals belong to this category. The radioisotope here is a transition metal that is associated with an appropriate carrier by means of coordinate linkages eg. 99mTc-Tetrofosmin (myocardial imaging).
4. **Particulate formulations** - Here the carrier is a particulate/macroaggregate and the radioisotope may either be encapsulated within the carrier or attached to the surface by suitable chemistry eg. 90Y-Glass microspheres (liver cancer therapy).

Based on the intended application, radiopharmaceuticals may be classified as **diagnostic** and **therapeutic**.

1.2.1. Diagnostic Radiopharmaceuticals

Diagnostic radiopharmaceuticals aid in imaging organ morphology and function, or metabolic abnormalities associated with various clinical conditions like cancer, infection etc. In general they are applied at extremely low concentrations, not intended to have any pharmacological effect [12]. Radionuclides incorporated in this class of preparation have the following characteristics:

1. They primarily emit gamma radiation, with none to minimal amount of charged particle emissions.
2. They have a short half life, ranging from a few minutes to a few hours.
3. They have simple radiolabeling chemistry and are available in logistically and economically viable form.

The lower LET and greater penetration of gamma rays ensure that emissions from diagnostic radiopharmaceuticals localized inside the patient's body are conveniently detected on an externally placed imaging system, and have minimal interaction with the surrounding body tissues. An exception to the rule comes from positron emitting radiopharmaceuticals used in PET imaging. Here however, while the initial positron emission is particulate, it travels only a very short distance in tissue (typically less than 1mm) losing its kinetic energy in the process, then interacts with a nearby electron thereby getting annihilated. This annihilation of matter leads to the release of two high-energy (511keV) gamma photons in diametrically opposite directions. The coincident detection of these gamma photons is registered by the imaging system. Hence the detection process still depends on the emission of gamma rays. Fluorine-18 (18F) is one of the prominent positron emitters used in PET-based diagnostic imaging today. Predictably, the high LET alpha or beta emitting radioisotopes are not used for diagnostic imaging. Tab. 1.1 gives some of the typical imaging applications for diagnostic radiopharmaceuticals (data sourced from Table 16.6 p316 of [10], suitably adapted for presentation here).

Of the various diagnostic radioisotopes, Technetium-99m aka 99mTc is the most widely used. It accounts for about 80% of all diagnostic studies [11], amounting to nearly 30 million scans annually, and has justifiably been named the "Workhorse" of

Organ / Function	**Diagnostic Radiopharmaceuticals Used**
Brain	Perfusion: [18F]-fluorodeoxyglucose (FDG), 99mTc-Ethylene Cysteine Diamine (ECD); Neuroendocrine receptors: [18F]-DOPA
Heart	Perfusion: 99mTc-Tetrofosmin, 99mTc-Sestamibi; Metabolism: [18F]-FDG, [123I]-β-methyl-iodophenylpentadecanoic acid (BMIPP); Blood Pool: 99mTc-Human Serum Albumin (HSA)
Lungs	Perfusion: 99mTc-HSA microspheres; Ventilation: 99mTc-Diethylenetriaminepentaacetic acid (DTPA) aka Technegas
Thyroid	[131I]-Sodium Iodide
Bone	99mTc-Methylene diphosphonate (MDP)
Liver	99mTc-sulfur colloid, 99mTc-phytate
Kidneys	Imaging: 99mTc-Dimethylmercaptosuccinic acid (DMSA), 99mTc-Glucoheptonate (GHA); Renography: 99mTc-Mercaptoacetyltriglycine (MAG_3), 99mTc-EC
Infection/Inflammation	Infection: 99mTc-Ciporofloxocin; Inflammation: 99mTc-Human Immunoglobulin G (HIgG)
Tumors	67Ga-Citrate, 111In-Octreotide / 68Ga-DOTA Octreotide derivatives, [123/131I]-meta-iodobenzylguanidine (MIBG), [18F]-FDG

Table 1.1.: Typical imaging applications for diagnostic radiopharmaceuticals.

nuclear medicine. The overwhelmingly large utilization of 99mTc is due to its highly suitable radiation characteristics, convenient half-life and ease of availability [11, 12]. 99mTc has a mono-energetic (140 keV) photon emission accounting for 88% of its radiation abundance. This photon is not significantly attenuated within the body and has optimal characteristics for being collimated and recorded by the imaging system. Technetium-99m has no clinically significant charged particle emission (only a small fraction of low-energy Auger electrons), which limits potential hazardous effects. The physical half-life of 6.03 hours makes it convenient in the hospital setup to perform radiolabeling, quality control, administration into the patient and in vivo scanning at multiple time points to obtain necessary clinical information. It is conveniently obtained from a “generator”. In this generator, the parent radionuclide Molybdenum-99 (99Mo), which has been obtained from the reactor either as one of the products of the nuclear fission of Uranium-235 or by neutron irradiation of stable Molybdenum-98 target, is loaded onto an alumina column. 99Mo undergoes β-decay with a half-life of 66.7 hours to give 99mTc daughter product. When isotonic saline is passed through this column, 99mTc is selectively eluted out while the remaining 99Mo is retained on the alumina. The column can be repeatedly eluted with saline (after giving adequate time to allow for build-up of 99mTc) so long as the yield of 99mTc is sufficient for imaging purposes. A 99Mo-99mTc generator in the radiopharmacy has a typical shelf life of around a week. The entire operation can be performed in conditions that maintain the purity and sterility necessary to meet clinical standards. Technetium is also advantageous from the point of view that it has a very diverse redox chemistry. In different complexes it may exhibit oxidation states varying from -1 to +7, the specific oxidation state depending upon the chelating ligand and the reaction conditions. Thus it can be manipulated to form complexes with a wide range of ligands suitable for different diagnostic purposes.

1.2.2. Therapeutic Radiopharmaceuticals

Therapeutic radiopharmaceuticals as the name suggests are employed in curative or palliative treatment of different clinical conditions. They have been defined as radiolabeled molecules designed to deliver therapeutic doses of ionizing radiation to disease sites with high specificity in the body [13]. While their major application is in the therapy of tumors of various origins, other conditions like thyroid disorders, rheumatoid arthritis, arterial restenosis etc. have also been treated using this class of radiopharmaceuticals. Radionuclides incorporated in these preparations have the following characteristics:

1. They have charged particle emissions such as α, β, Auger electrons or Coster-Kronig (C-K) electrons [14]. Charged particle emissions have higher LET than gamma rays, allowing for therapy via the generation of excited and ionized atoms and free radicals in surrounding medium/tissue. These formations are responsible for DNA damage in cells via the induction of single strand breaks [11]. Also, charged particles have lower energy deposition range, which implies lower penetration into adjacent non-specific regions as compared to electromagnetic radiations.
2. Typical therapeutic radionuclides have half life ranging from several hours to few days. The choice of radionuclide employed for a given therapy depends on the emission characteristics and half-life of the isotope and its suitability to the intended application; beta-emitters with millimeter range penetration are effective for large tumors and alpha-emitters with 50-100 micron penetration are restricted to very small tumors or micrometastases, while C-K and Auger electrons with their sub-micron range may only be applied in situations where they can be transported adjacent to nuclear DNA to exert their therapeutic effect [14].
3. As with diagnostic radionuclides, they must have logistically feasible labeling chemistry, suitable in vivo pharmacokinetics and economic viability [13].

Alpha particles possess the highest LET and correspondingly lowest penetration (less than 0.1mm) among charge particle emissions. They have the potential to

Clinical Condition	**Therapeutic Radiopharmaceutical Used**
Thyroid carcinoma	[131I]-Sodium iodide
Neuroendocrine tumors	[131I]-MIBG
Non-Hodgkin's Lymphoma	131I- labeled Tositumomab, 90Y-labeled Ibritumomab (anti-CD20 antibodies)
Metastatic bone pain	[32P]Sodium orthophosphate, 153Sm-Ethyelenediaminetetramethylene phosphate (EDTMP)
Arthritic joint pain	[32P]chromic phosphate aggregates, 90Y-Silicate colloid, 166Ho-Hydroxyapatite
Endovascular restenosis	32P-coated stent

Table 1.2.: Typical applications of therapeutic radiopharmaceuticals, data adapted from [10]

cause more irreparable double stranded DNA breaks, more severe chromosomal damage during mitosis and greater frequency of chromosomal rearrangements than lower LET emissions like β-particles. However, although studies have been done in animals and in human trials using α-emitters, the requirement for such radiopharmaceuticals to be localized adjacent to the DNA limits their utility in the clinical working scenario. Similarly, Auger electrons also have very low penetration in tissue. Hence primarily β-emitting radioisotopes are used for preparation of therapeutic radiopharmaceuticals. Tab. 1.2 gives some examples of clinically employed therapeutic radiopharmaceuticals.

Yttrium-90 (90Y) is one of the prominent radionuclides used for the development of therapeutic radionuclides. 90Y emits β-radiations, getting converted to stable Zirconium (90Zr) in the process. It is obtained from a generator in which Strontium-90 (90Sr) as the parent radionuclide undergoes β-decay with a half life of 28.8 years to give 90Y. Traditionally column-based solvent extraction techniques have been used to separate 90Y from 90Sr for use in the clinical environment, but these techniques are tedious. In recent years novel electrochemical generator techniques have been specially developed for the extraction of high specific activity 90Y, which have been commercially adapted for use in the radiopharmacy setup [15]. The long half-life of

90Sr coupled with its near limitless availability from spent fuel confers significant logistical and economical advantages to the use of 90Y as a therapeutic radionuclide. 90Y is a pure beta-emitter with 100% radiation abundance of high energy β-particles [E_β (max) = 2.28MeV]. It has a comparatively long tissue penetration range (12mm max), allowing for homogenous dose distribution in affected organ / tissue even if the radiopharmaceutical is heterogeneously localized. The half life of 90Y is 64 hours, which is convenient for manufacture and delivery of the final radiopharmaceutical to the patient, and at the same time short enough to a achieve critical dose rate with reduced long-term adverse consequences [12].

In the work proposed towards this thesis, it has been attempted to prepare and evaluate some novel radiopharmaceuticals for use in cancer. Using 99mTc as a diagnostic radioisotope, tracers of different classes have been developed for the detection of sentinel lymph nodes, an important component of prognosis in cancers of several origin. Using 90Y as a therapeutic isotope, various preparations have been attempted towards the treatment of liver cancer. Suitable animal models have been employed for the testing of these novel preparations. The following chapters will delve into the details of the work done and results obtained. The studies performed herein are ultimately dedicated towards the development of new diagnostic and therapeutic tools for nuclear medicine clinicians in their ongoing battle against cancer and thereby benefit society at large.

2. PLGA BASED SLN DETECTION TRACERS

2.1. BACKGROUND

2.1.1. The Basis of Sentinel Lymph Node (SLN) Detection

The major causes of the poor clinical prognosis for several types of cancers are metastasis and relapse. Metastasis refers to the ability of malignant cells from a primary tumor site to migrate to another region and subsequently give rise to secondary lesions. The development of multiple secondary lesions at different sites adds an element of uncertainty to the effectiveness of directed treatment. If cancer cells are not systematically removed / destroyed at all lesion sites, there is a possibility of relapse of the disease, thereby prolonging and complicating the therapy and follow-up regimen.

Metastasis occurs when malignant cells shift from the primary tumor site, and this shifting occurs by lymphatic drainage at the primary tumor site. The lymphatic network, with its wide capillaries and gradual flow rate, has been postulated to be a particularly suitable vehicle for the incubation and transport of cells [16]. Tumor cells may be transported via the lymphatic vessels to the lymph nodes and thereon, eventually getting into the blood circulation. The scientific literature provides examples of studies that have linked the spreading of tumor cells to the axillary lymph nodes to the prognosis of the disease [17], including quotations from work done as far back as 1752, when HF Le Dran postulated that the spread of breast cancer via the lymphatic system to the lymph nodes and beyond would result in systemic disease. It has been proposed in several studies that the tumor cells are trapped in the lymph node by mechanical barriers and the phagocytic action of lymph node macrophages [18, 19], while others have suggested that tumor cells may pass through unaffected after a period of harboring in the lymph node. The overall behavior may depend on the origin and nature of the cancer cells as much as or perhaps more than the capacity of the lymph node to trap and retain them [20]. The exact role of the lymph nodes with respect to the retention/harboring has not been clearly understood, with contradictions between studies that claim a possible immune response for these lymph nodes [21] and those which suggest that lymph nodes may be serving as a breeding ground for future tumors due to loco-regional down-modulation of the immune response in the adjacent lymph nodes [22]. While historically it was believed that only the terminal collecting lymph trunks communicate with the bloodstream, recent reviews of available literature have concluded that other modes of lymphovenous communication may be operating for transport of tumor cells from the lymphatic drainage into the circulatory system [20]. Initially, radical removal of axillary lymph nodes used to be carried out to arrest metastasis, followed by pathological examination of the dissected nodes using hematoxylin-eosin staining [23]. The progression of tumor cells via the lymphatic system to distal regions was the rationale provided for radical techniques like complete elective lymph node dissection (ELND) employed in cancer treatment even without prior evidence of metastasis [24, 25, 26]. However this approach has severe repercussions for both the patients and the clinicians. Patients undergoing total ELND are at risk for acute wound problems, chronic lymphedema, nerve injury, and anesthetic complications, and require prolonged and more expensive hospital care than patients with surgery at the primary site alone [38]. In addition, the biopsy examination of a large number of regional lymph nodes proves a burden for establishing the presence/absence of malignant cells. Typically in such cases, the biopsy would be limited to histological examination of hematoxylin-eosin stained slides of a restricted number of tissue sections. The study of Cochran et al [27] states that by this technique only a small fraction of the node would be examined and there is a greater chance of false negative inference of metastasis. By reducing the number of nodes necessary to be clinically examined for presence of metastasis, it becomes feasible to employ more sophisticated and in-depth techniques like immunohistochemistry (for example, using anti S-100 protein antibodies in melanoma [28]) for better detection of occult metastasis.

The first node to receive lymphatic drainage from the region of primary tumor was denoted by Morton's group as the "Sentinel Node" [38]. The term Sentinel Node was earlier used by Cabanas [39] in penile cancer to identify the node anatomically located adjacent to the inferior epigastric vein, which he proposed to be a harbor for metastatic cells. Cabanas also postulated that if the sentinel lymph node tested negative for the presence of metastasis, metastasis via the lymphatic pathway may be deemed unlikely and radical surgery for the groin region could be avoided. However, as put forth in Morton's review [38], several subsequent studies have suggested that the sentinel node for a given region does not have a fixed anatomic location but depends on the lymphatic pattern for that region. Hence, to detect the possible presence of metastatic cells in the sentinel node from a site of primary tumor, it becomes necessary to detect the individualized pattern of lymphatic drainage towards the nearby lymph nodes so as to identify the relevant nodes for excision and detailed biopsy examination. Since the 1950's, nuclear medicine scientists have made use of radioisotope techniques to study the pattern of lymphatic drainage for various relevant regions of the body with respect to the treatment of cancer [29, 30]. This method of mapping of lymph nodes by imaging of the associated radioactivity is referred to as 'lymphoscintigraphy'. Over the years several colloidal preparations were developed employing various routes and having differing physico-chemical properties, which were tested for lymphoscintigraphy [40]. Some of these have been detailed in the discussion of the history of radiopharmaceuticals development for this application. Apart from colloids / nanoparticles incorporating radioactivity, the literature has several other examples of preparations proposed towards possible use in SLN detection. The review of Jain et al [31] provides an exhaustive look at many such possibilities, including liposomes using avidin-biotin interactions [32] or encapsulating blue-dye [33], fluorescent dendrimers [34] and quantum dots [35, 36], each of which have their corresponding advantages and disadvantages. The aim of the current work is to develop suitable nuclear medicine techniques for detection and imaging of SLN's, hence further discussion shall be restricted to the work done in the field of lymphoscintigraphy agents.

2.1.2. The History of Lymphoscintigraphy Agents

One of the first lymphoscintigraphy agents in clinical use was radioactive colloidal gold (198Au) [37]. With a particle size range of 3-5 nm, 198Au is quickly transported in the surrounding lymphatic network and helps in rapid mapping of lymphatic drainage patterns. However, there are significant disadvantages as well [40]: 198Au has a half-life of 2.7 days and emits a gamma photon of 412keV energy (alongside a 0.96MeV electron). This means that a significant radiation dose is administered at the site of injection, leading to possible scarring of the tissue. Also, the high emission energy of the gamma photon is not suitable for imaging due to its lower spatial resolution. With the advent of 99mTc as an ideal diagnostic radionuclide, several agents based on 99mTc were explored for lymphoscintigraphy.

Some of the early particulate 99mTc-labeled agents used for lymphoscintigraphy include 99mTc-antimony trisulfide colloid and 99mTc-sulfur colloid. In the case of the antimony trisulfide colloid, the size of the particulates varied from 3-30 nm depending on the preparation, and were covered by a layer of polyvinylpyrrolidone for stabilizing the particle [41]. 99mTc-antimony trisulfide colloid was tested in multiple centers, but owing to the lack of favorable response to the implementation of lymphoscintigraphy as a prognostic device at the time, its usage did not gain adequate support for acceptance in the clinic.

As very comprehensibly reviewed by Eshima et al [40], 99mTc-labeled sulfur colloid is prepared through numerous pathways, resulting in a wide range of particle sizes. There are two primary protocols for the formation of 99mTc-labeled sulfur colloid: 1) Passing hydrogen sulfide gas through acidic solution of 99mTc-pertechnetate, followed by oxidation, which generates colloidal sulfur 2) Reaction of thiosulfate with acid by adding acidified pertechnetate to thiosulfate in the presence of gelatin or other stabilizing agents. The latter method which gives large size particles is used more commonly, and in this case the particle size can be influenced to a certain extent by controlling heating time for colloid formation reaction [42]. It has been postulated that the process of formation of 99mTc-labeled sulfur colloid involves the formation of a 99mTc-colloid nucleus around which sulfur may accumulate in colloidal form to generate an in situ labeled nanocolloid [43]. The preparation involves a heating reaction and typically produces a bimodal distribution of colloidal particulates, regardless of the route of production. Nevertheless, sulfur colloid is a commercially available lymphoscintigraphy agent for clinical use in the United States [44].

99mTc-labeled human serum albumin (HSA) in soluble form was tested as a lymphoscintigraphy agent and on intradermal injection was shown to successfully map the lymphatic pathway. However its non-particulate nature renders its transit through the lymphatic network very rapid with only a small degree of retention in the sentinel node. Hence any delay in identifying the sentinel node would lead to lead to false-negative results [45].

Better results were obtained with the use of HSA as a colloidal preparation, which has been licensed in Europe for use as a lymphoscintigraphy agent [42]. Here, >95 % of the colloidal particles are <80 nm in diameter. Nanocolloidal HSA is prepared as a kit containing HSA and stannous chloride for reduction, with some other constituents for stabilization and cryo-protection of the preparation during freeze-drying. The radiolabeling procedure depends on the binding of reduced technetium to albumin. HSA employed for this purpose must be sourced carefully and certified before use as free of blood borne pathogens like Hepatitis B, Hepatitis C and Human Immonodeficiency Virus (HIV) 1 and 2. Anaphylactic reactions to administration of HSA as a lymphoscintigraphy agent are rare but have been reported [42]. Also, the formation and 99mTc-labeling of HSA nanocolloid calls for a significant amount of tin (II) chloride to be added to the formulation. If oxygen is present beyond a certain level during addition of pertechnetate to the cold kit vial, tin (II) chloride has a tendency to react with pertechnetate to form stannous technetium colloid, which is not associated with the HSA particles [40]. Hence sufficient care must be taken to minimize presence of oxygen during the formation of nanoparticles and during the addition of pertechnetate to prepare the radiopharmaceutical.

2.1.3. Rationale for the Planned Work

Characteristics of an Ideal SLND Tracer

A survey of the history of lymphoscintigraphy agents gives insight into the expected characteristics for an ideal SLND agent. These may be summarized as follows:

1. An ideal SLND radiotracer should show rapid and appreciable uptake in the sentinel node, so as to give an unambiguous scintigraphic image for pre-surgical localization and accurate detection during surgery using a hand-held gamma probe.
2. It should show selective retention in the sentinel node with minimal passage into the subsequent nodes and thereon to the bloodstream where it may localize in other non-specific regions.
3. It should be retained in the sentinel node for sufficient period to allow for both convenient imaging and detection during surgery.
4. It should adhere to all other characteristics of a good radiopharmaceutical, including absence of toxicity. immunogenicity and/or any possible other hazard during preparation / administration of the radiopharmaceutical.

At present, there is no single radiotracer for SLND that fully satisfies all these criteria. Hence, there remains a scope for continued development of novel SLND ligands that come closer to the ideal characteristics. To this end, work has been done in this topic on the development and biological evaluation of novel SLND ligands using suitable biocompatible materials.

Poly [lactide (co-glycolide)] is a well-known nanocarrier in pharmaceutical applications [46, 47, 48, 49]. It has been widely employed in clinical trials as a vehicle for the in vivo delivery of various drugs. The physico-chemical properties of the nanocarrier are a function of the relative proportion of lactic acid and glycolic acid in the co-polymer and the formulation employed for generation of the nanoparticles. Based on their extremely favorable properties of biocompatibility and degradability, PLGA formulations have long been approved by the FDA as suitable in vivo carriers for drugs requiring controlled release [50]. PLGA can be formulated as particles of desired nanometer range size with a narrow distribution. This can be achieved by several techniques of which one of the well-established means is emulsion solvent evaporation technique. Here, an organic solution containing the co-polymer is poured into an aqueous phase under homogenization to generate nanoparticles. Subsequently the organic phase is evaporated off. Once optimized, the formulation can be carried out under aseptic conditions. The particle diameter range of PLGA nanoparticles is expected to be more controlled than for sulfur colloid used for SLND. PLGA also has the advantage over HSA nanocolloid in that it does not require handling of potentially hazardous blood products. Therefore it poses a lower risk of allergic reaction from the patient. Hence, a PLGA based 99mTc-labeled SLND tracer that fulfills the necessary criteria of uptake and retention can offer definite benefits over the currently employed SLND kits.

However, prior to this work, there has been no report of using PLGA nanoparticles for SLND. Hence PLGA nanoparticles with different modifications were developed with the intent of testing their biological suitability as 99mTc-labeled in vivo tracers for detection of sentinel nodes. First "plain" PLGA nanoparticles were formulated, which depended on direct 99mTc-labeling of the co-polymer itself. Subsequent to that, modified PLGA nanoparticles were prepared in order to assess their impact on the diagnostic radiolabeling and in vivo biological efficacy. Two approaches were undertaken to produce different PLGA derivatives:

1. In situ encapsulation of a 99mTc-chelating ligand inside the PLGA nanoparticles. Mebrofenin is a lipophilic molecule already used in nuclear medicine as a liver function imaging agent [52]. It is known to form stable complexes with 99mTc under moderate reaction conditions. Mebrofenin is soluble in ethanol and remains in solution when mixed with PLGA dissolved in acetone prior to emulsification in aqueous medium. It is expected to have favorable encapsulation efficiency during the process of nanoparticle formation. Hence mebrofenin was selected as a suitable ligand for encapsulation.
2. Derivatizing the surface groups of PLGA with 99mTc-chelating groups. Diethylenetriamine pentaacetic acid (DTPA) is a very well known 99mTc-chelator. It has been employed as a bifunctional chelating agent in the formation of several radiotracers relevant to nuclear medicine. The surface of the PLGA nanoparticles is expected to bear terminal carboxylic acid groups. They can be conjugated with a suitable amino-group bearing derivative of DTPA, like para-aminobenzyl DTPA (p-aminobenzyl-DTPA). In a typical conjugation protocol, the terminal carboxylic acid groups are first activated using EDC and NHS. Subsequently they are modified by reaction with p-aminobenzyl-DTPA to give suitable chelating centers for radiolabeling with 99mTc.

It is expected that such types of modifications may have advantages over plain PLGA nanoparticles in terms of the radiolabeling yield and stability of the labeled product, and in consequence may also influence the in vivo biological efficacy.

2.2. MATERIALS AND METHODOLOGIES

2.2.1. Materials

2.2.1.1. For Plain PLGA Nanoparticles

For the preparation of plain PLGA nanoparticles, 50/50 Poly DL lactide-co-glycolide was procured as a gift from PURAC Asia Pacific Pvt. Ltd. (Singapore). d-α-tocopheryl polyethylene glycol 1000 succinate (Vitamin E TPGS) was from Eastman Chemical Company, USA. Ethanol A.R. grade, Acetone A.R. grade, glucose, mannitol, sucrose, lactose and fructose were purchased from S.D. Fine Chemicals Ltd, India. Poloxamer 188 (Pluronic® F68) and Poloxamer 407 (Pluronic® F127) were gifted by BASF India Ltd. Ultrapure water obtained from a Milli Q Plus system (Millipore, France) was used in preparation and analysis of PLGA nanoparticles. Trehalose was a gift from Gangwal Chemicals Pvt. Ltd., India. 0.45 µm membrane filters were purchased from Pall Life Sciences, India.

Ultraturrax® T25 homogenizer used during the process of nanoparticle preparation was from Janke & Kunkel, IKA Labortechnik, Germany and subsequent magnetic stirring was done on an instrument from Remi, India. Dynamic Light Scattering (DLS) measurements were carried out using a Malvern Autosizer 4800 instrument with 7132 digital correlator (Malvern, UK) and Argon ion laser was from Coherent Innova, USA. Lyophilization was performed in the FreeZone 4.5 freeze-dryer (Labconco Corporation, USA).

Saline used for 99mTc labeling, purification and in vivo biological evaluation studies was prepared using ultrapure water from Aquamax-Ultra 370 water purification system (Young Lin, Korea) and purged with nitrogen gas (Inox Chemicals, India) before use, to minimize oxygen content. Sodium chloride and stannous chloride (AR Grade) were obtained from Sigma, USA. 99mTc was obtained as pertechnetate by elution with saline from an in-house 99Mo-99mTc generator at the Isotope Applications & Radiopharmaceuticals Division, BARC. PD10 columns (GE Healthcare, UK) containing Sephadex G-25 resin were employed for purification of the labeled product.

Orbital shaker-incubator used for radiolabeling reaction was from Biosystem Scientific Co., India. Sodium iodide (thallium) counters from Electronics Corporation of India Limited (ECIL), India were used for radioactivity measurement studies while UV absorption studies were conducted on the V-530 UV-Vis Spectrophotometer (Jasco, Japan). Scintigraphic imaging studies were carried out with the Millennium MPS gamma camera system (Wipro-GE Medical Systems, India).

2.2.1.2. For Modified PLGA Nanoparticles

For the preparation of mebrofenin-loaded and DTPA-conjugated PLGA nanoparticles, PLGA was procured from Lakeshore biomaterials Inc. Mebrofenin was obtained from the Board of Radiation and Isotope Technology (BRIT), India. 1-Ethyl-3-[3-dimethylaminopropyl] carbodiimide hydrochloride (EDC) and N-hydroxysuccinamide (NHS) were purchased from Sigma-Aldrich, India. 90Y was obtained as yttrium chloride by elution from an in-house 90Sr-90Y generator at the Isotope Applications & Radiopharmaceuticals Division, BARC. Other materials used were as described above.

Energy Dispersive X-ray Spectroscopy (EDS) for assessment of DTPA conjugation was performed on the JEOL JSM-7600F Scanning Electron Microscope, at the Sophisticated Analytical Instrument Facility (SAIF), Indian Institute of Technology (IIT) - Bombay. IR spectra were recorded on a JASCO FT/IR-420 spectrophotometer, Japan.

2.2.2. Preparation of Nanoparticles

2.2.2.1. Plain PLGA Nanoparticles

The PLGA nanoparticles were synthesized by emulsion solvent evaporation. PLGA solution in acetone (22 mg in 5 ml) was emulsified with 0.05 % w/v solution of Vitamin E TPGS in double distilled water (20 ml) using Ultraturrax® T25 at 17500 rpm for 5 min. The emulsion formed was stirred using a blade-type stirrer at 2000 rpm for 8 hours to evaporate the organic phase, which resulted in the formation of nanoparticles. The process was optimized with respect to the effect of different non-ionic surfactants (Vitamin E TGPS, Tween 80, Pluronic® F 127, Pluronic® F 68). The effect of these parameters on the particle size and size distribution of the resulting product was studied using DLS techniques. After preparation, the nanoparticles were subjected to freeze-drying. Before and after this process, their mean particle diameter and polydispersity index (PI) were determined by DLS techniques.

2.2.2.2. Modified PLGA Nanoparticles

A. “Base” PLGA Nanoparticles

Using the PLGA material obtained from Lakeshore Biomaterials Inc., base PLGA nanoparticles were prepared by solvent evaporation technique for standardization prior to mebrofenin-loading and DTPA-conjugation. An existing optimized protocol (optimization data not shown here) for preparing PLGA nanoparticles using this material was employed. As per the protocol PLGA was dissolved in acetone, and 1.75 % Vitamin E TGPS was employed as the surfactant in aqueous phase. Both the phases were sonicated for 10 min and the organic phase was poured into aqueous phase under continuous dispersion using Ultraturrax® T25 for 5 min at 17500 rpm followed by magnetic stirring at 2500 rpm for 6 hours to evaporate the organic solvent completely and to give a nanoparticulate dispersion. After preparation, the nanoparticles were subjected to freeze-drying. Before and after this process, their mean particle diameter and PI were determined by DLS techniques.

B. Mebrofenin-loaded PLGA Nanoparticles

Mebrofenin-loaded PLGA nanoparticles were prepared by a technique similar to that employed for base PLGA nanoparticles (sec. 2.2.2.2A). Briefly, 50 mg of PLGA and 10 mg of mebrofenin were dissolved separately in 3 ml of acetone and 5 ml of ethanol respectively and mixed together. Aqueous phase was identical to that used in preparation of base PLGA nanoparticles. As described above for base PLGA nanoparticles, the two phases were sonicated for 10 min and the organic phase was poured into the aqueous phase under continuous dispersion using Ultraturrax® T25 for 5 min at 17500 rpm. This was followed by magnetic stirring at 2500 rpm for 8 hours to evaporate the organic solvent completely and to give a nanoparticulate dispersion. After preparation, the nanoparticles were subjected to freeze-drying. Before and after this process, their mean particle diameter and PI were determined by DLS techniques.

The encapsulation efficiency of mebrofenin inside PLGA was determined by measuring the concentration of free mebrofenin in the dispersion medium after emulsification, and comparison with the initial concentration of added mebrofenin. For this, the emulsified mixture was centrifuged through Nanosep® molecular filtration tubes at 17000 rpm for 40 min. After suitable dilution, the filtrate was spectrophotometrically assayed for unencapsulated mebrofenin at 205 nm and its concentration was determined by comparison against a set of mebrofenin standards (1-9 µg/ml linear range).

C. DTPA-conjugated PLGA Nanoparticles

Base PLGA nanoparticles were prepared as described in sec. 2.2.2.2A and freeze-dried. The terminal -COOH groups on the surface of base PLGA nanoparticles were conjugated with the amino group of p-aminobenzyl-DTPA using NHS and EDC for activation. Conjugation was carried out using various DTPA:PLGA ratios (5:1, 10:1 and 20:1) to ascertain the ratio that would result in the highest conjugation yield. For the reaction, 30 mg of freeze-dried PLGA nanoparticles were reconstituted in 500 µl water, to which were added 100 µl each of 10 mg/ml NHS and 20 mg/ml EDC solution in water. This was stirred on a magnetic stirrer at room temperature for 30 min. Then, appropriate amounts of p-aminobenzyl-DTPA dissolved in 0.1 M phosphate were added to obtain the selected PLGA:DTPA ratios. The pH of the reaction mixture was adjusted to near 7.0 using KOH. The reaction mixture was stirred at room temperature on a magnetic stirrer for 2 hours and transferred to 4 °C for overnight incubation with stirring. It was then again stirred at room temperature for 2 hours. The extent of DTPA conjugation was studied by labeling the conjugation reaction mixture with 90Y-chloride. In brief, to a 50 µl aliquot of the reaction mixture were added 250 µl 0.05 M ammonium acetate buffer (pH 5.5), 1:1 amount of 89Y-chloride proportional to DTPA and a trace amount of 90Y-chloride. Labeling was carried out at 37 °C for 2 hours in an orbital shaker-incubator. At the end of the labeling, the mixtures were characterized by paper chromatography (Whatman no 3) with water:acetonitrile mixture (1:1) as the mobile phase. The ratio giving highest conjugation yield was selected for further work. After conjugation, the reaction mixture was centrifuged in an Amicon molecular filter tube at 3000 g for 20 min to remove free DTPA. PLGA nanoparticles retained in the filter were washed twice with phosphate buffered saline (pH 7.4) using the same procedure. They were then suspended in the same buffer and dispensed into vials for lyophilization. After freeze-drying, their mean particle diameter and PI were determined by DLS techniques.

2.2.3. Freeze-drying of PLGA Nanoparticles

The samples were lyophilized in a laboratory freeze-dryer (n=3) using the following regimen. The shelf temperature was initially reduced to -40 °C and the sample was held therein for 8 hours. The temperature was then increased from -40 °C to -15 °C at 0.3 °C/minute with the chamber pressure maintained at 0.08 mbar for primary drying. These conditions were maintained for 6 hours. The secondary drying was achieved by further increasing temperature to 25 °C at 0.5 °C/minute, with chamber pressure maintained at 0.08 mbar for 4 hours. During the entire process the temperature of the cold-trap was maintained at -52 °C. Different concentrations of cryoprotectants and stabilizer were added to the formulation to assess optimum concentration. The final samples were stored at 4 °C until analysis.

After freeze drying, the products were tested for reconstitution characteristics by the addition of double distilled water. Rehydration was observed visually after gentle manual agitation of the samples, leading to the formation of aqueous solution. Mean particle diameter and PI of the reconstituted product were then determined by DLS.

2.2.4. Characterization of PLGA Nanoparticles

The mean particle diameter and PI of the optimized formulation, pre and post-lyophilization were assessed by DLS at 25 °C. The light source was argon ion laser operated at 514.5 nm with a maximum output power of 2 W. Immediately before measurement, each sample was diluted tenfold with double distilled water and filtered through 0.45 µm membrane filter, which enabled the nanoparticles to pass through while retaining any external impurities possibly present in water used for sample dilution, which could affect the particle size determination.

For DTPA-PLGA nanoparticles the conjugation of DTPA groups onto the surface of PLGA nanoparticles was confirmed by testing lyophilized DTPA-PLGA preparation (prepared using optimized DTPA:PLGA ratio) with a combination of FT-IR, Zeta-potential and EDS, using the standard protocols for these techniques. Plain PLGA nanoparticles were used for comparison for all the analyses.

2.2.5. 99mTc-labeling of PLGA Nanoparticles

2.2.5.1. Plain PLGA Nanoparticles

Plain PLGA nanoparticles reconstituted with saline from the lyophilized form were labeled with 99mTc by direct reduction technique with stannous chloride, adapting from the protocol reported by Tafaghodi et al [51]. Briefly, 5 mg of lyophilized PLGA preparation was reconstituted by addition of 3.7-37 MBq of 99mTc (as pertechnetate) in 1 ml saline to obtain the nanoparticle suspension. Stannous chloride (2 mg/ml in saline) was added to this suspension and the mixture was mixed vigorously on a vortex mixer, followed by extended shaking (80 rpm) in an orbital shaker-incubator to aid in the radiolabeling. The reaction was optimized with respect to stannous chloride content, reaction temperature and time. In the standardized protocol, the reaction was carried out using 250 µg stannous chloride for 60 min at 37 °C.

2.2.5.2. Mebrofenin-loaded PLGA Nanoparticles

The modified PLGA derivatives were labeled with 99mTc using stannous chloride as the reducing agent. Mebrofenin-PLGA nanoparticles were radiolabeled following a procedure similar to that for plain PLGA nanoparticles. In the optimized labeling protocol, to 5 mg of mebrofenin-loaded PLGA nanoparticles were added 37-185 MBq of [99mTc] pertechnetate in saline and 250 µg of stannous chloride (in 50 µl). The total reaction volume was maintained at 1 ml using saline containing 0.1 % Tween-20 (to prevent aggregation of the nanoparticles). The reaction was carried out for 60 min at 37 °C with constant shaking at 80 rpm on an orbital shaker-incubator.

2.2.5.3. DTPA-conjugated PLGA Nanoparticles

In the case of DTPA-PLGA, labeling with 99mTc was carried out as follows: 37-185 MBq of [99mTc] pertechnetate in saline was added to 5 mg of DTPA-PLGA nanoparticles along with stannous chloride keeping total reaction volume at 1 ml using saline containing 0.1 % Tween-20. The reaction was carried out for different time periods at room temperature with intermittent shaking.

2.2.6. Purification and Characterization of 99mTc-labeled PLGA Nanoparticles

Purification of 99mTc-labeled PLGA nanoparticles as well as their characterization in terms of the radiolabeling yield and stability was performed by size-exclusion chromatography using a PD10 column containing Sephadex G-25 resin. Beforehand, the elution pattern of unlabeled plain PLGA nanoparticles was ascertained using PD10 column elution followed by spectrophotometric estimation at 220 nm. Unlabeled

PLGA nanoparticles were found to be eluted near the void volume fraction, and this was taken the basis for future estimations.

The purification protocol for the 99mTc-labeled PLGA derivatives was as follows:

PD10 column was washed with 5 column volumes of phosphate buffered saline (containing 0.1 % Tween-20). After completion of the respective 99mTc-labeling reactions for the various PLGA derivatives, the reaction mixture was loaded on to the column and elution was performed up to 3 column volumes using PBS (0.1 % Tween-20). 1 ml fractions were collected and measured for 99mTc activity on a well-type sodium iodide (thallium) scintillation detector with suitable energy window. Radiolabeling yield was calculated from the radioactive peak fraction corresponding to elution pattern for PLGA. This purified 99mTc-labeled PLGA derivative fraction was used for further studies.

In the case of plain PLGA nanoparticles and mebrofenin-loaded PLGA nanoparticles, it was observed that 99mTc activity from the reaction mixture not associated with the PLGA nanoparticles was being retained on the PD10 column. It was inferred that the high requirement of tin (II) chloride for the radiolabeling procedure led to the formation of reduced 99mTc colloid, which was being retained on the column. Subsequently, the PD10 column was washed with 5 % hydrogen peroxide solution. This led to elution of the residual 99mTc activity from the column, confirming the inference. The PD10 column was then washed with at least five column volumes of PBS (0.1 % Tween-20) before using for next elution.

Stability of the purified 99mTc-labeled PLGA derivatives was assessed by repeated PD10 column elution using the procedure described above and correcting for radioactive decay of 99mTc. Stability was assessed for 24 hours, which is sufficient for the intended application of the labeled product.

After allowing for decay of the 99mTc activity in the radiolabeled preparations, the nanoparticles were assessed again for their particle size characteristics to see if there was any effect of the radiolabeling protocol on the nanoparticle morphology.

2.2.7. Biological Evaluation of 99mTc-labeled PLGA Derivatives

The various 99mTc-labeled PLGA derivatives were tested for their biological suitability as SLN detection tracers through animal experiments. Wistar Rat was selected as the appropriate species for animal studies and footpad injection was employed for testing the in vivo localization pattern of the tracers. The efficacy experiments performed in animal models included in vivo activity distribution measurement studies and scintigraphic imaging studies. The procedures followed herein were in concurrence with the institutional guidelines governing the conduct of animal experiments.

2.2.7.1. In Vivo Radioactivity Distribution Measurement

The rats were anesthetized via the intraperitoneal route with a 1:10 mixture of xylazine:ketamine. This is a commonly used anesthesia formulation, where xylazine functions as a sedative and ketamine functions as a muscle relaxant. In case additional boosters were required ketamine alone was used.

In the footpad model for assessment of SLN detection tracers, the radiolabeled preparation is injected subcutaneously in the footpad of the animal and its transit to the nearest (popliteal) node and beyond along a well-understood pathway is studied using suitable methods. In this technique the popliteal node serves as the sentinel lymph node. After the anesthesia had taken effect, 50 µl of the appropriate 99mTc-labeled PLGA derivative was administered to each animal subcutaneously in the footpad region. Following this, a gentle massage of the administered region was performed using an absorbent gauze pad for approximately 1 min. The rejection criteria for any injected animal were the observation of bleeding at the site of injection or measurement of more than 0.5 % of 99mTc activity from the administered dose on the absorbent gauze pad. The animals were then kept in separate sets for different incubation periods under normal conditions, with water provided ad libitum. In the case of in vivo distribution measurement studies, 5 min prior to the end of the respective incubation periods, the animals in each set were administered with 50 µl of Patent Blue dye solution (1 % w/v in saline) in the same region using a protocol identical to administration of the 99mTc-labeled PLGA derivative. This was done for visual identification of the nodes along the lymphatic pathway adjacent to the site of injection (Fig. 2.1).

Figure 2.1.: Visual identification of lymph nodes with blue dye (popliteal node near tibia).

At the end of the respective incubation periods, the animals were sacrificed by exposure to a carbon dioxide saturated atmosphere. The relevant organs and tissues, including the popliteal (sentinel) and iliac (secondary) nodes, were excised for determination of the in vivo distribution of 99mTc activity from the labeled preparation. Radioactivity measurement was done on a flat bed-type sodium iodide (thallium) detector. Activity retained in each organ/tissue was expressed as a percentage of the total injected dose (% ID). As the popliteal node serves as the sentinel node in this procedure, Popliteal Extraction (PE) is an indicator of the suitability of a preparation as an agent for SLN detection. PE was calculated using the formula given below [54]:

$PE = (\%ID_{popliteal} - \%ID_{iliac})/\%ID_{popliteal}$

2.2.7.2. Scintigraphic Imaging Studies

Scintigraphic imaging studies were performed in Wistar Rat, using the same amount of nanoparticulate PLGA derivatives as for the in vivo radioactivity distribution measurement studies with ~1.2 MBq radioactivity administered per animal. The protocols followed for anesthesia of the animals and administration of 99mTc-labeled PLGA nanoparticles were the same as for the radioactivity distribution measurement studies. The administration of blue dye however was not required in this case. The animals were placed with their dorsal side facing the camera. Scintigraphic images were acquired at various time-points with the Genie Acq Image Acquisition software (Release 3.0). The acquisition parameters were as follows - Matrix 256 × 256, Pixel size ~2.2 mm, Zoom 1.33, 5 min acquisition time. Image processing was achieved using the Xeleris image processing software (Version 1.0272).

2.2.8. Toxicity Studies

The ligand showing good promise in the in vivo biological efficacy studies was taken up for performing studies to evaluate possible toxicity from the cold ligand. Here, 100-fold concentration of the cold ligand (or normal saline in controls) was injected in Wistar rats using a protocol indentical to the one described in sec. 2.2.7.1. Post-injection, the animals were kept under normal conditions for 15 days and then sacrificed. Blood, serum and tissue samples were taken for performing relevant toxicity assays.

2.2.8.1. Hematology Studies

The following hematological parameters were measured in the whole blood samples: Red blood cell (RBC) count, white blood cell (WBC) count, platelet count and hemoglobin concentration.

Blood cell counts were performed by hemocytometry using Neubauer's Chamber slide. Hemoglobin concentration was measured using the Drabkin's reagent method. Drabkin's reagent contains sodium bicarbonate, potassium ferricyanide and potassium cyanide. In the reaction with alkaline cyanide and ferricyanide, hemoglobin in most forms in the the blood is rapidly converted to cyanmethemoglobin. This can be measured colorimetrically at 540 nm. Whole blood was reacted with Drabkins's reagent as per the kit instructions and allowed to stand for 15-20 min at RT. The reaction mixture was then read at 540 nm and plotted on a standard curve generated using cyanmethemoglobin standards to obtain the concentration of hemoglobin in the blood sample.

2.2.8.2. Liver Function Studies

From the serum samples the following liver function assessment parameters were measured: Asparate aminotransferase (AST) / serum glumatate oxaloacetate transaminase (SGOT) activity, alanine aminotransferase (ALT) / serum glumatate pyruvate transaminase (SGPT) activity, serum albumin and serum bilirubin concentration.

AST/SGOT catalyses the following reaction: Aspartate + α-ketoglutarate → oxaloacetate + glutamate. The kit for measurement of serum AST activity contains a substrate mixture (aspartate and α-ketoglutarate) and a color reagent in the form of a diazonium salt that selectively reacts with oxaloacetate to form a colored product that can be estimated photometrically at 530 nm. Serum samples were reacted as per the kit protocol. The colored product was read at 530 nm and compared with a control containing a calibrated value of AST activity to obtain the activity of AST in the sample.

ALT/SGPT catalyses the following reaction: Alanine + α-ketoglutarate → pyruvate + glutamate. The kit for measurement of serum ALT activity contains a substrate mixture (alanine and α-ketoglutarate) and 2,4-dinitrophenylhydrazine. Pyruvate formed in the SGPT-catalysed reaction selectively reacts with 2,4-dinitrophenylhydrazine to form 2,4-dinitrophenylhydrazone complex. This is dissolved using the color developer reagent containing 0.5 N sodium hydroxide and the resultant solution is read spectrophotometrically at 505 nm. Serum samples were reacted as per the kit protocol. The colored product was read at 505 nm and compared with a control containing a calibrated value of AST activity to obtain the activity of AST in the sample.

The colorimetric assay kit for estimation of serum albumin uses bromocresol green (BCG) dye reagent that reacts with albumin to give a colored complex with an absorbance maxima at 620 nm. The sample was measured against a standard curve prepared using known stock solution of albumin provided in the kit.

The kit for estimation of total bilirubin in serum uses an aqueous diazotized sulfanilic acid reagent to modify bilirubin in the sample to an azobilirubin colored product that can be measured colorimetrically at 550 nm. The absorption of the product is directly proportional to the concentration of total bilirubin and comparison with a standard as provided in the kit gives a value of bilirubin concentration in the sample.

2.2.8.3. Histological Studies

Samples of tissue from popliteal node, footpad and liver were suspended in 10 % neutral buffered formalin for 24-48 hours for preservation of the tissue structure. After allowing adequate time for fixation they were washed several times with tap water to remove all traces of formalin. Finally they were suspended in 70 % ethanol solution and stored at 4 °C before making histological blocks and slides. Histological blocks were prepared using the standard protocol for paraffin block making as follows: The fixed tissues were immersed in a graded series of ethanol baths of increasing concentration (70 % - 95 % - absolute ethanol). They were then immersed in xylene for clearing. Finally molten paraffin wax was added over the tissues placed in suitable orientation and allowed to cool and harden for formation of the paraffin tissue blocks. These were stored at room temperature and taken for making slides as required.

Using the paraffin blocks, ≤5 µ thick sections were taken for making slides. These slides were stained with the established Hematoxylin - Eosin staining procedure. The active staining component of hematoxylin is its oxidation product hematin. Hematin in acidic conditions binds to the lysine residues of nuclear histones, thereby staining the chromatin. In the procedure hematin stain was allowed to saturate, and then rinsed off with tap water, giving a bluish-purple tint to the nuclei. The extent of hematin saturation was then reduced to clear the background, using 0.3 % acidified alcohol as a differentiator. After washing off the differentiator with tap water, eosin was used as a counter-stain, which colors the other cellular components pink. After eosin staining the stained sections were dehydrated by exposure to absolute ethanol and xylene, then mounted with coverslips for histological examination.

2.3. RESULTS

2.3.1. Plain PLGA nanoparticles

2.3.1.1. Optimization of Formulation

The formulation for plain PLGA nanoparticles was optimized with respect to various surfactants and surfactant concentrations to achieve optimal particle size in terms of diameter and size distribution range. The results are depicted in terms of particle size distribution in Fig. 2.2 and mean of particle diameter and PI in Fig. 2.3 (n=3).

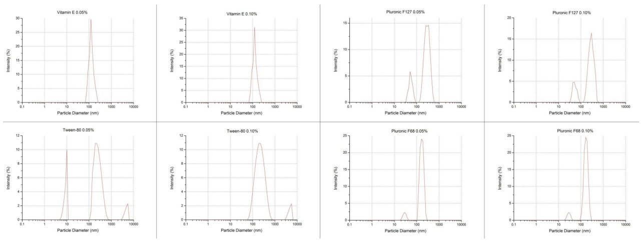

Figure 2.2.: Effect on particle size distribution of various surfactants in emulsion solvent evaporation based generation of PLGA nanoparticles.

It becomes evident from these results that using Vitamin E TPGS as a surfactant facilitates a low particle size and narrow distribution (as represented by the polydispersity index, PI) under all the tested experimental concentrations. A decrease in the particle size and PI was observed . as the concentration of Vitamin E TGPS was increased from 0.05 to 0.1 % w/v, only a marginal decrease in the particle size was observed. Hence a concentration of 0.05 % w/v Vitamin E TGPS was finalized for further work. Among the other surfactants tested Pluronic® F 127 and Pluronic® F 68 resulted in a comparable average particle size when they were used at the same concentration levels. However, these surfactants gave a very non-homogeneous size distribution, as indicated by the high PI values in these cases. The results obtained

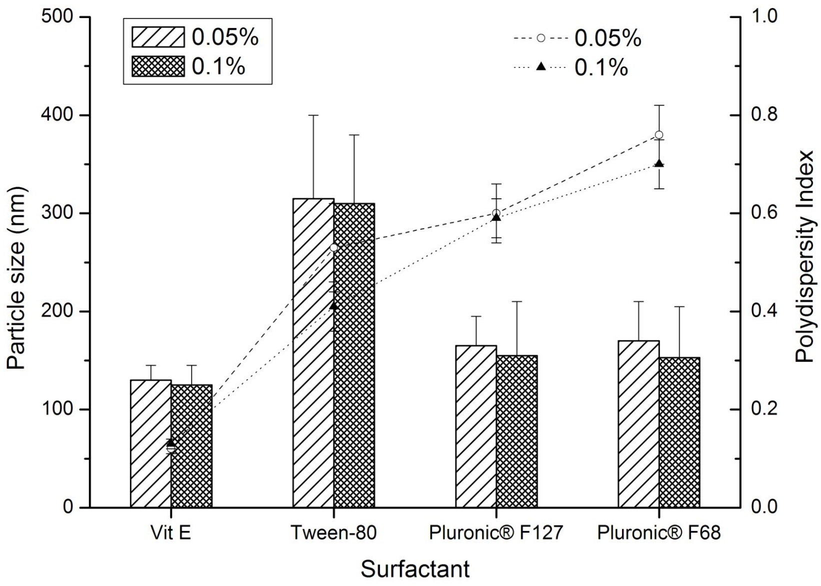

Figure 2.3.: Effect of surfactant on the particle size and PI of the nanoparticles, prior to freeze-drying (n=3). Columns are associated with particle size and lines are associated with polydispersity index.

with Vitamin E TPGS may be attributed to its superior emulsification ability, which ultimately governs the particle size as the solvent evaporates.

The various concentrations of the solid sugar or sugar-stabilizer mixture used as the cryoprotectant was dissolved in the final nanoparticle formulation before being subjected to the drying process. The effect of the cryoprotectant formulations on the particle size distributions of PLGA nanoparticles post-lyophilization is depicted in Fig. 2.4. Mean particle diameters and the PI of the lyophilized products after reconstitution are shown in Fig. 2.5.

The particle size analysis of the reconstituted products showed that the particle diameter results were in accordance with the physical nature of the freeze dried cake and the reconstitution velocity. Formulations with mannitol alone, or in combination with 1 % Poloxamer, showed increased particle size. In terms of particle

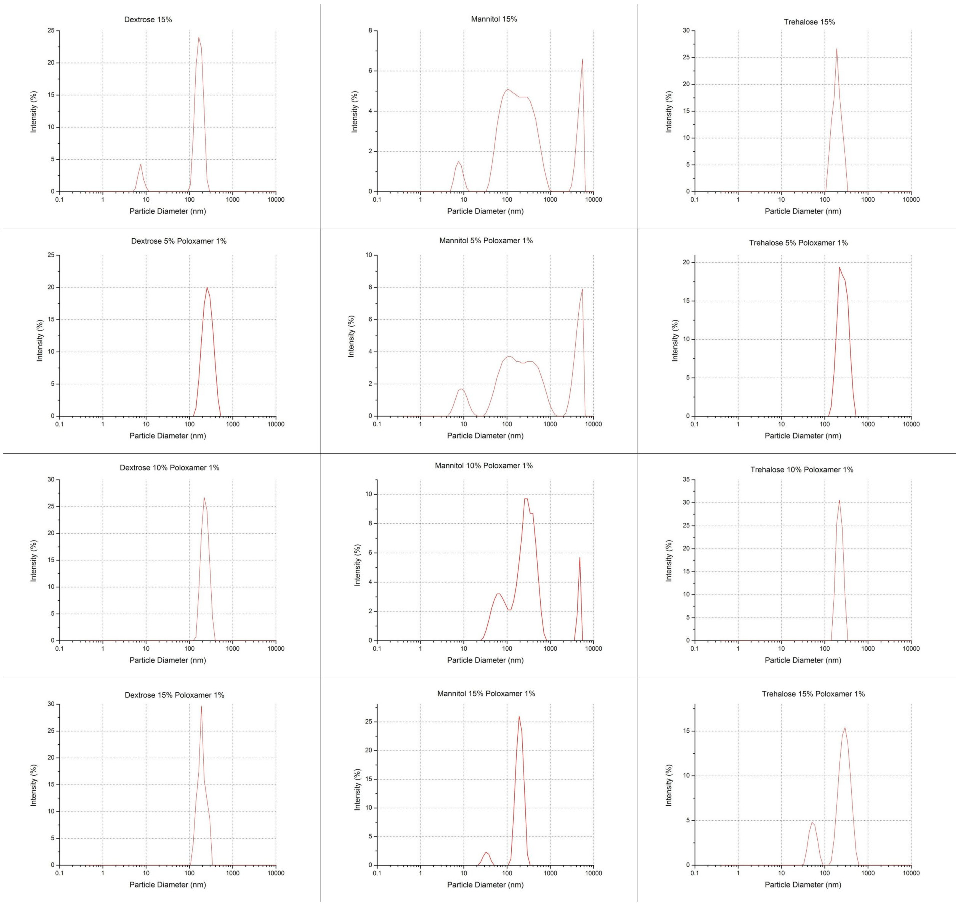

Figure 2.4.: Effect of various cryoptotectants on the particle size distribution of plain PLGA nanoparticles reconstituted after lyophilization.

diameter, the results obtained with Trehalose alone at a concentration of 15 % and in combination with 1 % Poloxamer as well as those obtained with a combination of 15 % Dextrose and 1 % Poloxamer were similar (~180 nm). However, the combination of 15 % Trehalose and 1 % Poloxamer resulted in a wider particle size distribution as indicated by the PI of the sample. The distributions with 15 % Trehalose and 15 % Dextrose with 1 % Poloxamer were comparable. In this respect, the later combination would be preferred at an industrial scale, in event of scale-up of nanoparticles, as Dextrose is more economical.

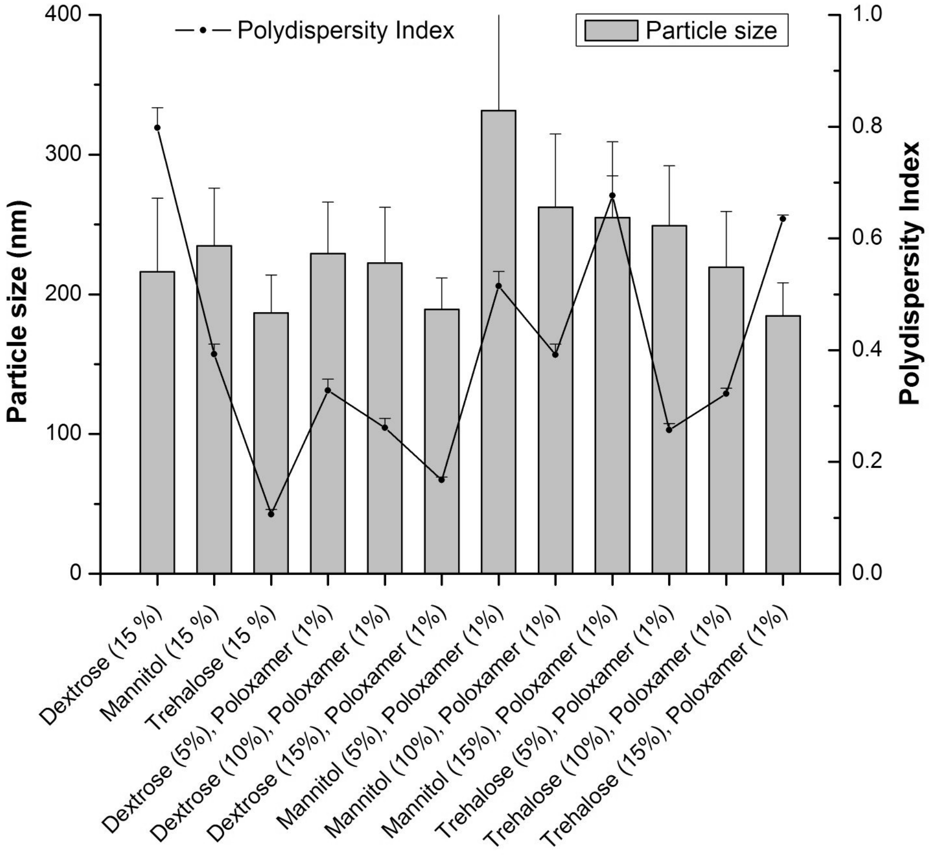

Figure 2.5.: Particle diameters and the PI of the reconstituted nanoparticles post freeze-drying (n=3)

2.3.1.2. 99mTc-labeling of PLGA Nanoparticles

Following the absorbance at 220 nm, plain PLGA nanoparticles were found to be eluted in the region of the void volume with PBS (0.1 % Tween-20) elution on PD-10 column. Using the optimized labeling procedure, approximately 70 % of the added 99mTc activity was associated with the PLGA nanoparticles and the labeled product could be easily separated on a PD-10 size exclusion column (Fig. 2.6a).

The effect of reaction time and temperature on 99mTc-labeling yield is shown in Fig. 2.6b. Under reaction conditions of 60 min at 37 °C, an increase of tin (II)

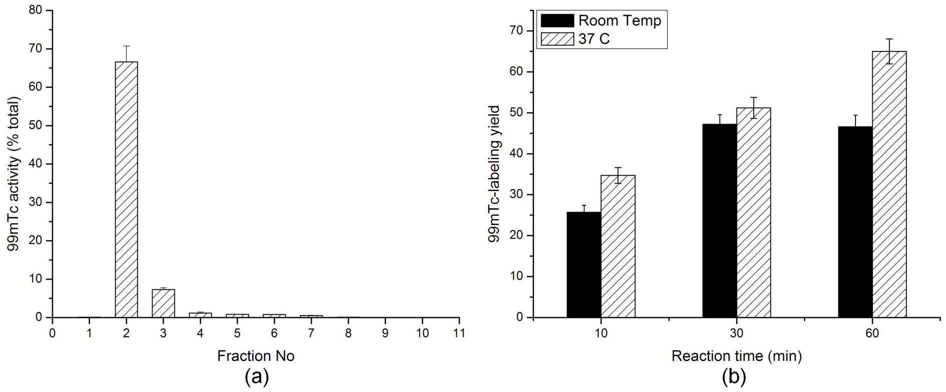

(a)

(b)

Figure 2.6.: a) Elution profile of 99mTc-labeled PLGA on PD-10 column based on the radioactivity profile of elution in saline b) Effect of reaction conditions on 99mTc-labeling yield of PLGA (n=3, columns are associated with Time and lines are associated with $SnCl_2$content).

chloride content in the reaction mixture from 250 µg to 500 µg improved the labeling yield by less than 5 %, hence it was decided to use the lower tin (II) chloride concentration. The labeled product was found to be stable (>90 % retention of activity in PLGA fraction) for up to 12 hours when stored at 4 °C in saline. From the particle size analysis it was observed that exposure to the conditions of 99mTc-labeling did not significantly alter the particle size distribution.

2.3.1.3. In Vivo Radioactivity Distribution and Scintigraphic Imaging Studies

The in vivo distribution pattern of PLGA nanoparticles labeled with 99mTc as observed from the measurement of retained activity in excised organs / tissues is given in Tab. 2.1. 99mTc activity appears to be extracted in significant amounts from the site of injection. 99mTc-PLGA shows accumulation in the popliteal and iliac nodes, which appears to be stable over the tested period of 3 hours.

Organ	**15 min**	**60 min**	**180 min**
Liver	1.71±0.4	1.63±0.21	0.84±0.14
	(0.20±0.05)	(0.19±0.02)	(0.10±0.02)
Intestine	3.08±0.76	4.68±0.53	6.71±1.04
	(0.19±0.05)	(0.30±0.03)	(0.42±0.07)
Stomach	4.84±1.15	7.48±0.26	10.72±1.36
	(1.25±0.3)	(1.93±0.07)	(2.76±0.35)
Kidney	0.44±0.01	0.54±0.08	0.87±0.24
	(0.27±0.01)	(0.34±0.05)	(0.54±0.15)
Heart	0.13±0.01	0.11±0.02	0.05±0.01
	(0.16±0.01)	(0.13±0.02)	(0.06±0.01)
Lungs	0.25±0.05	0.25±0.07	0.14±0.02
	(0.19±0.04)	(0.19±0.05)	(0.10±0.01)
Spleen	0.06±0.02	0.09±0.01	0.03±0.01
	(0.12±0.04)	(0.18±0.02)	(0.06±0.02)
Blood	4.03±0.84	4.7±0.34	2.35±0.34
	(0.24±0.05)	(0.28±0.02)	(0.14±0.02)
Node Uptake			
Popliteal Node	1.05±0.60	1.37±0.60	1.75±0.65
	(210.0±120.0)	(274.0±120.0)	(350.0±130.0)
Iliac Node	0.24±0.09	0.56±0.14	0.59±0.18
	(48.0±18.0)	(112.0±28.0)	(118.0±36.0)
Site of Injection	62.86±5.82	47.91±1.77	46.57±4.29
PE (%)	76.17±3.68	61.28±16.92	65.77±2.83

Table 2.1.: In vivo distribution of plain PLGA nanoparticles in Wistar Rat model, data given as %ID per organ (%ID per gram) n=3.

Scintigraphic images confirming localization of 99mTc-labeled PLGA nanoparticles in the sentinel node at 15 min and 60 min are shown in Fig. 2.7. PE is good in the initial time interval (15 min) and competitive with the result that was obtained with commercially available sulfur colloid kit Nanocis® (PE 81±2.94 %). Although the PE value is lower at the 60 min mark, it remains stable even at 180 min post-injection. The absolute node uptake is lower than what we observed for 99mTc-labeled Nanocis (4.88±2.63 %ID at 180 min in popliteal node) but that would appear to be related more to the stability of the 99mTc label than as a characteristic of the labeled nanoparticle preparation. Apart from the nodes, radioactivity is observed to accumulate in the blood, liver, stomach and intestine. As there is no observed bleeding during subcutaneous administration in any of the animals included in the study, this pattern of retention indicates that the 99mTc label may be getting separated in vivo from the PLGA nanoparticles. It may then go into the circulation and subsequently accumulate in the above-listed organs.

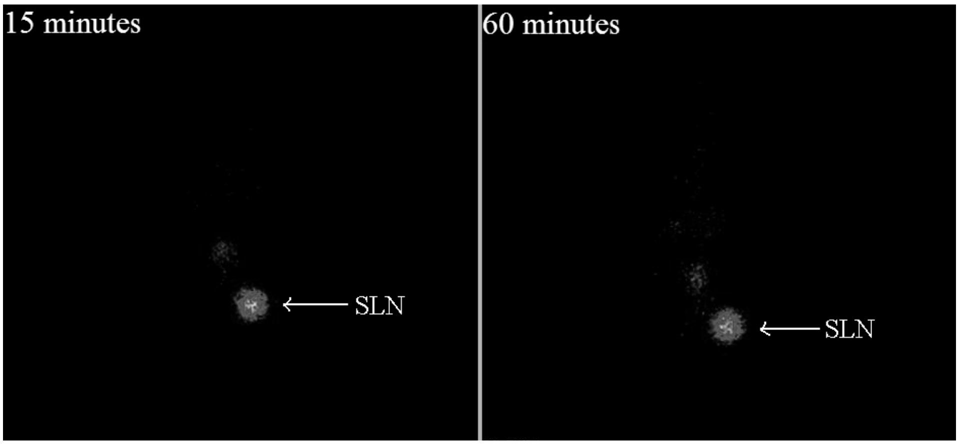

Figure 2.7.: SLN imaging in Wistar rat using plain PLGA nanoparticles.

From the above observations it may be hypothesized that technetium-99m in reduced form is adsorbed as a layer onto the surface of the PLGA nanoparticles. This may be getting re-oxidized to some extent in vivo and thereby separated from the nanoparticles. Further work is necessary to modify process of generating 99mTc-labeled PLGA nanoparticles to ensure a more stable association of 99mTc activity with the PLGA nanoparticles and study the impact of that on biological efficacy of the preparation as an SLND agent. Loading the PLGA nanoparticles with a suitable ligand for complexation with 99mTc may provide a more optimal radio-tracer, as may tagging the surface of PLGA nanoparticles with a suitable 99mTc-chelating agent. But the prima facie results observed with plain PLGA nanoparticles do indicate the potential of PLGA as promising polymeric biocompatible substrate towards development of a suitable nanoparticle ligand for SLN detection.

With the intention of realizing better labeling and in vivo properties for a PLGA-based SLN detection tracer attempts was made to modify the PLGA in two directions, the results of which are discussed further:

1. Loading PLGA nanoparticles with 99mTc chelating mebrofenin ligand.
2. Conjugating the surface of PLGA nanoparticles with 99mTc chelating DTPA groups.

2.3.2. Mebrofenin-loaded PLGA nanoparticles

2.3.2.1. Optimization of Formulation

Particle size distribution profile (Fig. 2.8) reveals the post-lyophilization size distribution against intensity (%) for mebrofenin loaded PLGA nanoparticles with different concentrations of sucrose cryoprotectant. With 10% sucrose, the mean particle diameter (nm) was found to be 224±6.15 nm, and a PI value of 0.26±0.027 showed the formulation to be homogeneously dispersed with narrow particle size distribution. The encapsulation efficiency for mebrofenin as determined by spectrophotometry was 51±2.3%.

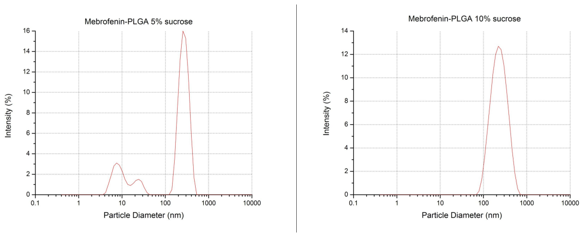

Figure 2.8.: Particle size distribution of Mebrofenin-loaded PLGA nanoparticles

2.3.2.2. 99mTc-labeling of Mebrofenin Loaded PLGA Nanoparticles

In the case of mebrofenin-PLGA, after 60 min labeling reaction at 37 °C, approximately 66 % of 99mTc-activity was associated with the PLGA elution fraction in the PD10 column (Fig. 2.9), which is similar to the result previously obtained for plain PLGA nanoparticles [53].

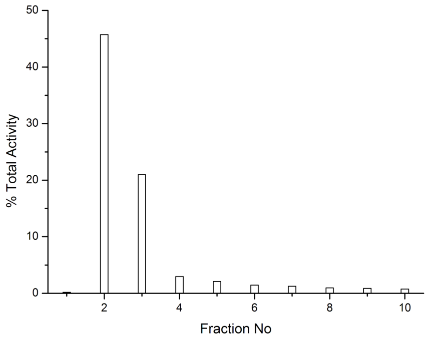

Figure 2.9.: PD10 column elution pattern of 99mTc-Mebrofenin-PLGA using phosphate buffered saline (pH 7.4) as eluant

Studies with reduced amounts of nanoparticle or tin (II) chloride used for the reaction led to decreased labeling yield. By repeated column elution and measurement of activity, the complex in the eluted fraction was found to be stable overnight at room temperature. Given the lower labeling yield, it was decided to perform purification of the labeled product by passing through a PD10 column with phosphate buffered saline as eluant before using for any animal studies.

Mebrofenin-loaded PLGA nanoparticles, did not show improvement in 99mTc-chelating ability as compared to plain PLGA nanoparticles. This suggests that the encapsulated mebrofenin is not available for complex formation. Since free mebrofenin is known to be easily labeled with 99mTc, it may be possible that post-encapsulation, mebrofenin is hermetically enclosed within a hydrophobic PLGA covering, and not accessible to 99mTc-pertechnetate from the aqueous phase, and the bulk of the activity may simply be reacting with tin (II) chloride to give reduced 99mTc colloid that is either overlaid on the surface of PLGA nanoparticles or present as free colloid in the reaction mixture, which are separated during PD10 purification.

2.3.2.3. In Vivo Radioactivity Distribution and Scintigraphic Imaging Studies

The in vivo 99mTc-activity distribution profiles for mebrofenin-PLGA complex (Tab. 2.2) shows some improvement over the previously reported 99mTc-labeled plain PLGA nanoparticles in terms of reduced accumulation in non-specific regions, such as liver and gastrointestinal tract.

Organ	**60 min**		**180 min**	
Liver	0.20±0.02	(0.02±0.00)	0.62±0.23	(0.07±0.03)
Intestine	0.17±0.00	(0.01±0.00)	0.36±0.05	(0.02±0.00)
Stomach	0.03±0.01	(0.01±0.00)	0.04±0.01	(0.01±0.00)
Kidney	0.25±0.02	(0.16±0.04)	0.83±0.12	(0.52±0.07)
Heart	0.05±0.01	(0.06±0.01)	0.04±0.01	(0.05±0.01)
Lungs	0.07±0.03	(0.05±0.02)	0.05±0.00	(0.04±0.00)
Spleen	0.07±0.02	(0.14±0.04)	0.03±0.01	(0.06±0.02)
Blood	1.01±0.17	(0.06±0.01)	1.18±0.5	(0.07±0.03)
Node Uptake				
Popliteal Node	0.39±0.25	(78.00±50.00)	1.35±0.14	(270.00±28.00)
Iliac Node	0.07±0.03	(14.00±6.00)	0.18±0.02	(36.00±4.00)
Site of Injection	89.18±0.4		82.07±2.16	
PE (%)	80.21±5.5		86.89±0.37	

Table 2.2.: In vivo distribution profile for Mebrofenin-PLGA in Wistar rat, data given as %ID per organ (%ID per gram) n=3.

The scintigraphic profile of 99mTc-Mebrofenin-PLGA is seen in Fig. 2.10. At 60 min p.i. the popliteal / sentinel node uptake for mebrofenin-PLGA is lower than that for plain PLGA nanoparticles but at 180 min p.i. it is similar in the extent of SLN uptake with better popliteal extraction value (1.35% SLN uptake with 86.89% PE compared to 1.75% uptake with 65.77% PE for 99mTc-labeled plain PLGA nanoparticles [53]). One may speculate here that the hydrophobicity of mebrofenin and its possible impact on the overall surface charge of the nanoparticles could affect the rate of migration from the site of injection, making it slower in extraction than plain PLGA nanoparticles.

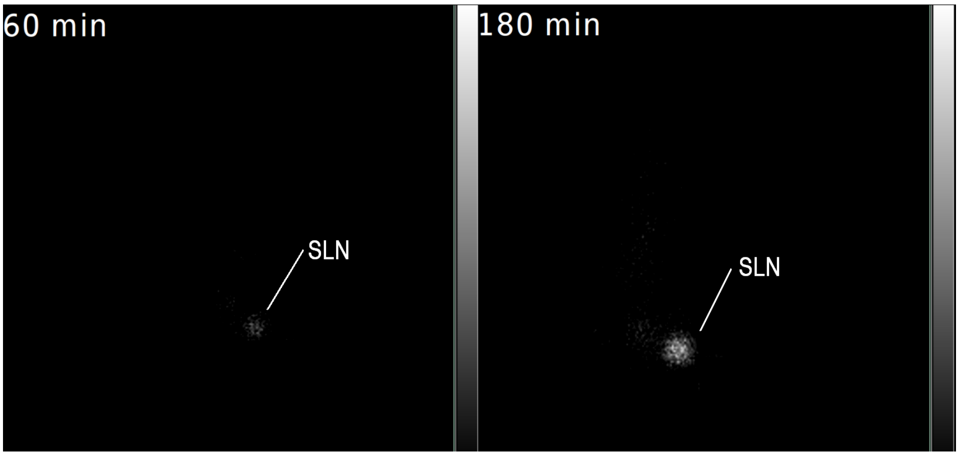

Figure 2.10.: SLN imaging using Mebrofenin-PLGA- in Wistar rat (SOI = site of injection)

It is notable that the in vivo stability of the complex as measured by the decrease in accumulation of 99mTc-activity in non-specific regions is greater than what was observed for 99mTc-labeled plain PLGA nanoparticles, suggesting that mechanisms other than surface adsorption of reduced 99mTc colloid may also be playing a role in this radiolabeling process. However, mebrofenin-loading appears unsuitable as an approach for the preparation of a PLGA-based nanoparticulate SLND tracer on account of its lack of improvement to the 99mTc-labeling yield.

2.3.3. DTPA-Conjugated PLGA Nanoparticles

2.3.3.1. Optimization of Formulation

Fig. 2.11 depicts the size distribution of base PLGA nanoparticles after freeze-drying with different concentrations of sucrose cryoprotectant, and also the size distribution profile of DTPA-conjugated PLGA nanoparticles. With 10% sucrose cryoprotectant, base PLGA nanoparticles show post-lyophilization diameter of 158.7±3.3 nm with a narrow PI of 0.152±0.011. DTPA-conjugated nanoparticles even when freeze-dried in absence of cryoprotectant showed a useful particle diameter (212.0±9.66 nm) and homogenous distribution with a narrow PI (0.21±0.04).

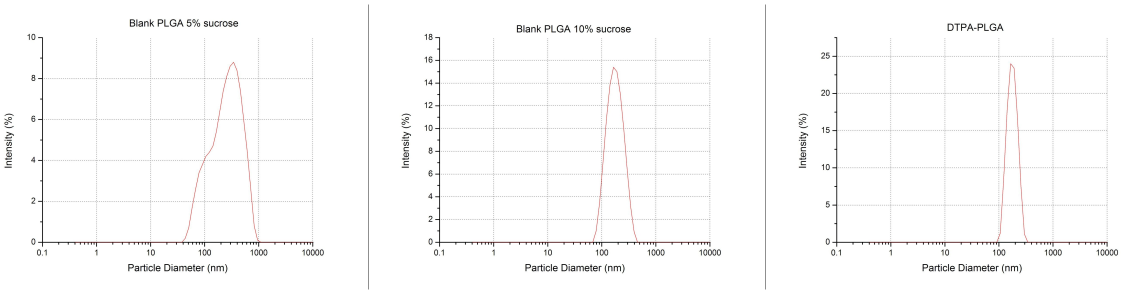

Figure 2.11.: Particle size distribution of plain and DTPA conjugated PLGA nanoparticles

The successful conjugation of the p-NH2-Bz-DTPA ligand on to the terminal carboxylic acid groups on the PLGA nanoparticle surface was confirmed using EDS, zeta-potential and FT-IR techniques. Tab. 2.3 shows the details of EDS analysis of lyophilised DTPA-PLGA nanoparticles confirming the presence of Nitrogen atoms from DTPA. The mean zeta-potential (n=3) of plain PLGA was determined to be -4.61 mV (±0.96) while that of DTPA-PLGA was estimated to be -8.87 mV (± 0.72). IR spectrum of DTPA-PLGA (Fig. 2.12) shows peak at 1637 cm-1, characteristic of the carbonyl group in the amide linkage that would be formed between terminal carboxyl group on the PLGA nanoparticle surface and amino group of p-NH2-Bz-DTPA. The above results reliably confirm the presence of exposed functional groups from DTPA on the surface of PLGA nanoparticles in the conjugate.

Fig. 2.13 shows the results of paper chromatography of the conjugation mixtures in water:acetonitrile (1:1) after labeling with 90Y, which shows a distinct separation between the movement patterns of 90Y-DTPA-PLGA formed in the vari-

EDS Pattern	**Plain PLGA nanoparticles**	**DTPA-PLGA nanoparticles**
Element	**Weight % (Atomic %)**	**Weight % (Atomic %)**
1) Carbon	49.72 (56.85)	60.52 (66.72)
2) Oxygen	50.28 (43.15)	32.29 (26.72)
3) Nitrogen	0.00 (0.00)	6.54 (6.18)

Table 2.3.: Elemental analysis of DTPA-PLGA and plain PLGA nanoparticles to confirm DTPA conjugation with PLGA nanoparticles.

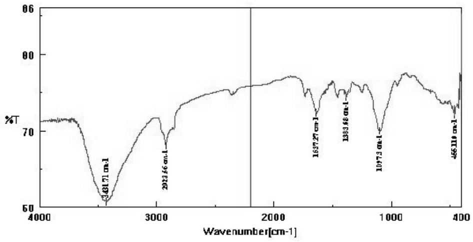

Figure 2.12.: IR spectrum of DTPA conjugated PLGA nanoparticles.

ous DTPA:PLGA conjugation mixtures and 90Y-p-aminobenzyl-DTPA. It is seen here that a ratio of 20:1 of DTPA:PLGA provides a high extent of conjugation – Considering a molecular weight of ~70kD for PLGA and 0.508kD for DTPA, 85% labeling yield corresponds to approximately 17 DTPA residues conjugated per PLGA molecule. Hence DTPA:PLGA in a ratio of 20:1 was chosen for doing further work. Particle size analysis performed after lyophilization of the DTPA conjugated PLGA (Fig. 2.11) indicated a particle size of 212.0±9.66, similar to that obtained for mebrofenin-loaded nanoparticles, and a PI value of 0.21±0.04, reflecting a sufficiently narrow distribution profile.

2.3.3.2. 99mTc-labeling of DTPA-conjugated PLGA Nanoparticles

The PD10 column elution pattern of 99mTc-DTPA-PLGA is shown in Fig. 2.14a, while Fig. 2.14b shows the comparative chromatographic elution patterns of 99mTc-

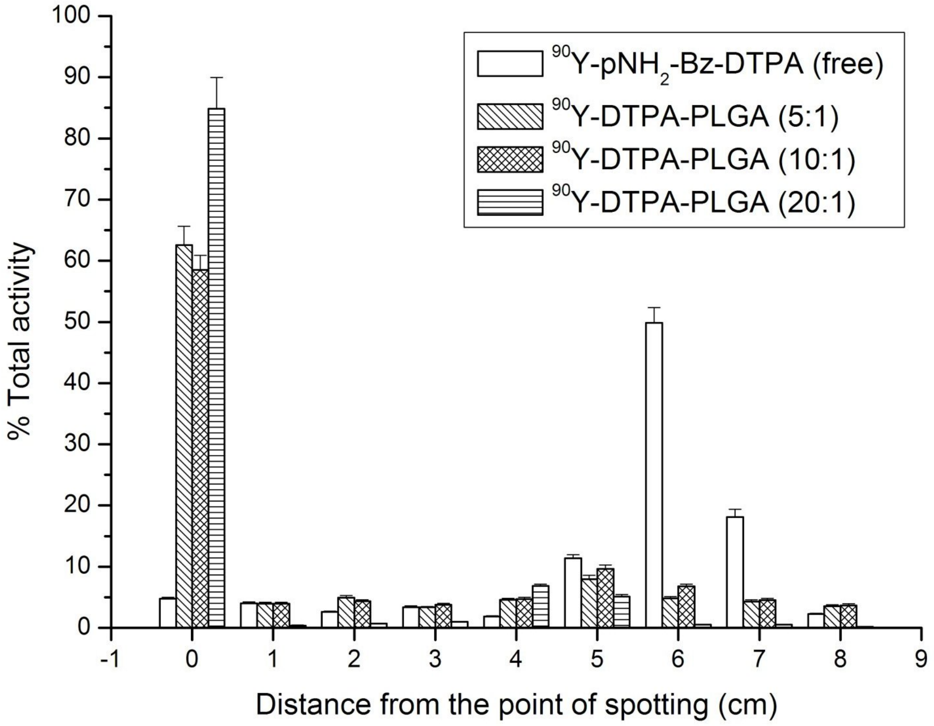

Figure 2.13.: Paper chromatography pattern of 90Y-labeled p-aminobenzyl-DTPA and 90Y-labeled DTPA-PLGA conjugation mixtures with DTPA:PLGA ratios of 5:1, 10:1 and 20:1 in water:acetonitrile (1:1)

DTPA-PLGA and 99mTc-p-aminobenzyl-DTPA after paper chromatography in saline.

As can be deduced from the above figures, >90 % 99mTc-labeling of the nanoparticles was obtained after reaction for 15 min at room temperature using as little as 75 µg of tin (II) chloride for reduction of 99mTc. As with 99mTc-mebrofenin-PLGA, the complex was found to be stable overnight at room temperature. Given the adequacy of the labeling yield, 99mTc-DTPA-PLGA prepared was used for animal studies without further purification.

In comparison to both plain PLGA and mebrofenin-loaded PLGA nanoparticles, DTPA conjugated PLGA nanoparticles exhibited significantly improved 99mTc-labeling, showing higher product yield even with a lower concentration of reducing

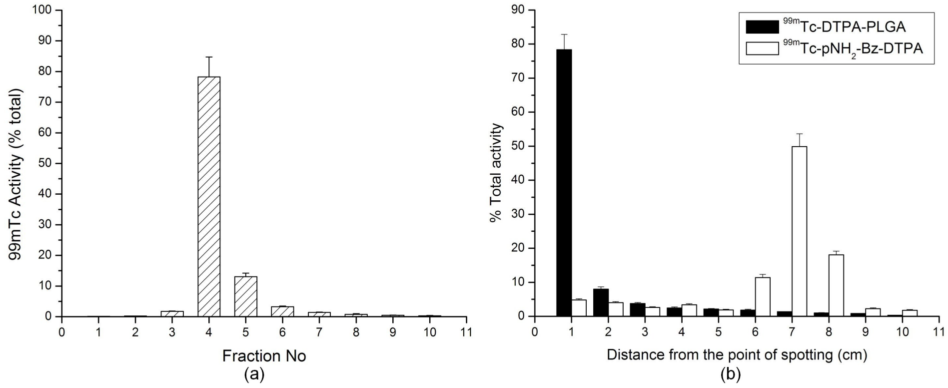

Figure 2.14.: a) PD10 column elution pattern of 99mTc-DTPA-PLGA using phosphate buffered saline (pH 7.4) as eluant b) Paper chromatography pattern of 99mTc- DTPA-PLGA and 99mTc-p-aminobenzyl-DTPA in saline.

agent and more moderate labeling conditions. This indicates that DTPA groups on the surface of PLGA play a supporting role in formation of 99mTc-labeled PLGA nanoparticles. The product was found to be stable overnight and the good radiochemical yield precluded the need for any additional purification, which is an advantage in the clinical scenario.

2.3.3.3. In Vivo Radioactivity Distribution and Scintigraphic Imaging Studies

Tab. 2.4 shows the in vivo distribution pattern for 99mTc-DTPA-PLGA nanoparticles in Wistar rats after footpad injection. At both 60 min and 180 min p.i. the SLN uptake is significantly increased, showing more than twice the value observed for the other tested PLGA variants. Popliteal extraction increases from 67.62 % at 60 min p.i. to 82.89 % at 180 min p.i., mainly due to greater uptake from the site of injection into the sentinel node in this interim.

Fig. 2.15 shows the scintigraphic images of 99mTc-DTPA-PLGA at different timepoints. The in vivo efficacy of 99mTc-DTPA-PLGA is thus seen to be better than

Organ	**60 min**		**180 min**	
Liver	0.40±0.04	(0.05±0.00)	0.53±0.07	(0.06±0.01)
Intestine	0.39±0.04	(0.02±0.00)	0.55±0.06	(0.03±0.00)
Stomach	0.05±0.01	(0.01±0.00)	0.11±0.04	(0.03±0.01)
Kidney	0.23±0.07	(0.14±0.04)	0.48±0.12	(0.30±0.07)
Heart	0.02±0.02	(0.02±0.02)	0.05±0.05	(0.06±0.06)
Lungs	0.03±0.01	(0.02±0.01)	0.05±0.03	(0.04±0.02)
Spleen	0.03±0.03	(0.06±0.06)	0.02±0.02	(0.04±0.04)
Blood	0.34±0.34	(0.02±0.02)	1.85±0.67	(0.11±0.04)
Node Uptake				
Popliteal Node	2.56±0.02	(512.00±4.00)	3.47±0.11	(694.00±22.00)
Iliac Node	0.83±0.06	(166.00±12.00)	0.59±0.13	(118.00±26.00)
Site of Injection	71.94±0.06		69.60±0.70	
PE (%)	67.62±2.45		82.89±3.22	

Table 2.4.: In vivo distribution profile for 99mTc-DTPA-PLGA, data given as %ID per organ (%ID per gram), n=3.

the other PLGA variants tested in our studies, which may in part be related to the nanoparticle forming a stable 99mTc-complex with DTPA groups as opposed to surface adsorption of reduced 99mTc colloid. Also, particle sizing is determined by dynamic light scattering method, which essentially provides the hydrodynamic diameter of the nanoparticles. Given that mebrofenin is encapsulated within the PLGA, while DTPA groups are tagged on to the nanoparticle surface, there may be differences in actual nanoparticle size between the various types of preparations that may account for the difference in movement from the site of injection and uptake in the sentinel node. But with 3.47% SLN uptake and 82.89% PE at 180 min, 99mTc- DTPA-PLGA does not perform better in terms of nodal uptake and popliteal extraction than the results we had previously obtained with 99mTc-labeled commercially available sulfur colloid kit Nanocis, which showed ~4.88% SLN uptake with ~81% PE at 180 min p.i. [53] However, it shows greater clearance from the site of injection (~30% for DTPA-PLGA vs ~19% for Nanocis), which could give improvement in sensitivity of detection of the SLN due to reduced background from the site of injection.

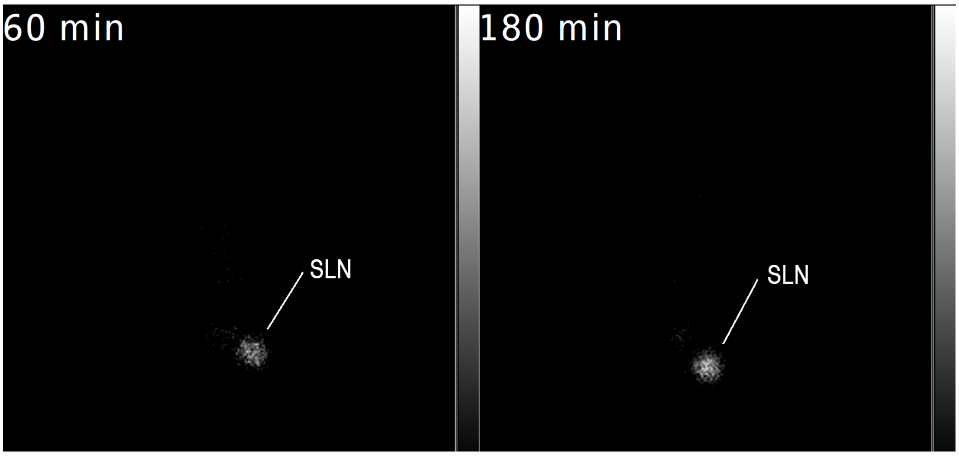

Figure 2.15.: In vivo scintigraphic image profile for 99mTc- DTPA-PLGA in Wistar rat (SOI = site of injection)

2.3.3.4. Toxicity Studies

Since DTPA-PLGA showed the most promising results with respects to 99mTc-labeling and in vivo distribution characteristics, it was taken for toxicity studies to assess its safety at pharmacologic concentrations. The effect of DTPA-PLGA on hematological parameters like RBC-WBC-Platelet count and hemoglobin concentration is depicted in Fig. 2.16. Fig. 2.17 gives the impact on differential WBC concentration. The results of possible effect on relevant serum biochemical parameters like SGOT-SGPT activity and albumin-bilirubin concentration are presented in Fig. 2.18. Comparative histology of relevant tissues for controls and DTPA-PLGA acute toxicity profile animals is shown in Fig. 2.19. These results do not indicate any major deviation in the mean values of the tested parameters from values obtained for the controls, suggesting the absence of any significant toxicity from the preparation in the model studied.

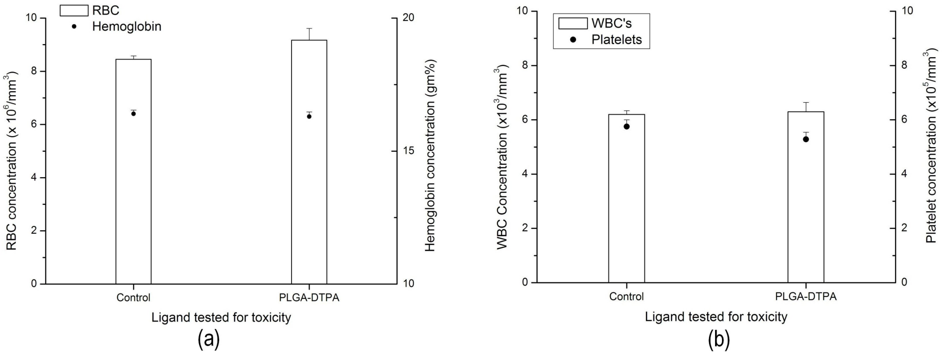

Figure 2.16.: Acute toxicity profile of DTPA-PLGA a) RBC count and hemoglobin concentration b) WBC and Platelet count

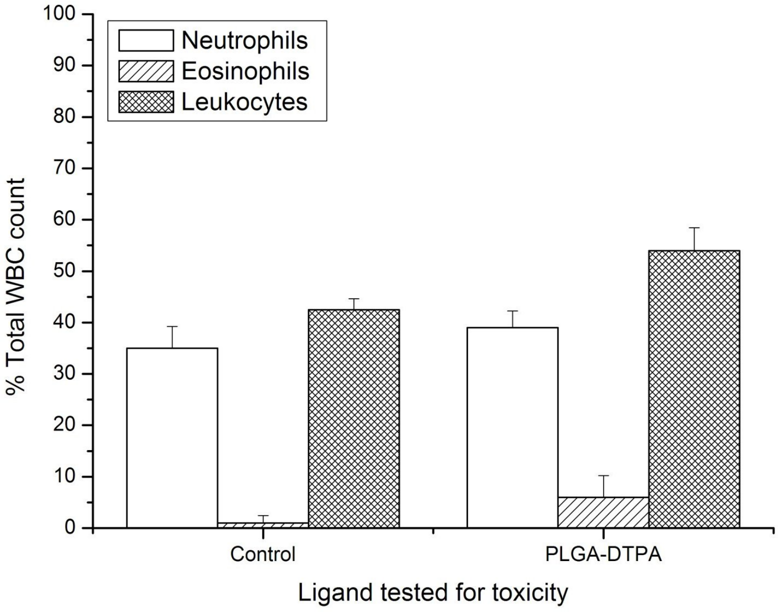

Figure 2.17.: Acute toxicity profile of DTPA-PLGA - differential WBC profile

2.4. SUMMARY

Three PLGA derivatives - plain PLGA, mebrofenin-PLGA and DTPA-PLGA were tested as SLN detection tracers. Of these, DTPA-PLGA appears to have the most suitable physico-chemical and biological properties. It shows efficient 99mTc-labeling under mild reaction conditions and effective in vivo localization and phar-

Figure 2.18.: Acute toxicity profile of DTPA-PLGA - serum levels of a) SGOT-SGPT activity b) Albumin and total bilirubin concentration

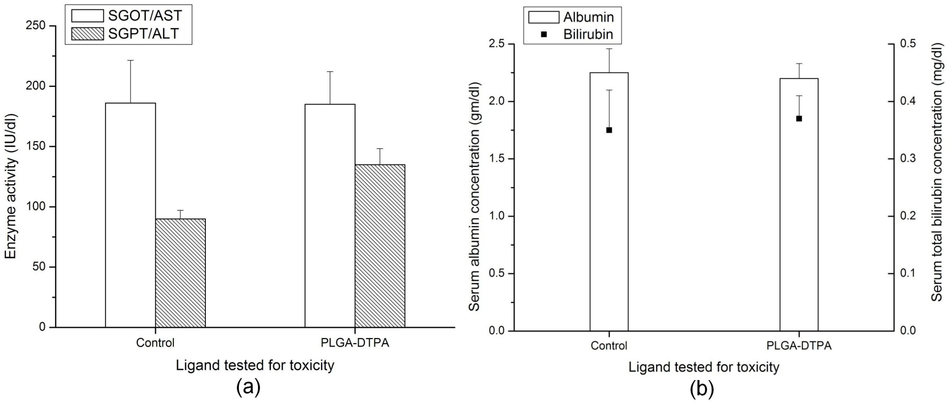

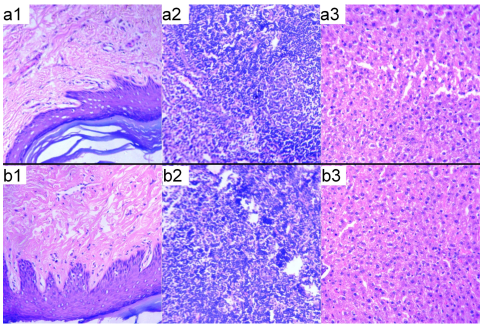

Figure 2.19.: Acute toxicity profile of DTPA-PLGA - comparative histology a) Control set (1 - SLN, 2 - footpad, 3 - Liver) and b) DTPA-PLGA exposed set (1 - SLN, 2 - footpad, 3 - Liver)

macokinetics, and toxicity studies indicate no significant hazard from administration of the preparation at clinically relevant concentrations. However, although ease of labeling over sulfur colloid and absence of potential hazard from handling of biological material (as in HSA nanocolloid) are advantages in its favor, the biological efficacy of the current preparation is not significantly improved over clinically employed preparations, hence it is required to work on further modification of the DTPA-PLGA nanoparticle to achieve sufficient advantage for acceptance as an alternative in the clinical setup.

3. MANNOSE-BASED SLN DETECTION TRACERS

3.1. BACKGROUND

3.1.1. Need For Receptor Targeting SLN Tracers

As mentioned in the outline of ideal characteristics for an SLN detection tracer (sec. 2.1.3), the desired in vivo properties for an ideal SLN detection tracer include rapid clearance from the site of injection, selective uptake in the SLN and minimal spread to other nodes/non-target regions. The conventional 99mTc-labeled nanoparticle agents developed for use towards this application have particle size as the single most important differential factor dictating the kinetics and selectivity of their uptake in SLN. As particle size is inversely proportional to rate of transport of the tracer from the site of injection to the lymphatic system and its further spread beyond the sentinel node, the currently employed agents of this class have a significant degree of retention at the site of injection and slower kinetics of transport thereon to the lymphatic network.

To alleviate this reliance on particle size and the compromise involved therein, mannose receptors expressed by macrophages located in the lymph node have been identified as a target for developing mannose-bearing ligands that will be receptor-specific for SLN detection [54, 55, 56]. It is envisaged that specific affinity of these ligands to the mannose receptor will lead to high uptake of a 99mTc-labeled mannose bearing tracer by the SLN macrophages, allowing for the design of ligands with significantly smaller particle size. Such ligands may be expected to exhibit a high rate of clearance from the injection site thereby resulting in lower radiation background, without an adverse impact on the selectivity of uptake in the sentinel lymph node. The first ligand of this type is Lymphoseek, a [99mTc]DTPA mannosyl dextran complex that has been patented and is in clinical trials for SLN mapping in different cancer types [54]. There are also reports on the use of 99mTc-labeled mannosyl human serum albumin [57] for the same purpose, and several research groups across the world are involved in the development of newer mannose-based SLN tracers that will take us nearer towards the characteristics of the ideal SLN radiotracer .

3.1.2. Rationale For The Planned Work

Taking the above-described goal into consideration, the development and biological evaluation of some novel mannose-based receptor-targeting radiotracers was undertaken. The aim was to develop products based on mannose-bearing ligands with well-understood radiolabeling chemistry using a known intermediate such as the 99mTc-tricarbonyl synthon $[99mTc(CO)_3(H_2O)_3]^+$. Two classes of ligands, synthesized in a collaborating laboratory as described briefly below, were selected for performing the biological evaluation:

1. **Dextran-Cysteine-Mannose Derivative (DCM20)** - DCM20 was synthesized by the reaction of dextran (mw 11800) with allyl bromide to give allyl dextran, followed by formation of dextran-S-cysteine which is subsequently mannosylated in part to give the final product. non-mannosylated cysteine residues serve as the bridge between the dextran backbone and the 99mTc synthon. The molecular weight of the final ligand is approximately 22kD [60].

2. **Dextran-Pyrazolyl-Mannose Derivatives (DAPM4 And DAPM8)** - Synthesis of dextran-pyrazolyl mannose derivatives was a multi-step sequential reaction wherein dextran was reacted with allyl bromide to form to allyl dextran, which was then converted to amino dextran derivative. Amino dextran was reacted with different ratios of pyrazolyl diamine chelator and subsequently mannosylated. In the final ligand pyrazolyl group serves as the bridge between dextran and the 99mtc synthon. Depending on the number of pyrazolyl residues per dextran molecule, two derivatives were obtained. One had 4 pyrazolyl residues per dextran (DAPM4) and the other had 8 pyrazolyl residues per dextran (DAPM8) [61].

These ligands were labeled with 99mTc and the labeling properies were assessed. The labeled complexes were then tested for their affinity to the mannose receptor using in vitro cell uptake assays. In vitro receptor binding studies were performed with RAW 264.7 macrophage precursor cells which have been reported in the literature to bear mannose receptors [58]. Their in vivo localization properties were evaluated using the wistar rat model as described in sec. 2.2.7.1.

3.2. MATERIALS AND METHODOLOGIES

3.2.1. Materials

DCM20 was synthesized by the group of Dr. Ioannis Pirmettis at the Institute Of Radioisotopes And Radiodiagnostic Products, NCSR "Demokritos", Athens, Greece. DAPM4 and DAPM8 derivatives were synthesized by the group of Dr. Isabel Santos at the Unidade De Ciências Químicas E Radiofarmacêuticas, ITN, Sacavém, Portugal. They were provided for biological evaluation as part of a coordinated research project (CRP) on The "Development Of 99mTc Radiopharmaceuticals For Sentinel Node Detection And Cancer Diagnosis" convened under the aegis of the International Atomic Energy Agency (IAEA). Mallinckrodt-Covidien, Holland provided isolink kit vials as a gift, for the preparation of the 99mTc-tricarbonyl synthon. 99mTc-pertechnetate for radiolabeling was obtained from an in-house 99Mo/99mTc generator by elution with isotonic saline. HPLC grade solvents were degassed before use for all HPLC analyses. Dulbecco's Modified Eagle's Medium (DMEM) and Dulbecco's Phosphate Buffered Saline (DPBS) used for cell culture and in vitro experiments were procured from Sigma, USA. Fetal Bovine Serum (FBS) used as a growth supplement in cell culture was procured from Hi-Media, India. RAW 264.7 macrophage precursor cells were procured from the National Center For Cell Science, Pune, India.

HPLC analyses were performed on a JASCO HPLC system (JASCO, Japan) equipped with a C-18 reversed phase HiQ Sil (5 Mm, 4×250 Mm) column. The system was coupled to a PU 1575 UV/visible detector (JASCO, Japan) and a NaI (Tl) radioactivity detector (Raytest, Germany). Sodium iodide (Thallium) counters from Electronics Corporation Of India Limited (ECIL), India were used for radioactivity measurement studies. Scintigraphic imaging studies were carried out with the Millennium MPS Gamma Camera System (Wipro-GE Medical Systems, India).

3.2.2. Preparation Of 99mTc-tricarbonyl Synthon and 99mTc-labeled Dextran-mannose Derivatives

The principle of the formation of tricarbonyl synthon is as follows: when carbon monoxide is flushed in an alkaline medium in the presence of sodium carbonate and sodium borohydride, 99mTc-pertechnetate can be reduced at elevated temperatures by forming a transient cationic complex, which is the tricarbonyl synthon (Fig. 3.1A). Suitable ligands bearing an imidazol ring at the terminal can react with this transient cationic complex to form a highly stable cationic 99mTc-complex, resistant under general conditions to oxidation/reduction reactions (Fig. 3.1B) [59].

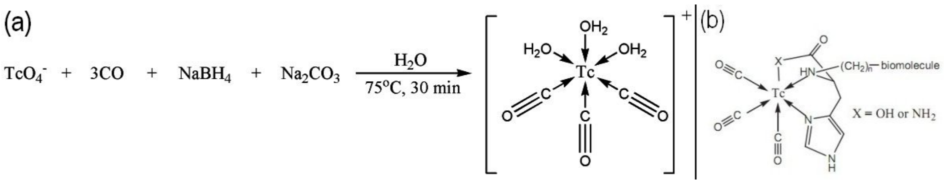

Figure 3.1.: a) Formation of 99mTc-tricarbonyl synthon b) 99mTc-labeling of suitable ligand through tricarbonyl linkage

Traditionally, carbonyl-based labeling required the reaction mixture to be flushed with carbon monoxide, which can be hazardous. However, in this case, the IsoLink® kit vial was used for preparation of the 99mTc-tricarbonyl synthon. this kit, available in freeze-dried form, contains a mixture of sodium tartrate, sodium tetraborate, sodium carbonate and sodium boranocarbonate. The synthon was prepared by adding 1-2 ml of 99mTc-pertechnetate (~370 MBq) to the contents of the kit vial and heating the contents of the vial at 100 °C for 20 min in a water bath. The yield of synthon formation was assessed by HPLC. The pH of the synthon was adjusted to 7.4 by addition of 0.1N HCl as required. In the case of DCM20, 0.5 ml of the 99mTc-tricarbonyl synthon [~37-92.5 MBq] was added to 50 µg of DCM20 ligand and reacted at 70 °C in a water bath for 30 min [62]. For the dextran-pyrazolyl-mannose derivatives, 1 ml [37-370 MBq] of the 99mTc-tricarbonyl synthon was added to 200 µg DAPM4 or DAPM8 and heated at 100 °C in a water bath for 30 min. Yield of the labeled ligand was estimated by HPLC.

The yields of 99mTc-labeling in formation of the tricarbonyl synthon as well as its conjugation of the various dextran-mannose ligands was assessed by reversed phase HPLC. HPLC was performed using water (Solvent A) And methanol (Solvent B) with 0.1 % trifluoroacetic acid in a gradient mode of elution. The gradient was set up as follows: 0-1 min 0 % B, 1-9 min 0-70 % B, 9-19 min 70 % B, 19-25 min 70-95 % B, 25-35 min 95-0 % B. The flow rate was maintained steady at 1 ml/min. The absence of any reduced 99mTc colloid in the 99mTc-tricarbonyl used for preparing the labeled conjugates was confirmed by paper chromatography (Whatman No. 1) using 5 % of 6 N HCl in methanol as the mobile phase. In this system, reduced 99mTc colloid remains at the origin (Rf=0) while free 99mTc-pertechnetate and 99mTc-tricarbonyl conjugate migrate towards the solvent front.

It was not attempted to separate unlabeled ligand from [99mTc(CO)$_3$]-labeled ligand. It is assumed that the labeled ligand functions similar to the free ligand in terms of in vitro receptor binding and in vivo pharmacokinetic behavior. All reported concentrations of the tracer refer to the total ligand concentration in the labeling reaction mixture.

3.2.3. In Vitro Biological Evaluation Studies

The mouse macrophage precursor cell type RAW 264.7 was employed as a mannose receptor-bearer to study the in vitro uptake of dextran-mannose derivatives. The cells were cultured in DMEM at 37 °C and 5 % CO2 atmosphere. 10 % FBS was added to the culture medium as a growth supplement. For splitting or harvesting, the cells were removed without trypsinization, by flushing of media and use of a cell scraper.

For the experiment, RAW 264.7 cells were plated out onto 24-well tissue culture plates at 10^5 cells per well in 400 µl DMEM containing 10 % fbs and incubated for 2 hours at 37 °C and 5 % CO2 atmosphere to allow for adherence to the well surface. At the end of this period, the wells were microscopically observed to confirm uniform adherence. 50 µl of varying concentrations of dextran-mannose ligands were added after 99mTc-labeling to the wells. For each concentration of the radioactive preparation, a set of ‘cold’ wells was also prepared to which, in addition to the tracer, 50 µl of 100-fold excess concentration of unlabeled D-mannose in DPBS was added in order to estimate the non-specific cell uptake of the mannosylated ligands in the presence of competitive inhibition from D-mannose. The total reaction volume in all the wells was maintained at 500 µl using DPBS. The reaction setup was incubated at 4 °C for 3 hours, with intermittent mixing at 30 min intervals. All reaction combinations were assayed in triplicate.

At the end of the incubation period, the supernatant in the wells was carefully aspirated and the adherent cell monolayers were washed twice with 1 ml ice-cold DPBS. Following this, 1 ml of 8 N sodium hydroxide was added to each well with adequate flushing for dissolution of the cell layer. The resulting suspension was taken into counting tubes and 99mTc radioactivity associated with the cells was measured on a well-type NaI (Tl) Counter. Receptor-mediated specific uptake of the mannosylated ligand in RAW 264.7 was quantified by subtracting the value of tracer uptake observed in the presence of 100-fold excess of D-mannose from the total uptake value (Without D-mannose). The dissociation constant of receptor binding (Kd) was obtained by preparing a Scatchard analysis, plotting [Bound Ligand Concentration / Free Ligand Concentration] v/s [Bound Ligand Concentration] ([B/F] v/s [B]). Calculation of [B/F] assumes that the bound ligand fraction is only a small component of total ligand concentration.

3.2.4. In Vivo Biological Evaluation Studies

In vivo biological evaluation studies were performed in wistar rat model using the footpad injection technique as described earlier in sec. 2.2.7.1 [61]. Both radioactivity distribution studies and scintigraphic imaging studies were carried out to assess the in vivo distribution pattern and biological efficacy of each of the 99mTc-labeled dextran-mannose ligands.

As these were designed to be receptor specific ligands, it was deemed important to assess the impact of varying ligand concentrations on the in vivo distribution pattern. Hence for each ligand, two different concentrations were taken for in vivo administration for assessment of their biological efficacy. In all cases the injection volume was maintained at 50 µl. Each of the mannosylated ligands was tested at 10 µg/animal and 2.5 µg/animal. This corresponded to ~ 0.5 nmol and 0.125 nmol per animal DCM20, 0.53 nmol and 0.13 nmol per animal for DAPM4, and 0.49 nmol and 0.12 nmol of ligand per animal for DAPM8. As with previously described in vivo studies, 99mTc-activity retained in each organ/tissue was expressed as a percentage of the total injected dose (%ID) and popliteal extraction (PE) was calculated using the formula given below [54]:

PE = $(\%ID_{popliteal} - \%ID_{iliac})/\%ID_{popliteal}$

3.2.5. Toxicity Studies

The ligands showing favorable 99mTc-labeling and in vivo distribution characteristics using the optimized protocols were taken up for performing toxicity studies. These studies, which include hematological, biochemical and histological assessment, were carried out using protocols identical to the one described for PLGA-DTPA nanoparticles Appendix A.

3.3. RESULTS

3.3.1. 99mTc-tricarbonyl DCM20 Conjugate

3.3.1.1. Formation Of 99mTc-tricarbonyl Synthon

The formation of 99mTc-tricarbonyl synthon was confirmed by HPLC. In the reported HPLC system, 99mTc-tricarbonyl synthon had a retention time of 5.3 min (Fig. 3.2A). The percentage of reduced 99mTc colloid in the 99mTc-tricarbonyl synthon was determined to be <1 % as confirmed by paper chromatography with 5 % of 6 N HCl in methanol as the mobile phase (Fig. 3.2B). The absence of any reduced 99mTc-colloid in the formation of the tricarbonyl synthon was corroborated by the quantitative elution of 99mTc-activity during HPLC of the synthon and the conjugates with the various dextran-mannose ligands.

3.3.1.2. 99mTc-labeling Of DCM20 Ligand

From the elution pattern of HPLC, [99mTc$(CO)_3$]-labeled DCM20 was observed to have a retention time of 13.6 min (Fig. 3.3). Based on HPLC, radiolabeling yield is determined to be greater than 90%, which is appreciably high. Hence further

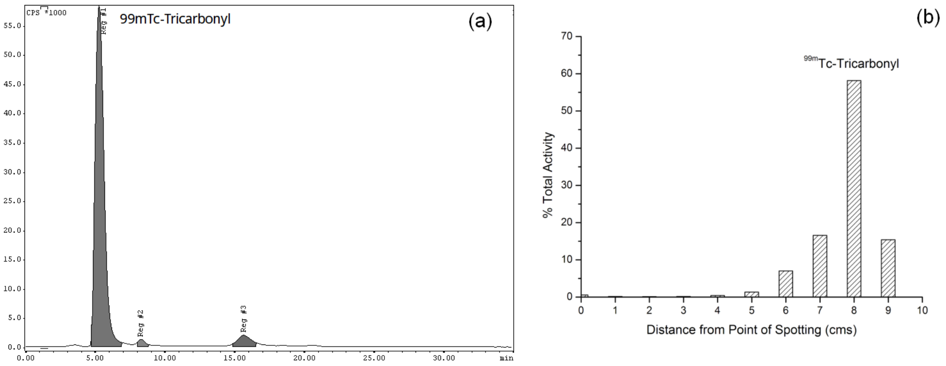

Figure 3.2.: Characterization of 99mTc- tricarbonyl synthon by (a) Reversed phase HPLC (b) Paper chromatography in 5% of 6N HCl in methanol

purification was deemed unnecessary before using the radiolabeled complex for in vitro and in vivo biological evaluation studies.

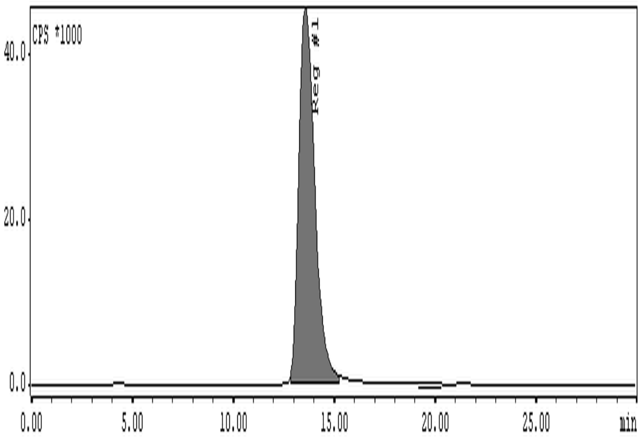

Figure 3.3.: HPLC pattern of 99mTc-tricarbonyl DCM20 conjugate

3.3.1.3. In Vitro Biological Evaluation

Fig. 3.4 shows the specific binding curve for the DCM20 ligand. Under the conditions of the reaction, DCM20 showed specific concentration-dependent uptake in the mannose receptor-bearing RAW 264.7 cell line. Fig. 3.5 depicts the Scatchard plot ([B/F] V/S [B]) for the same data. Using the Scatchard plot, binding affinity was quantified in terms of the dissociation constant (Kd) as 19.41nM.

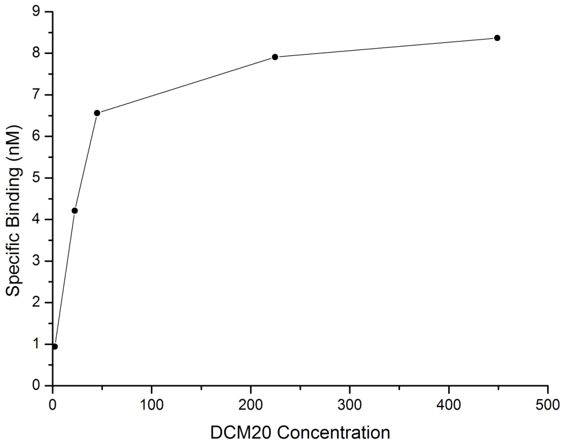

Figure 3.4.: Specific binding curve for DCM20 ligand in RAW 264.7 mannose receptor bearing cells (10^5 cells/0.5 ml)

3.3.1.4. In Vivo Biological Evaluation

DCM20 was administered in vivo at 10 µg/animal and 2.5 µg/animal total ligand concentration, and studies were performed for each concentration. The results of quantitative in vivo biodistribution studies are given in Tab. 3.1.

In the first set of experiments DCM20 ligand was administered at 10 µg / animal in 50 µl volume. Here, at 60 min, ~7.5 % of injected activity was localized in the sentinel node. However, there was also a significant accumulation of activity in the secondary node, which resulted in a low PE value of ~53 %. At 180 min, the PE increased to ~74 %, mainly due to washout of DCM20 from the secondary node. An appreciable amount of activity was also observed in the liver. It may be hypothesized that the mannose receptors of the SLN macrophages are saturated by the concentration of mannose-bearing ligand used, thereby causing the spread

Organ	**DCM20 10.0 µg/animal**				**DCM20 2.5 µg/animal**			
	60 min		**180 min**		**60 min**		**180 min**	
Liver	9.56±2.27	(1.11±0.26)	8.59±2.10	(0.99±0.24)	0.97±0.05	(0.11± 0.01)	1.16±0.12	(0.13±0.01)
Intestine	1.29±0.30	(0.08±0.02)	1.28±0.43	(0.08±0.03)	0.35±0.05	(0.02±0.00)	0.47±0.05	(0.03±0.00)
Stomach	0.47±0.20	(0.12±0.05)	0.22±0.08	(0.06±0.02)	0.21±0.03	(0.05±0.01)	0.44±0.11	(0.11±0.03)
Kidney	1.48±0.41	(0.92±0.25)	1.21±0.38	(0.75±0.24)	0.25±0.06	(0.16±0.04)	0.29±0.04	(0.18±0.02)
Heart	0.06±0.02	(0.07±0.02)	0.05±0.03	(0.06±0.04)	0.01±0.01	(0.01±0.01)	0.06±0.04	(0.07±0.05)
Lungs	0.08±0.03	(0.06±0.02)	0.08±0.02	(0.06±0.01)	0.02±0.01	(0.01±0.01)	0.04±0.03	(0.03±0.02)
Spleen	0.22±0.11	(0.44±0.22)	0.20±0.11	(0.40±0.22)	0.03±0.00	(0.06±0.00)	0.07±0.04	(0.14±0.08)
Blood	6.55±1.18	(0.39±0.07)	3.86±1.18	(0.23±0.07)	10.75±2.18	(0.64±0.13)	12.26±8.06	(0.73±0.48)
Node Uptake								
Popliteal Node	7.56±0.68	(1512.00±136.00)	6.67±3.13	(1334.00±626.00)	4.4±0.01	(880.00±2.00)	3.35±0.72	(670.00±144.00)
Iliac Node	3.42±0.08	(684.00±16.00)	1.91±1.10	(382.00±220.00)	0.02±0.01	(4.00±2.00)	0.05±0.08	(10.00±16.00)
Site of Injection	48.22±6.86		54.11±10.28		48.51±5.41		43.53±2.49	
PE (%)	53.47±7.10		73.80±6.90		99.64±0.21		98.02±3.06	

Table 3.1.: In vivo distribution profile for 99mTc-DCM20, data given as %ID per organ (%ID per gram), n=3.

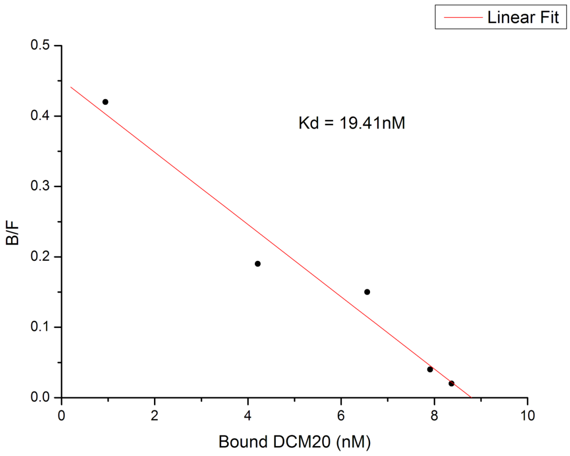

Figure 3.5.: Scatchard plot to calculate binding affinity of DCM20 ligand for RAW 264.7 mannose receptor bearing cells (10^5 cells/0.5 ml)

of unbound DCM20 to further nodes in the lymphatic system and subsequently to the blood circulatory system, leading to accumulation of activity in the liver. These instances of non-target accumulation indicated that DCM20 administered at this concentration is not entirely suitable toward use as a tracer for SLND at least in the tested animal model. Larger animals with greater mass of lymph node may show a better distribution profile.

In the second set of experiments, biodistribution studies were carried out delivering 2.5 µg of DCM20 tracer per animal in 50 µl. This made a significant difference to the in vivo distribution pattern as shown in Tab. 3.1. As early as 15 min p.i., ~4.5 % of the injected activity accumulated in the sentinel node. This is lesser than %ID value for sentinel node accumulation at the higher concentration, but appears to remain largely constant, with a gradual fall at 180 min. The importance of using a lesser amount of tracer was seen from the negligible activity accumulation in the secondary node at all tested time points up to 180 min. As a result, the PE value remained very high throughout the period of experiment, showing high selectivity of uptake in the sentinel node. In addition, there was rapid clearance of activity from the site of injection (footpad). The activity at the site of injection reduced from ~60 % at 15 min to ~43.5 % at 180 min. This would suggest a reduced radiation background and improved sensitivity of detection in actual clinical practice. There was also no appreciable accumulation of activity in the blood, liver or any non-target regions. These are highly desirable properties for a proposed tracer in sentinel lymph node detection in the clinic.

The scintigraphic imaging studies are depicted in Fig. 3.6 and they reflect the results of the biodistribution studies. A comparison of the images obtained for the different concentrations (10 µg ligand/animal and 2.5 µg ligand/animal) of DCM20 administered for the various time points shows a clear improvement with the use of lower concentration (2.5 µg ligand/animal), as the sentinel node is clearly demarcated throughout the period of study without appreciable counts in any other node or non-target region.

3.3.1.5. Toxicity Studies

As can be seen from the results of the hematological studies (Fig. 3.7 and Fig. 3.8), liver function biochemistry studies (Fig. 3.9) and histological examination (Fig. 3.10), animals exposed to relevant concentration of DCM20 ligand for single-dose acute toxicity assessment did not show any hazardous deviation in these parameters from control animals.

3.3.2. 99mTc-tricarbonyl DAPM4 and DAPM8 Conjugates

3.3.2.1. 99mTc-labeling of DAPM4 and DAPM8 Ligands

The yield of formation of the 99mTc-tricarbonyl synthon was estimated using HPLC and paper chromatography and the results were similar to those obtained in sec. 3.3.1.1.

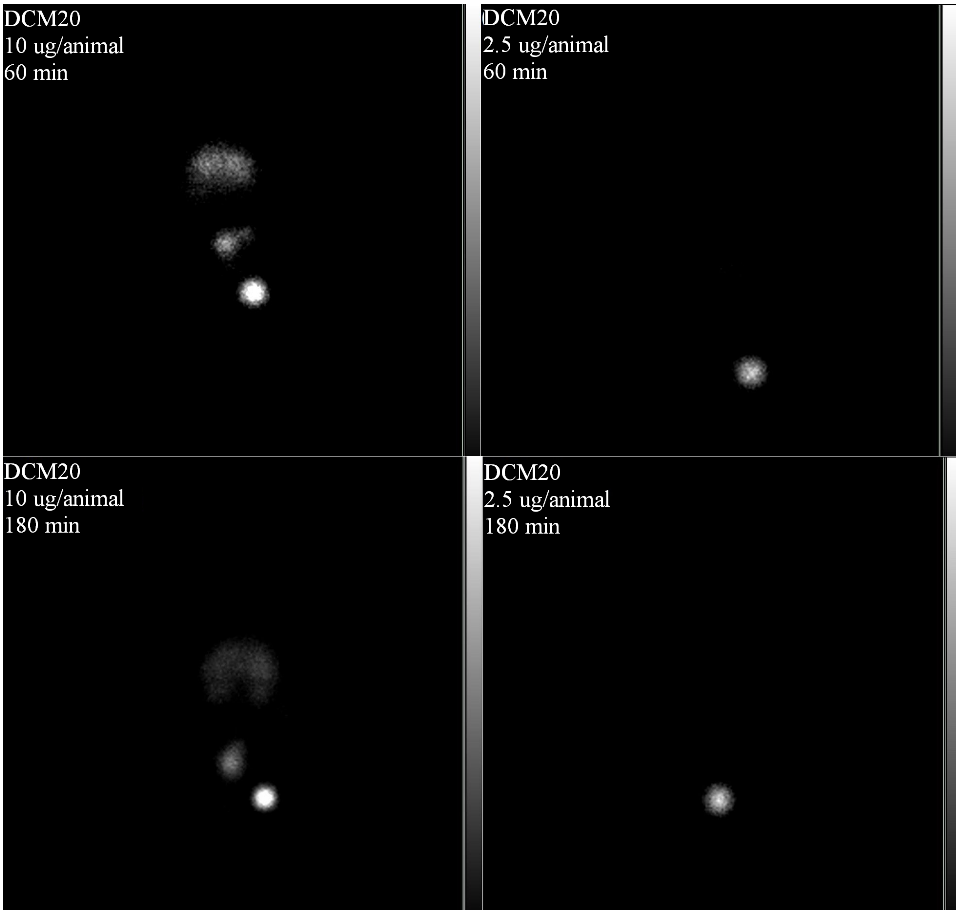

Figure 3.6.: Scintigraphic images showing comparison of in vivo distribution of different concentrations of DCM20 in Wistar rat model at corresponding time-points.

At 200 µg ligand content, both DAPM4 and DAPM8 ligands complexed 99mTc-tricarbonyl synthon in >90 % yields as confirmed by HPLC. Fig. 3.11a shows the HPLC pattern of 99mTc-tricarbonyl DAPM4 with a retention time of 15.3 min, while Fig. 3.11b is the HPLC pattern of 99mTc-tricarbonyl DAPM8 with a retention time of 15.5 min in the optimized HPLC solvent elution system. As the 99mTc-labeling yield was greater than 90 %, further purification of the radiotracers was not considered essential, hence not carried out.

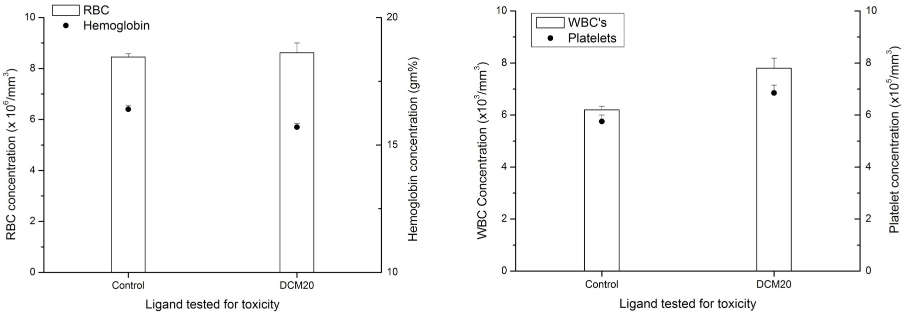

(a) (b)

Figure 3.7.: Acute toxicity profile of DCM20 a) RBC count and hemoglobin concentration b) WBC and Platelet count

3.3.2.2. In Vitro Biological Evaluation

Under the conditions of the study, a concentration dependent in vitro cell uptake of DAPM4 and DAMP8 ligands was observed in RAW 264.7. The results of these studies are summarized in Fig. 3.12, which represents the specific binding of the respective ligands with mannose receptors at 4 °C, after subtraction of non-specific uptake value from 'cold' wells having 100-fold excess D-mannose. Non-specific binding decreased with increasing ligand concentration and varied from 14.8 % to 9.6 % for DAPM4, and 15.2 % to 9.9 % for DAPM8.

Using the data for specific uptake, Scatchard plots were constructed (Fig. 3.13). From the binding data, the affinity of DAPM4 was calculated to be 116.5 nM, while that of DAPM8 was estimated as 111.27 nM

The in vitro binding affinities of the dextran-pyrazolyl-mannose ligands to RAW 264.7 macrophage precursor cells under the conditions of text appear to be considerably lower than that observed for DCM20 in our study. But as will be seen from the results of the studies in animal model, it did not in this case lead to a

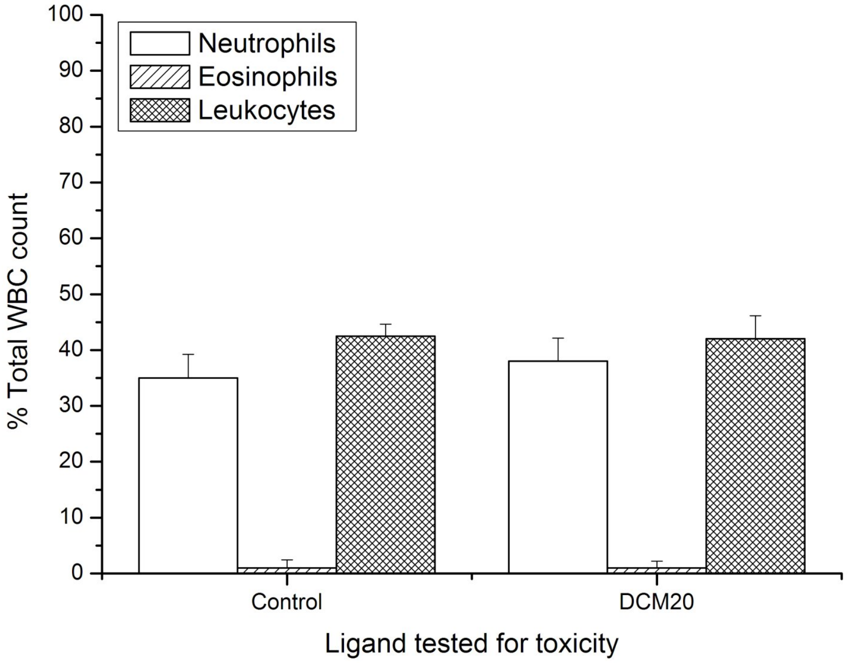

Figure 3.8.: Acute toxicity profile of DCM20 - differential WBC profile

proportionately decreased efficiency of SLN uptake in the animal model studies.

3.3.2.3. In Vivo Biological Evaluation

The in vitro binding affinity for pyrazolyl ligands in the study reported is admittedly low, especially in the higher concentration range, but as some promising data had been obtained in the preliminary animal studies [61], those studies were expanded upon, using different ligand concentrations to assess their effect on the sentinel node uptake and retention pattern.

The quantitative in vivo distribution pattern of DAPM4 at various time points is documented in Tab. 3.2. Fig. 3.14 shows the scintigraphic imaging pattern. For

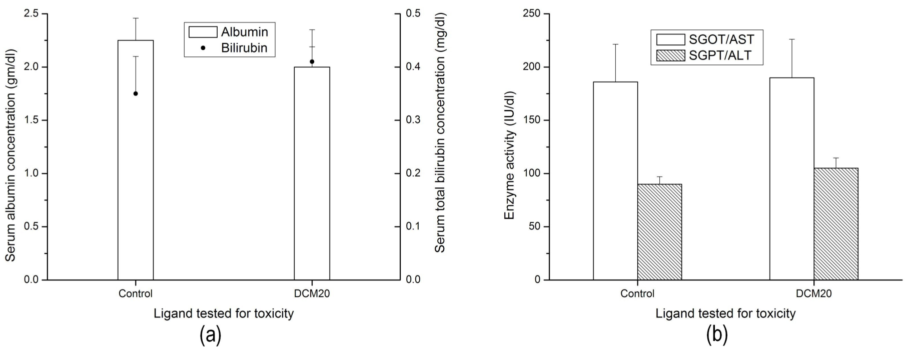

Figure 3.9.: Acute toxicity profile of DCM20 - serum levels of a) Albumin and total bilirubin concentration b) SGOT-SGPT activity

DAPM4, the use of lower ligand concentration led to a significant improvement in the localization properties, both in terms of percentage popliteal extraction (from 61.81 % to 90.39 % PE at 60 min) and clearance from the site of injection (from 16.15 % to 23.56 % clearance at 60 min). Significant amount of tracer diffusion from the site of injection appeared to occur with the first 15 min after subcutaneous administration. Thereafter the diffusion rate was more gradual. In the case of the lower ligand concentration, there was almost no further diffusion after 60 min p.i.

The in vivo localization of DAPM8 is quantitatively summarized in Tab. 3.3 with scintigraphic imaging pattern as depicted in Fig. 3.15. With DAPM8, lowering the injected ligand concentration from 200 µg/ml to 50 µg/ml improved clearance of 99mTc activity from the footpad region to some extent (from 18.42 % to 23.01 % at 60 min p.i.). However, the popliteal extraction of DAPM8 was not consistently improved at all the time points with the lower concentration, suggesting that improvement of the in vivo properties of a proposed SLN tracer by lowering of ligand concentration may not be uniform across all ligands and will need to be individually assessed for newer developed SLND ligands. As with DAPM4, significant amount of tracer diffusion from the footpad region appeared to occur within the first 15 min, after which the diffusion rate was more gradual.

Organ	DAPM4 10.0 µg/animal			DAPM4 2.5 µg/animal		
	15 min	**60 min**	**180 min**	**15 min**	**60 min**	**180 min**
Liver	2.42±0.47	4.80±1.03	6.49±0.09	3.80±0.35	4.96±0.38	6.39±0.50
	(0.28±0.05)	(0.55±0.12)	(0.75±0.01)	(0.44±0.04)	(0.57±0.04)	(0.74±0.06)
Intestine	0.55±0.07	0.75±0.06	0.95±0.17	0.57±0.04	0.89±0.06	1.22±0.10
	(0.03±0.00)	(0.05±0.00)	(0.06±0.01)	(0.04±0.00)	(0.06±0.00)	(0.08±0.01)
Stomach	0.15±0.03	0.30±0.05	0.52±0.17	0.13±0.04	0.24±0.02	0.37±0.03
	(0.04±0.01)	(0.08±0.01)	(0.13±0.04)	(0.03±0.01)	(0.06±0.01)	(0.10±0.01)
Kidney	0.53±0.02	1.12±0.27	1.20±0.01	0.61±0.05	0.50±0.04	0.77±0.06
	(0.33±0.01)	(0.70±0.17)	(0.75±0.01)	(0.38±0.03)	(0.31±0.02)	(0.48±0.04)
Heart	0.04±0.01	0.06±0.01	0.06±0.02	0.03±0.01	0.03±0.01	0.05±0.01
	(0.05±0.01)	(0.07±0.01)	(0.07±0.02)	(0.04±0.01)	(0.04±0.01)	(0.06±0.01)
Lungs	0.32±0.01	0.83±0.16	0.65±0.04	0.26±0.06	0.31±0.09	0.28±0.02
	(0.24±0.01)	(0.62±0.12)	(0.48±0.03)	(0.19±0.04)	(0.23±0.07)	(0.21±0.01)
Spleen	0.12±0.03	0.32±0.10	0.31±0.04	0.14±0.02	0.25±0.04	0.28±0.05
	(0.24±0.06)	(0.64±0.20)	(0.62±0.08)	(0.28±0.04)	(0.50±0.08)	(0.56±0.10)
Blood	2.14±0.01	0.91±0.02	0.96±0.37	1.15±0.23	1.00±0.25	1.04±0.11
	(0.13±0.00)	(0.05±0.00)	(0.06±0.02)	(0.07±0.01)	(0.06±0.01)	(0.06±0.01)
Node Uptake						
Popliteal Node	4.43±0.27	6.71±2.35	5.98±1.68	3.19±1.59	4.72±0.85	5.02±0.64
	(886.00±54.00)	(1342.00±470.00)	(1196.00±336.00)	(638.00±318.00)	(944.00±170.00)	(1004.00±128.00)
Iliac Node	1.09±0.40	2.59±1.06	1.41±0.50	0.54±0.13	0.46±0.28	0.34±0.11
	(218.00±80.00)	(518.00±212.00)	(282.00±100.00)	(108.00±26.00)	(92.00±56.00)	(68.00±22.00)
Site of Injection	89.14±2.09	83.85±1.37	79.50±5.02	81.19±1.58	76.44±1.26	77.12±2.85
PE (%)	68.55±1.35	61.81±2.42	76.65±1.73	81.73±4.13	90.39±4.48	92.94±3.38

Table 3.2.: In vivo distribution profile for 99mTc-DAPM4, data given as %ID per organ (%ID per gram), n=3.

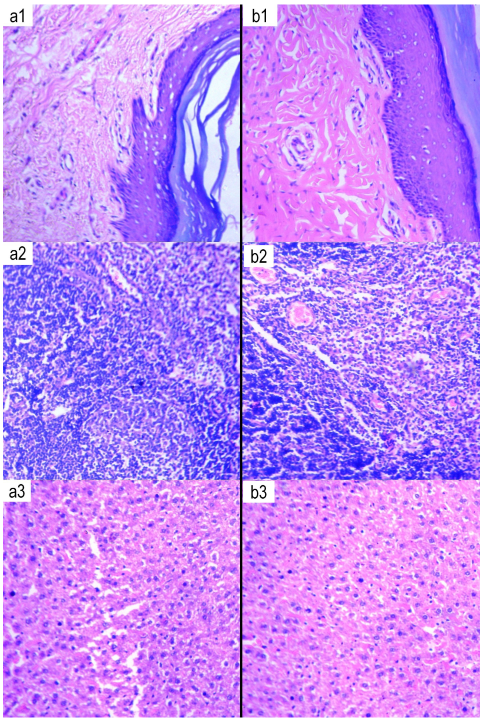

Figure 3.10.: Acute toxicity profile of DCM20 - comparative histology a) Control set (1 - SLN, 2 - footpad, 3 - Liver) and b) DCM20 exposed set (1 - SLN, 2 - footpad, 3 - Liver)

The results of the in vivo studies show specific uptake and retention of the labeled dextran-pyrazolyl-mannose ligands in the popliteal/sentinel lymph node of the Wistar rat model with favorable imaging properties in the tested conditions. Our conjecture is that the larger concentration of mannose receptor-bearing macrophages in vivo may be responsible for the appreciable uptake pattern of DAPM4 and DAPM8 ligands in animal studies despite the less favorable in vitro binding characteristics.

A head-to-head comparison with the results reported in the literature for 99mTc-labeled sulfur colloid or Lymphoseek® is not feasible due to differences in the various testing protocols. However, in simple terms of percentage popliteal extraction (at 60 min p.i.), DAPM4 (90.39 ± 4.48 % at 2.5 µg/animal) and DAPM8 (94.47 ± 2.45 % at 10 µg/animal) have displayed excellent localization characteristics favorably comparable to the reported values for filtered sulfur colloid (78.8 ± 6.5 %) and

Organ	**DAPM8 10.0 µg/animal**			**DAPM8 2.5 µg/animal**		
	15 min	**60 min**	**180 min**	**15 min**	**60 min**	**180 min**
Liver	2.42±0.47	5.44±1.06	6.84±0.01	2.54±0.54	3.45±1.11	4.30±0.27
	(0.28±0.05)	(0.63±0.12)	(0.79±0.00)	(0.29±0.06)	(0.40±0.13)	(0.50±0.03)
Intestine	0.55±0.07	0.61±0.57	1.28±0.17	0.52±0.07	0.64±0.15	1.10±0.13
	(0.03±0.00)	(0.04±0.04)	(0.08±0.01)	(0.03±0.00)	(0.04±0.01)	(0.07±0.01)
Stomach	0.15±0.03	0.42±0.01	0.74±0.07	0.14±0.02	0.38±0.19	0.39±0.02
	(0.04±0.01)	(0.11±0.00)	(0.19±0.02)	(0.04±0.01)	(0.10±0.05)	(0.10±0.01)
Kidney	0.53±0.02	1.18±0.20	1.67±0.28	0.59±0.17	0.82±0.19	1.21±0.01
	(0.33±0.01)	(0.73±0.12)	(1.04±0.17)	(0.37±0.11)	(0.51±0.12)	(0.75±0.01)
Heart	0.04±0.01	0.09±0.00	0.09±0.03	0.07±0.01	0.07±0.02	0.07±0.02
	(0.05±0.01)	(0.11±0.00)	(0.11±0.04)	(0.09±0.01)	(0.09±0.02)	(0.09±0.02)
Lungs	0.32±0.01	0.43±0.03	0.60±0.07	0.57±0.19	0.43±0.13	0.39±0.04
	(0.24±0.01)	(0.32±0.02)	(0.45±0.05)	(0.42±0.14)	(0.32±0.10)	(0.29±0.03)
Spleen	0.12±0.03	0.25±0.11	0.45±0.04	0.10±0.02	0.15±0.05	0.16±0.01
	(0.24±0.06)	(0.50±0.22)	(0.91±0.08)	(0.20±0.04)	(0.30±0.10)	(0.32±0.02)
Blood	2.14±0.01	1.72±0.81	1.55±0.65	1.78±0.31	3.38±2.02	2.68±0.29
	(0.13±0.00)	(0.10±0.05)	(0.09±0.04)	(0.11±0.02)	(0.20±0.12)	(0.16±0.02)
Node Uptake						
Popliteal Node	4.43±0.27	7.53±0.69	5.21±0.78	4.95±1.80	5.82±3.00	6.02±1.94
	(886.00±54.00)	(1506.00±138.00)	(1042.00±156.00)	(990.00±360.00)	(1164.00±600.00)	(1204.00±388.00)
Iliac Node	1.09±0.40	0.41±0.15	0.59±0.14	0.36±0.19	0.94±0.57	0.53±0.36
	(218.00±80.00)	(82.00±30.00)	(118.00±28.00)	(72.00±38.00)	(188.00±114.00)	(106.00±72.00)
Site of Injection	89.14±2.09	81.58±0.35	81.13±0.01	80.78±2.13	76.92±0.28	70.81±2.16
PE (%)	68.55±1.35	94.47±2.45	87.81±3.75	92.87±2.95	83.56±4.70	91.80±3.95

Table 3.3.: In vivo distribution profile for 99mTc-DAPM8, data given as %ID per organ (%ID per gram), n=3.

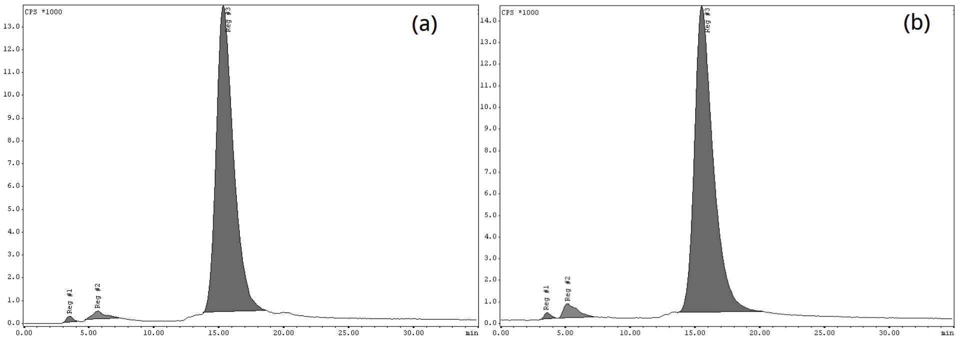

Figure 3.11.: HPLC pattern of (a) 99mTc-tricarbonyl DAPM4 conjugate (b) 99mTc-tricarbonyl DAPM8 conjugate

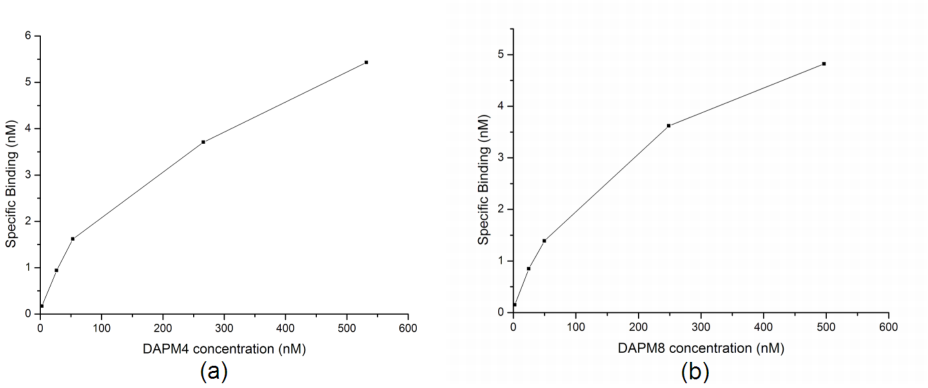

Figure 3.12.: In vitro specific binding pattern of (a) DAPM4 ligand and (b) DAPM8 ligand with RAW 264.7 cells

DTPA-mannosyl-dextran (90.1 ± 10.7 %) [54]. The kinetics of clearance from the site of injection for the pyrazolyl complexes appears to be closer to the value for 99mTc-labeled sulfur colloid (~19% at 180min p.i.). This is surprising given that the measured hydrodynamic particle size of the ligands used herein is significantly smaller than the colloid (less than 10 nm compared to particle diameter of 80-200 nm for typical SLN colloidal radiotracers like filtered sulfur colloid and albumin nanocolloid) and that mannose receptors, which can bind with and possibly internalize the ligand, are typically associated with the macrophages. It may possibly be a function of aggregation of the complexes at the tested concentration [61]. This will need to be addressed possibly with changes in the formulation that would prevent

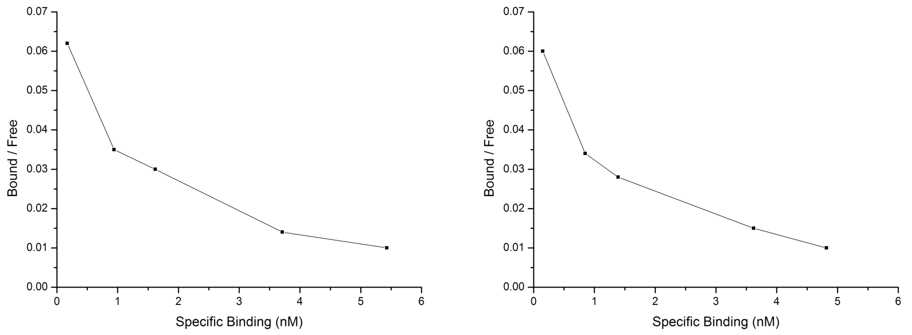

(a) (b)

Figure 3.13.: Scatchard plots for receptor binding curves of (a) DAPM4 ligand and (b) DAPM8 ligand

a possibility of such aggregation, since improved clearance is one of the proposed benefits of receptor-based SLN radiotracers, leading to better diagnostic sensitivity over colloidal tracers. With DCM20 and DAPM4, it is seen that with increase in the injected ligand amount there appears to be a displacement of the ligand from the SLN into adjoining lymph nodes and via the bloodstream to other organs. This could be a function of the ligand affinity, in which case future work may be in the direction of obtaining a higher affinity tracer for the purpose. However, such a pattern of displacement is not observed in the case of DAPM8 though it showed similar Kd value to DAPM4 in the in vitro studies. In any case, it is clear that preclinical in vivo studies of potential SLN tracers, especially those that target the mannose receptor, should be carried out using different injected concentrations to assess the impact of such variations on the localization of the tracer and thereby its usefulness as a radiotracer for SLN detection.

3.3.2.4. Toxicity Studies

The results of acute toxicity profile studies for the dextran-pyrazolyl mannose ligands DAPM4 and DAPM8 and presented in comparison to the controls with regards to hematological parameters (Fig. 3.16 and Fig. 3.17), biochemical parameters (Fig. 3.18) and histological examination (Fig. 3.19). In sum they suggest that

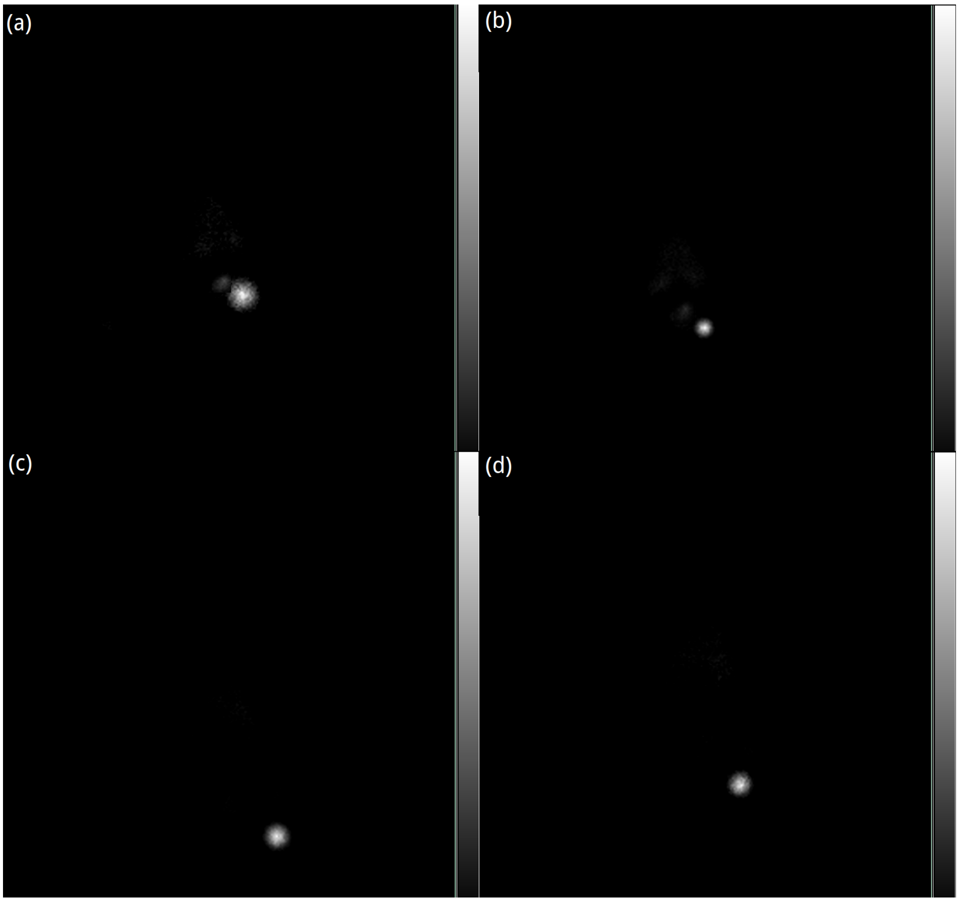

Figure 3.14.: Lymphoscintigraphy images in Wistar rat model of DAPM4 administered at 10 µg/animal for (a) 15 min (b) 60 min and 2.5 µg/animal for (c) 15 (d) 60 min

DAPM4 and DAPM8 do not induce any appreciable hazardous reaction when administered in pharmacologically relevant concentrations.

3.3.3. Summary

All the dextran-mannose ligands tested showed excellent (>90 %) 99mTc-labeling via the tricarbonyl core, and in the optimized protocol, displayed selective localization in the sentinel lymph node. DCM20 showed the highest popliteal extraction under optimal conditions. Acute toxicity profile studies with all the ligands proved negligible impact on tested toxicity parameters, indicating their safety for in vivo administration at pharmacologically relevent concentrations.

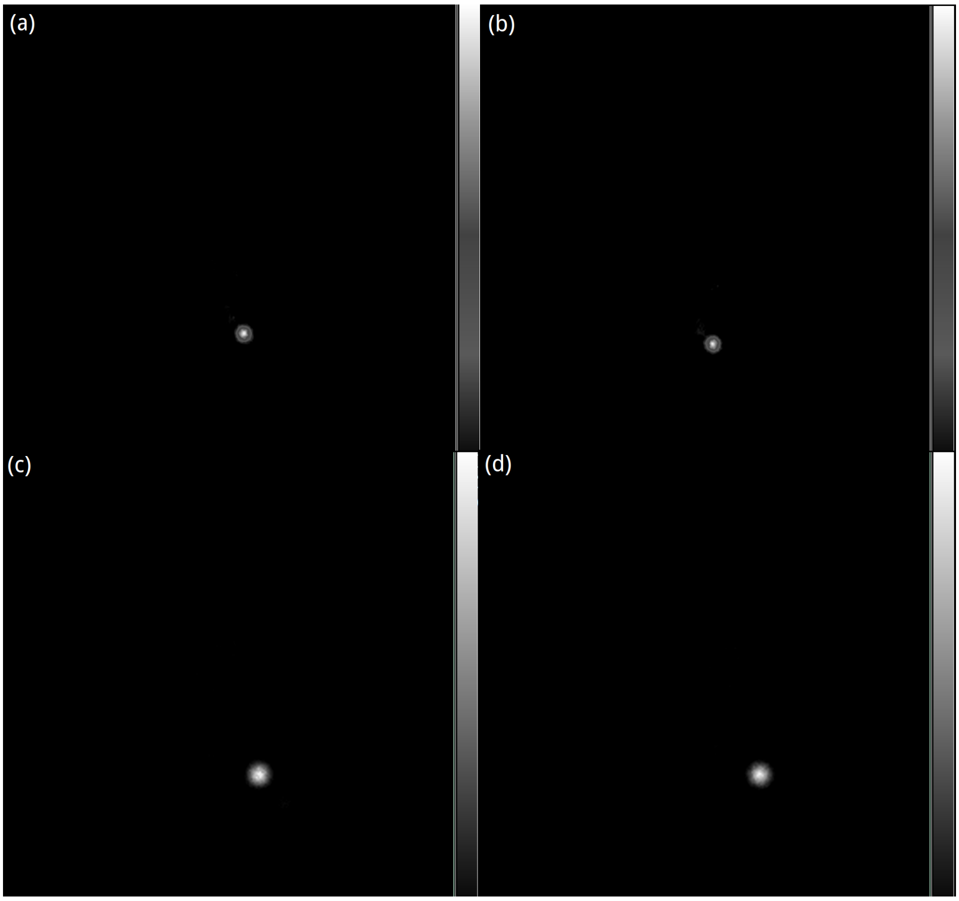

Figure 3.15.: Lymphoscintigraphy images in Wistar rat model of DAPM8 administered at 10 µg/animal for (a) 15 min (b) 60 min and 2.5 µg/animal for (c) 15 (d) 60 min

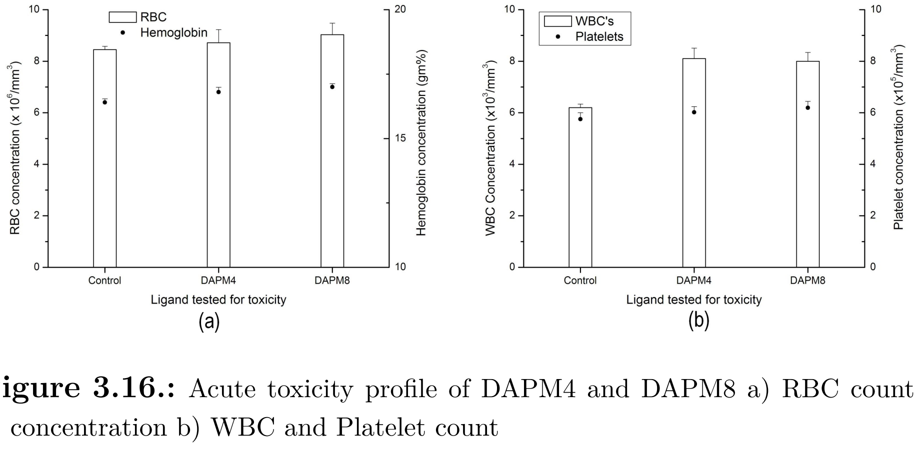

Figure 3.16.: Acute toxicity profile of DAPM4 and DAPM8 a) RBC count and hemoglobin concentration b) WBC and Platelet count

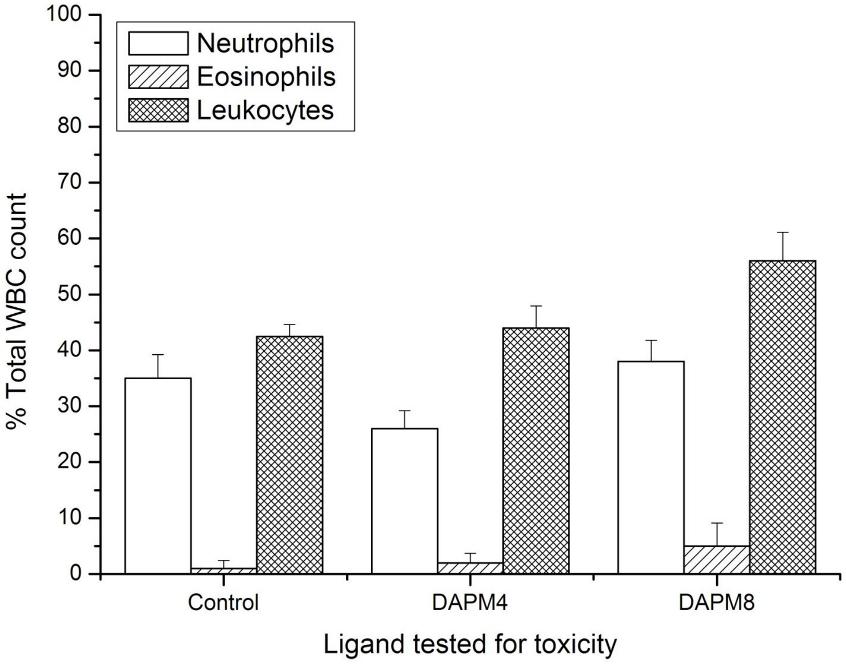

Figure 3.17.: Acute toxicity profile of DAPM4 and DAPM8 - differential WBC profile

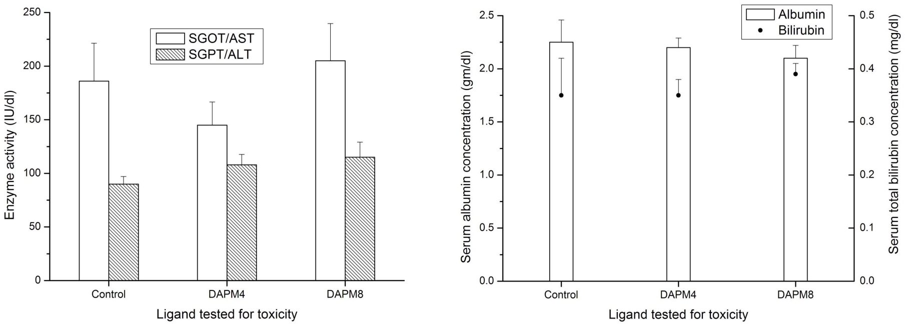

(a) (b)

Figure 3.18.: Acute toxicity profile of DAPM4 and DAPM8 - serum levels of a) SGOT-SGPT activity b) Albumin and total bilirubin concentration

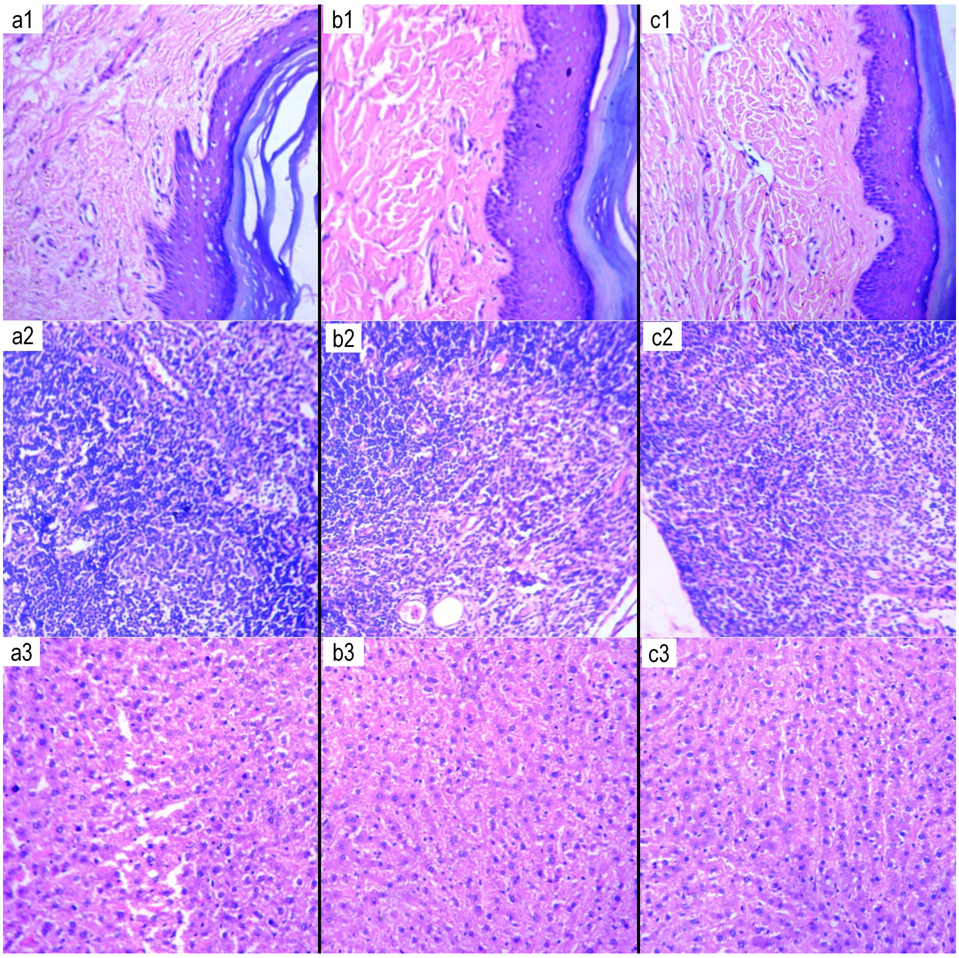

Figure 3.19.: Acute toxicity profile of DAPM4 and DAPM8 - comparative histology a) Control set (1 - SLN, 2 - footpad, 3 - Liver) and b) DAPM4 exposed set (1 - SLN, 2 - footpad, 3 - Liver) c) DAPM8 exposed set (1 - SLN, 2 - footpad, 3 - Liver)

4. RADIOPHARMACEUTICALS FOR LIVER CANCER THERAPY

4.1. BACKGROUND

4.1.1. Epidemiology of Liver Cancer

Cancer of the liver aka hepatocellular carcinoma (HCC) occupies the position of fifth most common malignant tumor [63], with a global incidence of more than 1 million patients each year [64, 65]. Its incidence in the developed regions of the West (North America and Western Europe) is low, with >10 cases per 100,000 population. However, in the case of Asian and African countries, there is a significant spike ranging from 50-150 cases per 100,000 population [66]. Even in the industrialized nations the growing incidence of Hepatitis C disease is expected to promote a noticeable increase of HCC cases in the next two decades. More than 80% of HCC patients have inoperable disease with very poor prognosis [67]. Hepatocellular carcinoma has a high mortality rate with less than 32% of patients surviving for more than 2 years and less than 5% achieving a 5-year survival rate owing to recurrence, metastases or the development of new primary sites [67, 68, 69]. The estimated median survival is only 8 months [70]. In East Asia, especially China, Japan, Korea, Taiwan, and Singapore, it is the major cause of death from cancer, as also in Zimbabwe, Ethiopia, and Mozambique [71]. This is in part due to late appearance of the symptoms, in which time the disease is widespread through the organ. Surgical resection as a mode of treatment is highly dependent on tumor mass, reserve liver function and the prevalence of metastases, hence is not a suitable option in many cases [72]. In fact, owing to the locally advanced and multi-focal nature of the disease, less than a quarter of established HCC patients are candidates for surgical intervention as the primary mode of treatment [73, 74, 75].

In addition to hepatocellular carcinoma, the liver is also a prime site for metastases of some other cancers. For instance liver metastases have been observed to develop in around half the total number of colorectal cancer cases [76, 77]. In fact, due to the extensive spread of the disease at the time of diagnosis, the first line treatment for colorectal cancer is either systemic chemotherapy or chemotherapy delivered via hepatic artery infusion [70].

4.1.2. Etiology of Liver Cancer

The development of hepatocellular carcinoma is, like with most other cancers, a multi-step process. Hepatocarcinogenesis is not as yet a thoroughly mapped out process and has several etiologies, which induce different genetic mutations. Both phenotypically and genotypically, HCC is extremely heterogeneous, a consequence of the numerous factors implicated in its development, the multitude of hepatocyte functions and the significantly advanced stage of the disease at which it becomes clinically symptomatic and detectable [66]. The sum of these various permutations of genetic alteration leads to the transformation of liver cells into the malignant phenotype. 3-5% of liver cirrhosis cases are said to develop HCC [78]. Conversely, 70-90% of HCC cases are linked to the development of cirrhotic liver, the specific molecular pathway being dependent on the cause of cirrhosis [66, 79]. The phenomenon of liver tissue injury and regeneration observed in cirrhosis is conducive to the formation of a mitogenic and mutagenic environment that ultimately fosters the malignant transformation. The major conditions linked to the development of liver cirrhosis are infection by hepatitis causing viruses (type B, C, D), exposure to hepatotoxic agents (e.g. Aflatoxin) and alcoholic liver disease. HCC occurs in 3-8% of patients having cirrhosis associated with type C hepatitis [79]. Other causes include metabolic disorders like hemochromatosis and alpha-1-antitrypsin deficiency, all of which lead to cirrhotic condition. The association of these chronic liver damage conditions to HCC is hypothesized to occur by the telomere shortening phenomenon. Studies have reported a strong correlation between telomere shortening and cirrhosis progression. It has also been noted that cancerous hepatocytes have shortened telomeres than their neighboring non-cancerous cells [80, 81]. On this basis it has been hypothesized that telomere shortening may have a tumor initiating effect [82]. In hepatocellular carcinoma, the rate of apoptosis in the malignant cells is downregulated compared to the surrounding normal liver cells. It has been observed from several studies that apoptosis is interrupted in different stages of hepatocarcinogenesis in rat liver. Studies on the effect of several non-genotoxic carcinogens have led to the hypothesis that they act by inhibiting the process of active cell death, thereby enhancing carcinogenesis by accelerated accumulation of initiated, preneoplastic and possibly neoplastic cells [83]. Fas, which is constitutively expressed in the normal hepatocytes, is partially or completely absent in several forms of hepatocellular carcinoma [84] and the expression of Fas has been correlated to the degree of differentiation of the hepatocytes; it is especially reduced in HCC's with poor differentiation, like in portal tumor thrombus or extra-capsular invasion [85]. On the other hand, the treatment of hepatocellular carcinoma with chemotherapeutic drugs is associated with upregulation of Fas expression and subsequent apoptosis [86].

4.1.3. Therapy of Liver Cancer

The treatment of liver cancer falls into the following major categories:

1. **Surgical Intervention** – this includes resection of the tumor or liver transplantation. Tumor resection may be recommended only in the cases where tumor is of small size, not multi-focal, and not located near any major intrahepatic vessels. Additionally it is essential that sufficient functional reserve of liver tissue exists and no significant metastases of the HCC has occurred [73, 87]. It is the treatment of choice in the cases of HCC without concomitant cirrhotic damage. However, in case of liver cirrhosis, a strict selection process must be applied to avoid the complications brought about by post-operative liver failure. As a result, the rate of resective surgery even in hospitals with extensive experience is only 10-37% of HCC cases [63], and only 25-38% of the patients that have undergone resective therapy successfully complete a 5-year survival period. Ideally liver transplantation would be the mode of treatment for widespread HCC since it would take care of the carcinoma as well as any

cirrhosis that could lead to future recurrence. Transplantation as a mode of therapy for liver cancer has proved very successful in clinical studies, showing ~70% 5-year survival rates with <15% recurrence when applied under appropriate selection criteria [88]. However the shortage of cadaveric liver donors becomes a limiting factor, especially as it is deemed important to truncate the waiting time for transplantation to less than 6 months. Living donor liver transplantation is possible, but it is a highly complicated procedure that comes with a 20-40% chance of morbidity for the patient and 0.3-0.5% for the donor [89].

2. **Systemic Chemotherapy** – this refers to the application of drugs for the treatment of cancer in a non-localized manner. In the case of liver cancer, several clinical trials have been performed for the assessment of various systemic chemotherapy molecules [90, 91]. Many well-known anti-cancer drugs including tamoxifen and octreotide have proved ineffective in the treatment of hepatocellular carcinoma, giving less than 20% response rate and almost no significant survival benefit [63, 92, 93]. While some like gemcitabine [94] and pravastatin [95] have shown some promise in studies, they cannot as yet be recommended for actual clinical practice.

3. **External Beam Radiotherapy** - Traditionally, external beam radiotherapy using Cobalt-60 source is one of the major modes of radiotherapy in the clinic. While beam radiotherapy has been tested for treatment of liver cancer, it has limited applicability herein, primarily due to the phenomenon of Radiation Induced Liver Disease (RILD) or radiation hepatitis, which is the predominant complication in patients receiving such therapy [74]. This is a clinical syndrome of anicteric hepatomegaly, ascites, and increased level of liver enzymes. It may extend for up to weeks or even months after therapy. While

some amount of improvement is obtained by taking a 3-dimensional approach to irradiation via conformal beam radiotherapy, there is still significant dose delivered to normal liver parenchyma to cause the adverse response described above [75].

4. **Percutaneous Intervention** – For cancerous lesions that are small and unresectable, percutaneous interventions are the optimal course of treatment. This may be achieved by the use of chemicals or thermal action. Ethanol or acetic acid are the chemicals of choice for percutaneous intervention [96]. Of these ethanol is the most widely used – in tumors <2cm diameter, it achieves 90-100% response rates, although for tumors ~5cm diameter the response efficiency drops to 50%. Because of the uncertainty in tumor necrosis, ethanol intervention is less successful as a curative treatment on its own, but it has good repeatability, which allows it to be used to address recurrence after resection or other tumor ablation methods for prolonging the survival or disease-free period [63]. Percutaneous ethanol interventions may also be considered for liver metastases. In the case of thermal therapy, the most prominent technique is radiofrequency thermal ablation (RFTA) which uses electric current to generate frictional heat in the tissue up to 100°C. Other approaches include microwave-heat induced thermotherapy, laser induced thermotherapy and cryoablation [96]. RFTA boasts an efficacy similar to that of ethanol intervention, but requires only one session and, in specific conditions, may be more successfully applied to hepatic tumors >5cm in diameter. However these techniques are again restricted in usefulness to smaller, less widespread lesions.

5. **Transarterial Intervention** – For HCC's that are unresectable and cannot effectively be treated by percutaneous interventions, transarterial intervention via embolization / chemoembolization forms one of the most widely used ther-

apy approaches [97]. Chemoembolization refers to a localized chemotherapy in which the presence of the drug is restricted to the region of interest by blocking / delaying its pharmacokinetics with the use of a suitable embolizing agent. Transarterial chemoembolization (TACE) has been clinically applied for more than three decades [98]. Here mainly lipiodol, which is composed of iodinated ethyl esters of fatty acids from poppy seed oil (37%w/w iodine) and used as a contrast agent in magnetic resonance imaging, is emulsified with the chemotherapeutic preparation to obtain the embolizing preparation. Under normal circumstances, using image guidance to identify tumor feeding vessels, an infusion is made with a catheter [99]. As described by Lewandowski et al [100], the overall goal of TACE is to deliver a high drug dose directly to the region of tumor in the liver, prevent rapid clearance of the drug, and induce ischemic necrosis of the tumor via embolization. Chemotherapeutic drugs like cisplatin, doxorubicin, methotrexate, paclitaxel etc. have been used in conjunction with embolizing agents to attain loco-regional therapeutic effect [101]. It can be applied in the case of multi-nodular lesions, but liver function should be sufficiently preserved in the course of the treatment regimen. A significant degree of extra-hepatic spread of the cancer will also hinder efficacy of this mode of treatment.

Embolization may be in conjunction with application of a therapeutic radiopharmaceutical preparation, in which case the procedure is referred to as radio-embolization. It has the advantage over systemic radiotherapy that it can be more specifically directed towards the region, restricting damage to the normal liver tissue and diminishing the possibility of RILD-related complications [102]. There are two principal approaches to radio-embolization for treatment of HCC in the clinic: 1) Using lipiodol as a carrier of radioactivity. The viscosity and lipophilicity of lipiodol are responsible for retention of the radiopharmaceutical in the region of interest. 2) Using a micron-range diameter particulate carrier (microsphere) that can adsorb or encapsulate the therapeutic radionuclide. Here the size of the particulate carrier is primarily responsible for localization of the radioactivity in the administered region.

The work in this thesis is devoted to the development of novel radio-embolization complexes, one lipiodol-based and one microsphere-based, that may serve as therapeutic vehicles for hepatocellular carcinoma.

4.2. MATERIALS AND METHODOLOGIES

4.2.1. Materials

Oxine (8-hydroxyquinoline), ammonium acetate, sodium chloride and sodium bicarbonate were obtained from Sigma, USA. Biorex 70 microparticulate resin was procured from Biorad, USA. Bio-Rex 70 resin has carboxylic acid functional groups attached to an acrylic matrix. Lipiodol was obtained from Guerbet, France. Ethanol and chloroform were procured from Merck, India. Double distilled water was used to prepare all solutions. Yttrium-90 (90Y) was obtained from an in-house 90Sr-90Y electrochemical generator through the cooperation of colleagues in the Radiochemicals and Radiation Sources Section of the Isotope Applications & Radiopharmaceuticals Division. All the reagents used were of AR Grade or better.

Sprague-Dawley rats employed in the animal studies were procured from the Animal House of ACTREC-TMC. N1S1 rat liver carcinoma cell line of Sprague-Dawley origin (ATCC CRL-1604) was procured by ACTREC towards use in development of orthotopic animal tumor model for this project. Ethicon brand surgical sutures (Johnson & Johnson, India) were used during surgical procedures.

For hemoglobin estimation, Drabkin's reagent was obtained from Sigma, USA. Kits for estimating serum levels of alanine aminotransferase and aspartate amino transferase were obtained from Bioquant, USA. Serum bilirubin was estimated using kit obtained from Bioscientific Corporation, USA.

Orbital shaker-incubator from Biosystem Scientific, India was used for radiolabeling reactions. Radioactivity measurements for 90Y-labeling studies were carried out using a well type NaI (Tl) scintillation detector (ECIL, India). Radioactivity measurements for in vivo distribution studies were performed on an integral line flat-bed NaI (Tl) scintillation detector (Harshaw, USA). In both cases the Bremsstrahlung radiation resulting from the beta-emissions of 90Y was measured.

4.2.2. Procedure for Making 90Y-labeled Therapeutic Preparations

4.2.2.1. 90Y-oxine in Lipiodol

The procedure for preparation and purification of 90Y-oxine and its dispersal in lipiodol was adapted from a previously reported protocol for making Lutetium-177 (177Lu) labeled oxine in lipiodol [103], with suitable modifications for labeling with 90Y. 5mg oxine was dissolved in 0.5ml ethanol and the alcoholic solution was mixed with an equal volume of reaction buffer. Ytttrium-90 (up to 185MBq) was added as 90Y-chloride and the reaction mixture was heated at up to 80°C in a water bath to form 90Y-oxine. The pH and the reaction time were varied to optimize the yield of 90Y-oxine. At the end of the reaction, 90Y-oxine was extracted into chloroform (1:1

volume with reaction mixture) and vortexed vigorously for 30 sec. The mixture was then allowed to stand and the aqueous (top) layer was separated from the chloroform (bottom) layer. Both were counted for their relative radioactive content. It is expected that 90Y-oxine will be extracted into chloroform while uncomplexed 90Y will remain in the aqueous layer. The yield of 90Y-oxine formation was assessed as the proportion of radioactivity in the chloroform layer. Chloroform was then allowed to evaporate off, using nitrogen purging if required. For stability studies the radiolabeled oxine was suspended in reaction pH buffer between extractions. To assess the stability of the 90Y-oxine, it was extracted with 1:1 chloroform:buffer mixture and the distribution of the radioactivity between the two phases was measured. The stability of 90Y-oxine was assessed at different times for up to a week in this manner.

For the intended application, 90Y-oxine needs to be dispersed in lipiodol. After chloroform was evaporated off, 2ml of lipiodol was added to the product vial. The vial was allowed to stand for 30 min with intermittent stirring to allow for leaching and dispersal of 90Y-oxine into the lipiodol phase. Extraction of 90Y-oxine into lipiodol was confirmed by measuring 90Y-activity associated with the lipiodol aliquot. To assess the stability of dispersion of 90Y-oxine in lipiodol, an aliquot of the final product was vigorously mixed with an equal volume of buffer, and the distribution of activity between the two phases was measured. The retention of 90Y-oxine in the lipiodol phase was taken as a measure of successful dispersion in lipiodol, a prerequisite for retention of 90Y-activity in the embolism.

4.2.2.2. 90Y-labeled Biorex 70 Microspheres

5mg of Biorex 70 microspheres were suspended in 1ml of freshly prepared 0.1M ammonium acetate solution. To this, up to 185MBq of 90Y-chloride was added. The pH was adjusted if necessary to ~5.0 using 0.1N HCl. The above reaction mixture was kept for mixing on an orbital shaker-incubator for different time periods at RT. At the end of the labeling reaction, the microspheres were collected by centrifugation at 2000rpm for 10 min and washed twice with phosphate buffered saline. The radioactivity counts associated with the microspheres and the supernatant of the reaction mixture was compared to assess 90Y-labeling yield. The stability of the labeled product was tested by suspending it in phosphate buffered saline and measuring the activity leached out into the supernatant at different time periods using the above technique. For the final application, the 90Y-labeled Biorex 70 microspheres were suspended in 2ml phosphate buffered saline.

4.2.3. Development of Animal Model for HCC by Orthotopic Induction

N1S1 cells were grown as a suspension culture in DMEM using 10% FBS as a supplement. When sufficient cell growth was obtained the cells were harvested by centrifugation at 1000rpm for 5 min and counted by hemocytometry. Cell viability was confirmed using Trypan blue staining. Cells were suspended at the desired final concentration in DMEM and used for the orthotopic induction studies.

Orthotopic administration of N1S1 cells in the liver of Sprague-Dawley rats was performed by a laparotomy protocol, described as follows: The animals were fasted for 12 hours prior to the induction procedure. For the experiment they were placed under anesthesia using isoflurane, delivered in a calibrated mixture with oxygen. The abdominal region was shaved with a hair clipper and surface sterilized by swabbing with 70% ethanol. An incision ~3cm long was made and the left lobe of the liver was exposed. The required aliquot of N1S1 cells was taken in a hypodermic syringe with 30G 1/2” needle. The needle was inserted beneath the lobular capsule and the suspension was slowly administered (15-20 sec). Successful administration was confirmed by the development of a pale colored sac in the region of injection. The incision was then closed using sutures at muscle and skin planes, and Vetbond® adhesive was applied for final sealing. The animals were then allowed to recuperate from the surgery. During the period of tumor development they were kept under normal conditions, food and water provided ad libitum. Tumor development was studied using different cell concentrations and development times. At the end of each time period, the animals were sacrificed. Tumor diameter was measured using vernier callipers. Blood was collected for hematology and serum biochemistry investigations, and liver tissues were taken for histological assessment.

4.2.4. Assessment of Tumor Development

4.2.4.1. Hematology Studies

The following hematological parameters were measured in the whole blood samples: Red blood cell (RBC) count, white blood cell (WBC) count, platelet count and hemoglobin concentration. The protocols followed were identical to those described in sec. A.1.

4.2.4.2. Liver Function Studies

From the serum samples the following liver function assessment parameters were measured: Asparate aminotransferase (AST) / serum glutamate oxaloacetate transaminase (SGOT) activity, alanine aminotransferase (ALT) / serum glutamate pyruvate transaminase (SGPT) activity and serum bilirubin concentration. The protocols followed were identical to those described in sec. A.2.

4.2.4.3. Histological Studies

Samples of liver tissue were suspended in 10% neutral buffered formalin for 24-48 hours for preservation of the tissue structure. After allowing adequate time for fixation they were washed several times with tap water to remove all traces of formalin. Finally they were suspended in 70% ethanol solution and stored at 4°C, allowing adequate time for decay of 90Y radioactivity (10 times half-life), before making histological blocks and slides. Further processing was as described in sec. A.3.

4.2.5. In Vivo Studies with 90Y-labeled Preparations

In vivo studies of the 90Y-labeled preparations were carried out in N1S1 tumor-bearing Sprague-Dawley rats. In these studies the preparation was administered via the hepatic vein. A separate set of experiments were done with unlabeled “cold” preparation to assess any possible effect of the carrier substances.

4.2.5.1. Administration of the 90Y-labeled / Cold Preparations via the Hepatic Vein

Although the clinical protocol for transarterial radio-embolization mandates that the therapeutic preparation should be administered into the hepatic artery (typically by passing a guided catheter through the femoral artery), the technical hurdles in achieving this in a rat model with the available facilities compelled the procedure to be performed via the hepatic vein instead. Given the smaller dimensions of rat liver as compared to the human liver, and the appreciable penetration range of β-emissions from 90Y (~12mm), it was hypothesized that some therapeutic effect would be seen in the model even using this less appropriate protocol. Prior to administering the preparation, the animals were fasted overnight, water provided ad libitum. On the day of the experiment, the animals were anesthetized with a mixture of xylazine:ketamine (1:10). Under anesthesia the abdominal region was shaved and swabbed with 70% ethanol. An incision of 3-4cm was made (Fig. 4.1a). The gastro-intestinal apparatus was carefully shifted to expose the hepatic vein (Fig. 4.1b). After sufficient mixing 100µl of the 90Y-labeled preparation was drawn into a syringe with 30G 1/2” needle. The preparation was slowly injected (20-25sec) into the hepatic vein (Fig. 4.1c). The site of injection was gently pressed with a gauze pad to stem any bleeding. The incision was then closed up at the muscle (Fig. 4.1d) and skin (Fig. 4.1e) planes using surgical suture. Healex® wound healing spray was applied over the sutured skin to supplement the sealing of the incision.

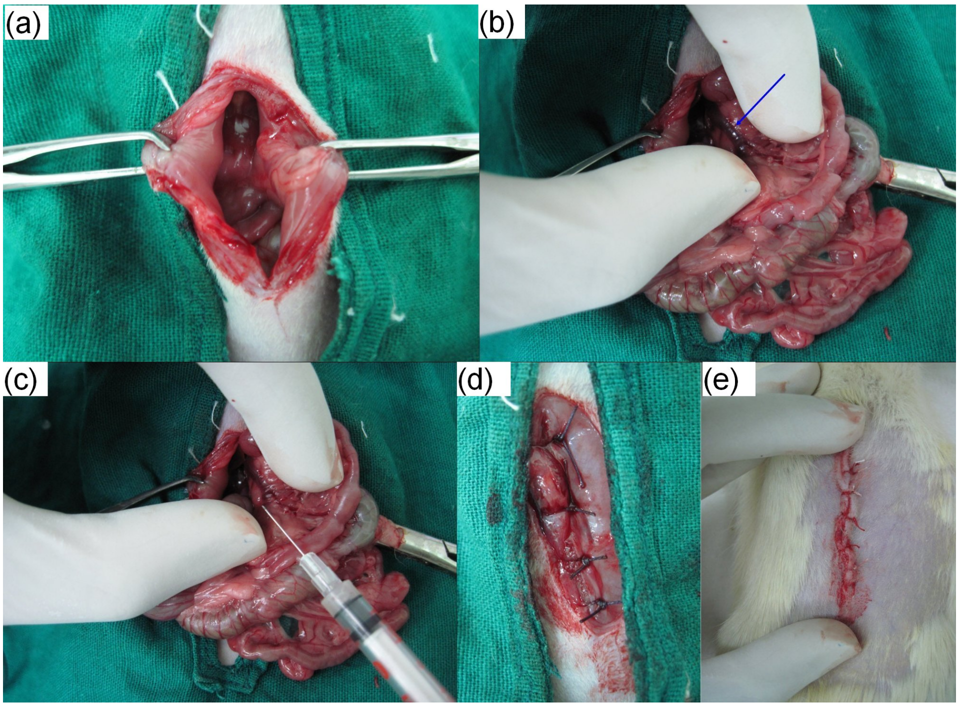

Figure 4.1.: a) Incision made to expose hepatic vein b) Localization of hepatic vein c) Labeled / cold preparation injected via the hepatic vein d) Suturing at muscle plane e) Suturing at skin plane.

At the end of the procedure, the animals were allowed to come out of anesthesia and recover. Food and water were provided ad libitum. They were kept under normal conditions till the time of sacrifice / biodistribution and monitored closely during this period for any signs of locomotive disability or excessive distress.

4.2.5.2. In Vivo Distribution and Efficacy Studies

Post administration of the therapeutic preparations, the animals were kept under normal conditions (water and food provided ad libitum) for the respective incubation periods, at the end of which they were sacrificed by exposure to a carbon dioxide saturated atmosphere. Blood was collected by cardiac puncture. The animals were then dissected and the relevant organs and tissues were excised for measurement of associated radioactivity to assess leakage of the radiolabeled preparation from the region of interest and spread to non-specific regions. Tumor diameter was measured using vernier callipers. In addition blood was collected to separate serum for relevant biochemical assays (as described in Appendix sec. A.2 and liver tumor / normal liver tissue samples were taken for histological analysis as detailed in Appendix sec. A.3 to assess the biological efficacy of the therapeutic preparations.

4.3. RESULTS

4.3.1. Preparation of 90Y-labeled Radiopharmaceutical Complexes

4.3.1.1. 90Y-labeled Oxine in Lipiodol

The results of optimization of the 90Y-labeling of oxine with respect to reaction time and pH are depicted in Fig. 4.2a. In the optimized reaction, 90Y-labeling of oxine carried out for 60 min at 80°C and pH 8.5 (using bicarconate buffer) was found to give >90% yield. Stability of the labeled product at 37°C as deduced from specific retention in chloroform phase after 1:1 extraction with buffer is seen from Fig. 4.2b to be reasonably adequate (~85%) for a 72 hour period, although it falls to about 60% by the end of 7 days. Extraction of 90Y-oxine into lipiodol was also found to be stable with >90 % of 90Y-activity associated with the lipiodol phase.

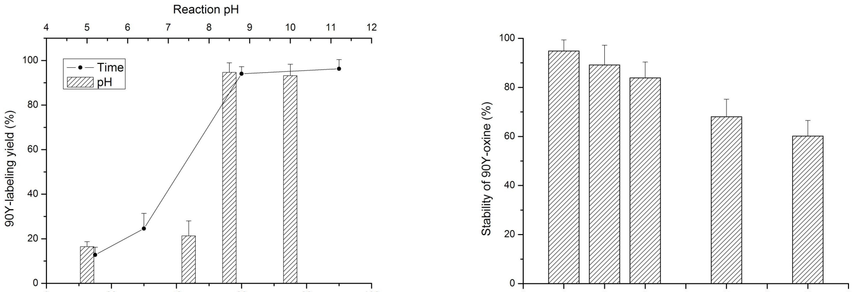

Figure 4.2.: a) Variation of 90Y-labeling yield of oxine with respect to reaction time [line graph, lower X-axis] and pH [bar graph, upper X-axis] b) Post-preparation stability of 90Y-labeled oxine at 37 °C.

4.3.1.2. 90Y-labeled Biorex 70 Microspheres

From Fig. 4.3a, which shows the variation in labeling yield with reaction time, it becomes evident that the binding of 90Y to the cationic Biorex 70 resin microspheres is extremely rapid and even as early as 15 min, the labeling yield is ≥95%. Stability in PBS was also excellent, with >95% of the 90Y-activity associated with the microspheres for as long as 7 days post-preparation at 37°C (Fig. 4.3b).

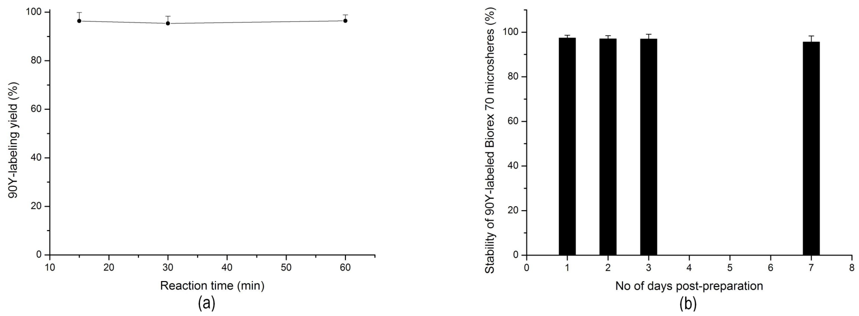

Figure 4.3.: a) Variation in yield of 90Y-labeled Biorex 70 microspheres with respect to reaction time b) Post-preparation stability of 90Y-Biorex 70 microspheres at 37°C.

4.3.2. Development of Animal Model for Liver Cancer

In the course of tumor development studies, 3 × 10ˆ6 N1S1 cells in 100µl volume of media was found to be the optimal concentration for achieving sizable and reproducible single lesion liver tumor model in a 3 week time period. All the animals survived the period of tumor development without any apparent ill effects. Fig. 4.4 shows the morphology of orthotopically induced N1S1 tumor (manifesting as a pale-colored lesion), in which a progressive increase in tumor size is observed over time.

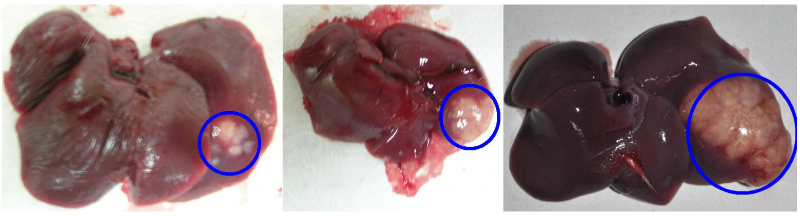

Figure 4.4.: Morphology of orthotopically induced N1S1 tumor at 1 - 2 - 3 weeks (3 × 10^6 cells in 100µl media injected in sub-capsular region of hepatic lobe).

On orthotopic tumor induction, the hematological parameters RBC count and hemoglobin concentration (Fig. 4.5a) did not appear to be much affected, but as seen in Fig. 4.5b, WBC concentration showed appreciable increase (~50%) in the course of development, although the variation in platelet concentration was very high to make a clear inference about the impact of tumor induction on the same.

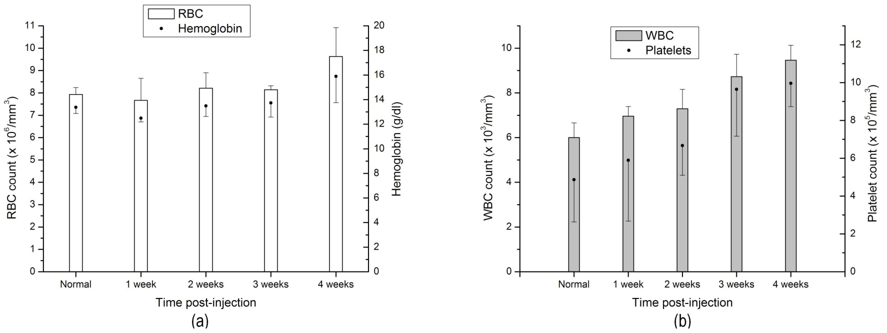

Figure 4.5.: Effect of N1S1 orthotopic tumor induction on a) RBC count and hemoglobin concentration b) WBC and platelet count.

With respect to liver function markers (Fig. 4.6a), there were variations in the activities of SGOT and SGPT, but they were not proportionate to the tumor proliferation, and serum total bilirubin showed large variance, hence no definite inference could be drawn from it. Serum alpha-fetoprotein (Fig. 4.6b) was the most consistent marker of proliferation of the implanted tumor. It showed rise with increase in tumor size, being almost exclusively a secretion product of hepatocellular carcinoma cells in adult animals.

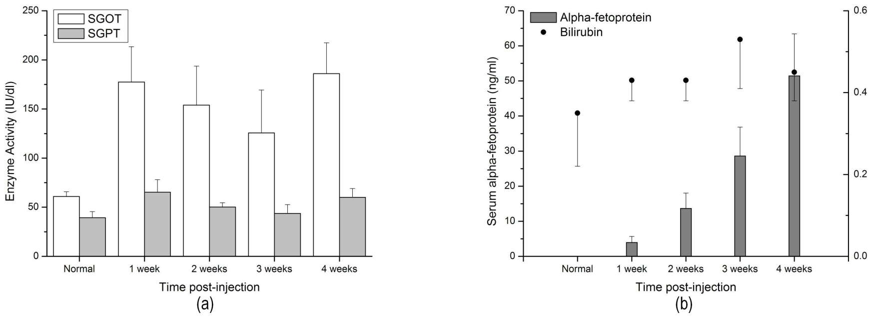

Figure 4.6.: Effect of N1S1 orthotopic tumor induction on serum levels of a) SGOT/SGPT activity b) alpha-fetoprotein concentration and total bilirubin concentration.

Fig. 4.7 compares the histological appearance of normal liver tissue and orthotopically implanted N1S1 tumor tissue. The implanted N1S1 tumor clearly shows loss of the normal cell architecture, accelerated proliferation, presence of fat vacuoles and other features associated with hepatocellular carcinoma tissue.

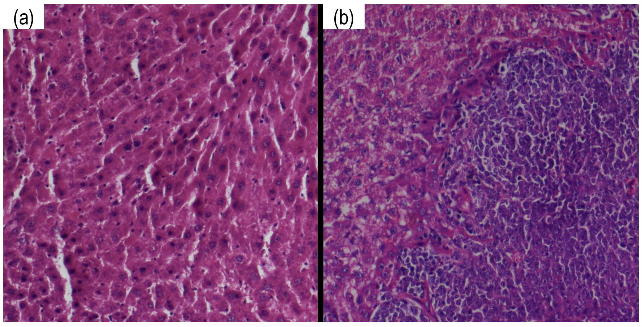

Figure 4.7.: Comparison of histological appearance of a) Normal liver tissue and b) Orthotopically implanted N1S1 tumor tissue.

4.3.3. In Vivo Distribution Studies

The results of the in vivo distribution studies for 90Y-labeled oxine in lipiodol are provided on per organ (Fig. 4.8a) and per gram basis (Fig. 4.8b). It is readily apparent that the labeled preparation is not retained in the liver, but shows significant 90Y activity leakage into non-target regions. The leakage is observed as early as 24 hours post-administration (only 48.41±5.19% retention in liver) and steadily increases with passage of time (only 23.8±2.61% retained in liver at 7 days). Critically, the most significant accumulation of leaked 90Y activity is in the bone, with 34.22±5.39% bone accumulation at 7 days. It is cause for serious concern, since it will lead to non-targeted exposure of bone marrow to 90Y radiation. The extent of leakage may be attributed to instability of the complexation between 90Y and oxine, thereby causing release of free 90Y, which has an affinity for bone tissue. This makes oxine in lipiodol unsuitable as a carrier of 90Y therapeutic dose for use in treatment of hepatocellular carcinoma.

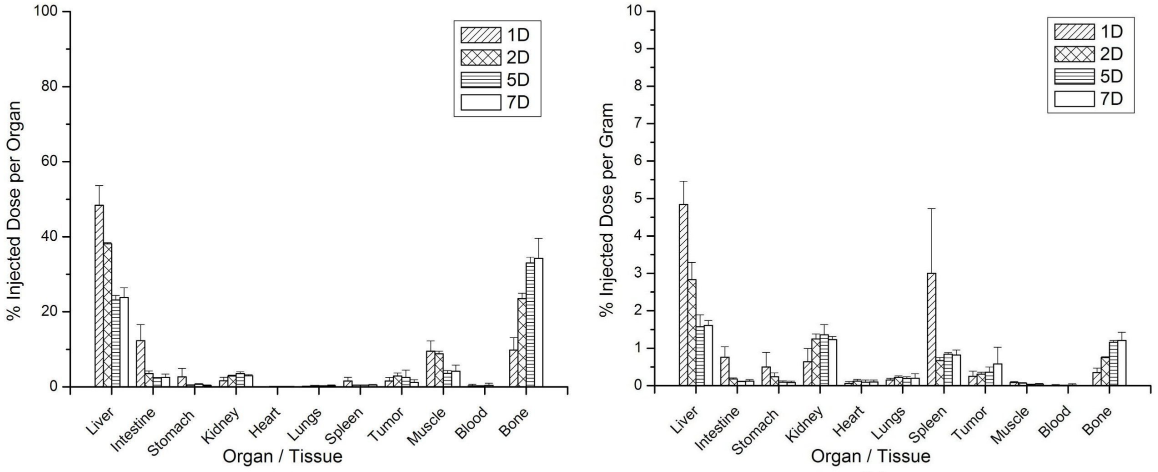

(a) (b)

Figure 4.8.: In vivo distribution profile of 90Y-labeled oxine in lipiodol in N1S1 orthotopic tumor bearing SD rats, data given in terms of %ID a) per organ b) per gram (n=4).

Fig. 4.9 a and b show the in vivo distribution of 90Y-labeled Biorex 70 microspheres in the tested orthotopic N1S1 tumor model in terms of per organ and per gram. It is evident that the Biorex 70 preparation is effectively localized in the liver tissue, with minimal leakage of 90Y activity to other organs. Even at 7 days post-administration 87.72±1.56% of injected dose is associated with the liver, indicating excellent stability of the radiolabeled preparation. The association of 90Y activity with non-target regions is also minimal. Throughout the period of study, accumulation of 90Y activity in the bone remains low, with only 0.56±0.97%ID bone activity measured at 7 days. This suggests that the preparation is unlikely to cause significant non-targeted dose to critical organs if used for therapy.

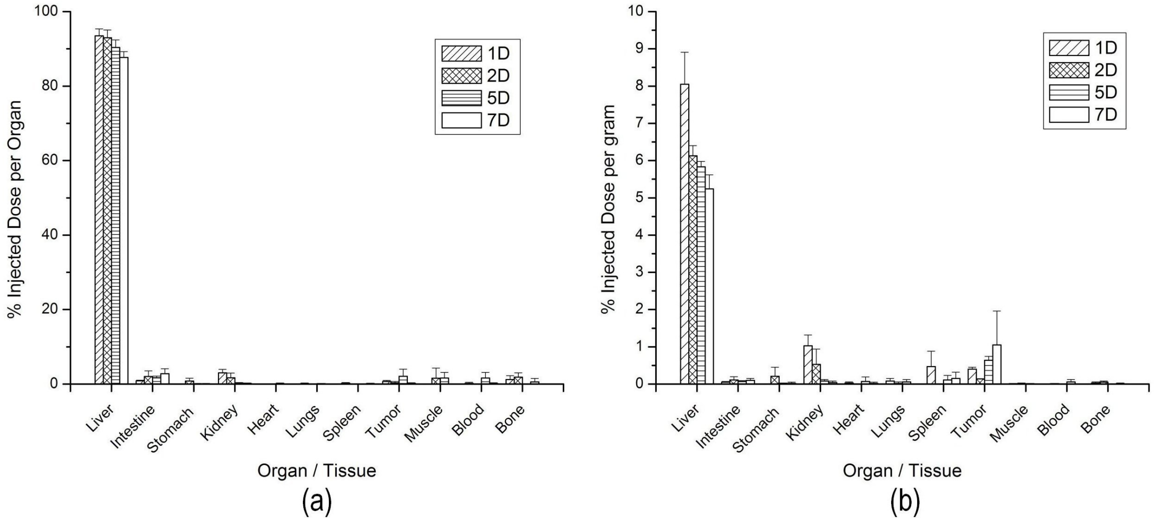

Figure 4.9.: In vivo distribution profile of 90Y-labeled Biorex 70 microspheres in N1S1 orthotopic tumor bearing SD rats, data given in terms of %ID a) per organ b) per gram (n=4).

4.3.4. Biological Efficacy Studies

4.3.4.1. Liver Tissue Histology

Tab. 4.1 gives the % weight of tumor to total liver weight for the different treatment groups, which provides insight into the effect on tumor dimensions of exposure to the cold and 90Y-labeled preparations.

Time points	**1D**			**2D**			**5D**			**7D**		
	Avg	**±**	**SD**	**Avg**	**±**	**SD**	**Avg**	**±**	**SD**	**Avg**	**±**	**SD**
Cold Oxine	31.03	±	2.28	26.02	±	3.17	23.23	±	2.21	26.80	±	3.75
90Y-Oxine	28.68	±	3.38	24.55	±	3.09	23.89	±	1.77	23.28	±	4.65
Cold Biorex 70	24.49	±	4.91	25.16	±	3.13	23.28	±	2.38	23.63	±	1.22
90Y-Biorex 70	27.33	±	2.52	22.33	±	3.06	13.50	±	2.83	11.76	±	1.05

Table 4.1.: Comparison of treatment groups in terms of percentage ratio of N1S1 tumor weight to total liver weight (n=4).

Comparison studies were performed with unlabeled "cold" oxine in lipiodol to assess biological efficacy of the 90Y-labeled product. The leakage of the preparation from the region of interest quite obviously diminished the therapeutic impact of the complex. As seen from Tab. 4.1, the ratio of tumor weight to total liver weight of orthotopic N1S1 tumor in animals treated with 90Y-labeled oxine in lipiodol was 23.28±4.65% at 7 days p.i. while animals administered with cold lipiodol in oxine showed tumors of only marginally higher average weight ratio (26.8±3.75%).

Histopathological sections of liver tissue from both sets of experiments are presented in Fig. 4.10. Examination of the sections does not show any significant gross changes in the tumor tissue in animals treated with 90Y-labeled oxine in lipiodol in comparison to administration with the cold preparation, suggesting that on account of leakage of 90Y activity from the liver, there is no significant impact of the therapy in the tumor.

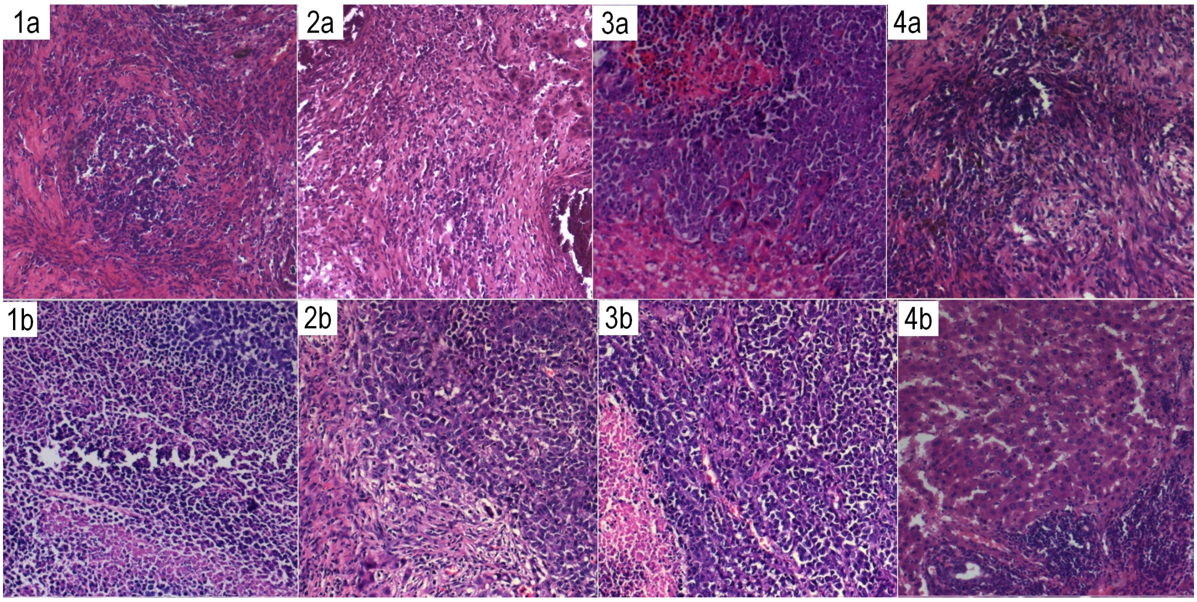

Figure 4.10.: Histological sections of N1S1 tumor tissue from animals administered with (1a-4a) cold oxine in lipiodol for 1, 2, 5 and 7 days and (1b-4b) 90Y-labeled oxine in lipiodol for the same time intervals.

In the studies for biological efficacy of 90Y-labeled Biorex 70 microspheres performed by comparison with cold Biorex 70 microspheres in terms of effect on tumor tissue and other parameters it was observed that while ratio of tumor weight to total liver weight in the animals injected with cold preparation was 23.63±1.22% at 7 days, it reduced significantly to 11.76±1.05% in the experimental set administered with 90Y-labeled preparation, indicating positive therapeutic effect of the beta-emissions from the radiopharmaceutical (Tab. 4.1). The effect on tumor histology is seen in Fig. 4.11. While cold Biorex 70 shows some embolic effect in terms of tissue damage surrounding the blood vessels, significantly more extensive damage and cell death is seen in the 90Y-treatment group, especially at 5 and 7 days post-injection. This is expected to be more pronounced in an actual clinical scenario where the radiolabeled preparation would be administered specifically through the hepatic artery into the regions of neo-angiogenesis.

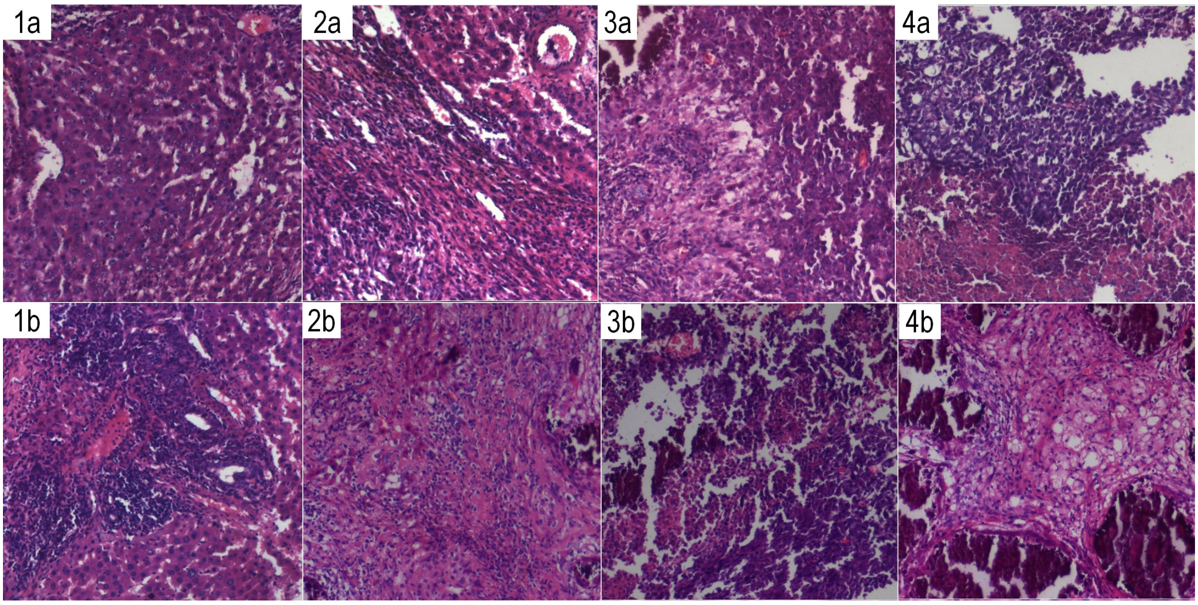

Figure 4.11.: Histological sections of N1S1 tumor tissue from animals administered with (1a-4a) cold Biorex 70 microspheres for 1, 2, 5 and 7 days and (1b-4b) 90Y-labeled Biorex 70 microspheres for the same time intervals.

4.3.4.2. Serum Biochemistry

Biochemical assays were performed on the sera of tested animals (from blood collected at the time of sacrifice) to assess impact of the treatment on relevant serum parameters, the results of which are presented here.

For both 90Y-incorporating and cold preparations of oxine in lipiodol and Biorex 70 microspheres, mean serum bilirubin level (Fig. 4.12) is seen to decrease in comparison to the mean value observed for N1S1 development control for 3 weeks and 4 weeks, but it may be noted from Fig. 4.6a that this is generally within the limits of standard deviation for the control values, and suggests that any impact of the treatment on liver function relating to serum bilirubin level is not definite.

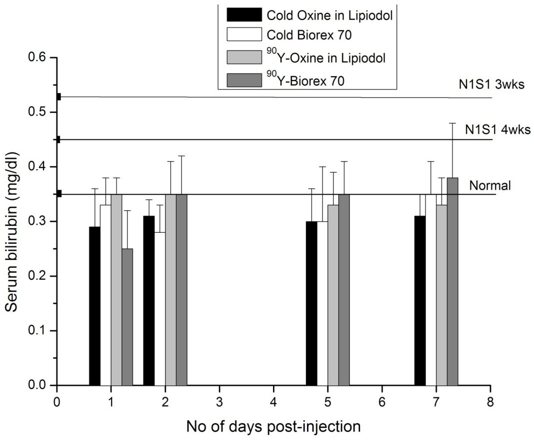

Figure 4.12.: Impact of 90Y-based radio-embolic treatment on serum bilirubin levels of N1S1-tumor bearing Sprague-Dawley rats (Compared against mean value of relevant controls).

The impact of treatment on liver function enzymes AST/SGOT and ALT/SGPT is shown in Fig. 4.13a and Fig. 4.13b respectively. In the case of 90Y-labeled oxine in lipiodol, there is initially a significant increase in the levels of both SGOT and SGPT (402.75±48.36IU/dl and 253.75±73.26IU/dl respectively, at 24 hours p.i.) and after which they fall (SGOT 232±74.14IU/dl, SGPT 67.5±12.4IU/dl at 7 days p.i.) to levels closer to those observed for N1S1 tumor controls (SGOT 186±31.31IU/dl, SGPT 60.0±9.0IU/dl at 4 weeks tumor development). This may be a result of leakage of the preparation from the site of embolism into the liver tissue (causing greater preliminary cell damage and enzyme release into the bloodstream) and subsequent loss of activity from the liver (leading to the fall in enzyme levels). In the case of 90Y-labeled Biorex 70 microspheres and the cold preparations, the increase in the levels of these enzymes is seen to be more moderate and sustained. Considering the significant impact of radiolabeled microsphere treatment on tumor size and tissue histology, it suggests that the cell damage from the microspheres is more controlled due to its stable retention in the liver capillaries and causes a less acute spike in serum levels of liver function enzymes in comparison to 90Y-labeled oxine in lipiodol.

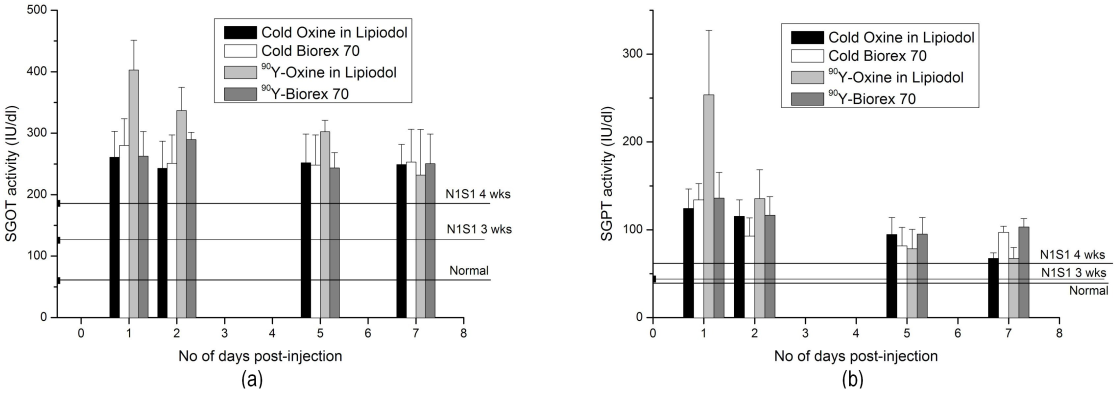

Figure 4.13.: Impact of 90Y-based radio-embolic treatment on a) SGOT and b) SGPT levels of N1S1-tumor bearing Sprague-Dawley rats (Compared against mean value of relevant controls).

As with the results of N1S1tumor development (Fig. 4.6b), serum alpha-fetoprotein levels show the best correlation with tumor spread (Fig. 4.14). In the case of animals administered with 90Y-labeled Biorex 70 microspheres, the mean level at 7 days p.i. is less than half that of N1S1 4 weeks control, corresponding with reduced tumor dimensions in those animals. In the case of the other tested preparations (cold Biorex 70 micropsheres, cold oxine in lipiodol and 90Y-labeled oxine in lipiodol), the drop in serum alpha-fetoprotein levels is much less, suggesting a lower impact of the embolic treatment. The levels are still significantly above normal on account of residual tumor tissue but this demonstrates that the sustained presence of 90Y activity gives a measurable therapeutic effect in the tested model for hepatocellular carcinoma.

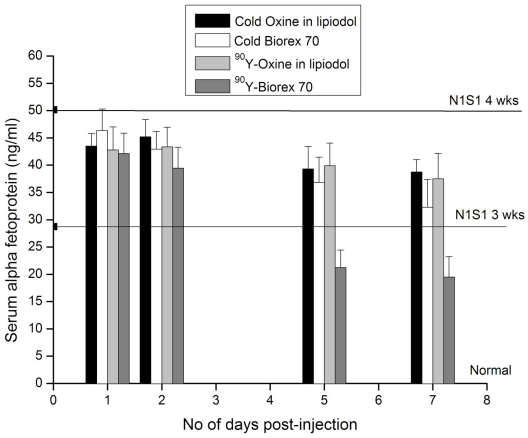

Figure 4.14.: Impact of 90Y-based radio-embolic treatment on serum alpha-fetoprotein levels of N1S1-tumor bearing Sprague-Dawley rats (Compared against mean value of relevant controls).

4.4. SUMMARY

Of the two 90Y-labeled preparations tested for possible application in therapy of hepatocellular carcinoma, Biorex 70 microspheres appear to be quite suitable. They show excellent 90Y-labeling yield and stability of labeled product, stable retention in the region of interest in the tested model, and demonstrate therapeutic effect as seen from measurement of relevant parameters in the period of study. Thus Biorex 70 microspheres show good potential to be taken up for further examination towards possible use in the clinic.

A. BIOLOGICAL EFFICACY AND TOXICITY STUDIES

Overview

This appendix is devoted to describing the assays common to the chapters on development of radiopharmaceuticals for sentinel lymph node (SLN) detection and liver cancer therapy. For SLN detection, these assays were used for determination of possible acute toxicity reaction from the unlabeled "cold" ligands, while in the case of liver cancer therapy, they were employed in assessing the biological efficacy of the therapeutic regimen with the tested radiopharmaceutical preparations. The tests described in this appendix fall into 3 major categories:

1. **Hematological Studies** - These tests are for assessment of effect of the preparation on blood parameters.
2. **Biochemical Studies** - These tests are primarily for the assessment of effect of the preparation on various liver function parameters. They include serum glutamate oxaloacetate transferase (SGOT) / asparate transaminase (AST), serum glutamate pyruvate transferase (SGPT) / alanine transaminase (ALT),

serum total bilirubin, serum albumin.

3. **Histological Examination** - Examination of tissues exposed to the preparation under study after necessary fixing and staining procedures to assess tissue-level phenomena like disruption of cellular architecture, presence of apoptotic / necrotic lesions, inflammation reaction etc.

A.1. Hematological Studies

Whole blood was collected from the animals by cardiac puncture in plastic BD Vacutainer® tubes (Beckton Dickinson, India) containing potassium salt of EDTA as a clot inhibitor and assayed hematology-wise on the same day. The following hematological parameters were measured in the whole blood samples: red blood cell (RBC) count, whole white blood cell (WBC) count, differential WBC count, platelet count, hemoglobin determination.

Blood cell counts were performed by hemocytometry using Neubauer's Chamber slide. Hemoglobin concentration was measured using the Drabkin's reagent method. Drabkin's reagent contains sodium bicarbonate, potassium ferricyanide and potassium cyanide. In the reaction with alkaline cyanide and ferricyanide, hemoglobin in most forms in the blood is rapidly converted to cyanmethemoglobin. This can be measured colorimetrically at 540nm. Whole blood was reacted with Drabkins's reagent as per the kit instructions and allowed to stand for 15-20 min at RT. The reaction mixture was then read at 540nm and plotted on a standard curve generated using cyanmethemoglobin standards to obtain the concentration of hemoglobin in the blood sample.

A.2. Biochemical Studies

For serum, whole blood was collected from the animals by cardiac puncture and taken into silicone-coated BD Vacutainer® tubes containing clot activator, and allowed to stand for sufficient time to allow seum to separate out. Serum was stored at -80°C till the time of assay. From the serum samples the following liver function assessment parameters were measured: Asparate aminotransferase (AST) / serum glumatate oxaloacetate transaminase (SGOT) activity, alanine aminotransferase (ALT) / serum glumatate pyruvate transaminase (SGPT) activity, serum albumin and serum bilirubin concentration.

AST / SGOT catalyzes the following reaction: Aspartate + α-ketoglutarate → oxaloacetate + glutamate. The kit for measurement of serum AST activity contains a substrate mixture (aspartate and α-ketoglutarate) and a color reagent in the form of a diazonium salt that selectively reacts with oxaloacetate to form a colored product that can be estimated photometrically at 530nm. Serum samples were reacted as per the kit protocol. The colored product was read at 530nm and compared with a control containing a calibrated value of AST activity to obtain the activity of AST in the sample.

ALT / SGPT catalyzes the following reaction: Alanine + α-ketoglutarate → pyruvate + glutamate. The kit for measurement of serum ALT activity contains a substrate mixture (alanine and α-ketoglutarate) and 2,4-dinitrophenylhydrazine. Pyruvate formed in the SGPT-catalyzed reaction selectively reacts with 2,4-dinitrophenylhydrazine to form 2,4-dinitrophenylhydrazone complex. This is dissolved using the color developer reagent containing 0.5N sodium hydroxide and the resultant solution is read spectrophotometrically at 505nm. Serum samples were reacted as per the kit protocol. The colored product was read at 505nm and compared with a control containing a calibrated value of AST activity to obtain the activity of AST in the sample.

The colorimetric assay kit for estimation of serum albumin uses bromocresol green (BCG) dye reagent that reacts with albumin to give a colored complex with an absorbance maxima at 620nm. The sample was measured against a standard curve prepared using known stock solution of albumin provided in the kit.

The kit for estimation of total bilirubin in serum uses an aqueous diazotized sulfanilic acid reagent to modify bilirubin in the sample to an azobilirubin colored product that can be measured colorimetrically at 550nm. The absorption of the product is directly proportional to the concentration of total bilirubin and comparison with a standard as provided in the kit gives a value of bilirubin concentration in the sample.

A.3. Histological Examination

Gross sections of the relevant tissues were taken and subjected to fixing as described in the relevant sections for SLN detection and liver cancer therapy.

Histological blocks were prepared using the standard protocol for paraffin block making as follows: The fixed tissues were immersed in a graded series of ethanol baths of increasing concentration (70% - 95% - absolute ethanol). They were then immersed in xylene for clearing. Finally molten paraffin wax was added over the tissues placed in suitable orientation and allowed to cool and harden for formation of the paraffin tissue blocks. These were stored at room temperature and taken for making slides as required.

Using the paraffin blocks, $\leq 5\mu$ thick sections were taken for making slides. These slides were stained with the established Hematoxylin - Eosin staining procedure. The active staining component of hematoxylin is its oxidation product hematin. Hematin in acidic conditions binds to the lysine residues of nuclear histones, thereby staining the chromatin. In the procedure hematin stain was allowed to saturate, and then rinsed off with tap water, giving a bluish-purple tint to the nuclei. The extent of hematin saturation was then reduced to clear the background, using 0.3% acidified alcohol as a differentiator. After washing off the differentiator with tap water, eosin was used as a counter-stain, which colors the other cellular components pink. After eosin staining the stained sections were dehydrated by exposure to absolute ethanol and xylene, then mounted with coverslips for histological examination.

Bibliography

[1] Williams FH. Early treatment of some epitheliomas by pure radium salts. N Engl J Med (1909) 160: 302-04.

[2] Rayudu GVS. Production of radionuclides for medicine. Semin Nucl Med (1990) 20: 100–11.

[3] http://www.who.int/diagnostic_imaging/imaging_modalities/dim_nuclearmed/en/index.html

[4] Kramer-Marek G, Capala J. The role of nuclear medicine in modern therapy of cancer. Tumor Biol (2012) 33: 629-40.

[5] Britton KE. Nuclear medicine, state of the art and science. Radiography (1995) 1: 13-27.

[6] Green MV, Seidel J. Single photon imaging. In: Nuclear Medicine - Diagnosis and Therapy. Harbert JC, Eckelman WC, Neumann RD (Eds.). 1st Edition, Thieme Medical Publishers, New York (1996) 87-120.

[7] Weissleder R. Molecular imaging in cancer. Science (2006) 312: 1168-71.

[8] Harbert JC. Atomic and nuclear structure. In: Nuclear Medicine - Diagnosis and Therapy. Harbert JC, Eckelman WC, Neumann RD (Eds.). 1st Edition, Thieme Medical Publishers, New York (1996) 3-21.

[9] Sood DD, Reddy AVR, Ramamoorthy N. Production and separation of isotopes. In: Fundamentals of Radiochemistry, 1st Edition, Indian Association of Nuclear Chemists and Allied Scientists, Mumbai (2000) 221-55.

[10] Sood DD, Reddy AVR, Ramamoorthy N. Applications of radioisotopes in healthcare. In: Fundamentals of Radiochemistry, 1st Edition, Indian Association of Nuclear Chemists and Allied Scientists, Mumbai (2000) 301-26.

[11] Hamoudeh M, Kamleh MA, Diab R, Fessi H. Radionuclides delivery systems for nuclear imaging and radiotherapy of cancer. Adv Drug Deliver Rev (2008) 60: 1329–46.

[12] Liu S. Bifunctional coupling agents for radiolabeling of biomolecules and target-specific delivery of metallic radionuclides. Adv Drug Deliver Rev (2008) 60: 1347-70.

[13] Volkert WA, Hoffman TJ. Therapeutic Radiopharmaceuticals. Chem Rev (1999) 99: 2269-92.

[14] Ecran MT, Caglar M. Therapeutic Radiopharmaceuticals. Curr Pharm Design (2000) 6: 1085-121.

[15] Chakravarty R, Pandey U, Manolkar RB, Dash A, Venkatesh M, Pillai MRA. Development of an electrochemical generator for separation of 90Y suitable for targeted therapy. Nucl Med Biol (2008) 35: 245-53.

[16] Tobler NE, Detmar M. Tumor and lymph node lymphangiogenesis — impact on cancer metastasis. J Leukocyte Biol (2006) 80:691–96.

[17] Shayan R, Achen MG, Stacker SA. Lymphatic vessels in cancer metastasis: bridging the gaps. Carcinogenesis (2006) 27: 1729-38.

[18] Fisher B, Fisher E. Barrier function of lymph node to tumor cells and erythrocytes. I. Normal nodes. Cancer (1967) 20: 1907-13.

[19] Fisher B, Fisher E. Barrier function of lymph node to tumor cells and erythrocytes. II. Effect of x-ray, inflammation, sensitization and tumor growth. Cancer (1967) 20: 1914-19.

[20] Harish K. Sentinel node biopsy: Concepts and current status. Front Biosci (2005) 10: 2618-44.

[21] Reiss CK, Volenec FJ, Humphrey M, Singla O, Humphrey LJ. The role of the regional lymph node in breast cancer: a comparison between nodal and systemic reactivity. J Surgical Oncol (1983) 22: 249-53.

[22] Cochran AJ, Morton DL, Stern S, Lana AM, Essner R, Wen DR. Sentinel lymph nodes show profound downregulation of antigen-presenting cells of the paracortex: implications for tumor biology and treatment. Modern Pathol (2001) 14: 604-08.

[23] Morton DL, Wanek L, Nizze JA, Elashoff RM, Wong JH. Improved long-term survival after lymphadenectomy of melanoma meta-static to regional nodes. Analysis of prognostic factors in 1134 patients from the John Wayne Cancer Clinic. Ann Surg (1991) 214: 491-99.

[24] Snow H. Melanotic cancerous disease. Lancet (1892) 2: 872-74.

[25] Halsted W. The Results of Operations for the Cure of Cancer of the Breast Performed at the Johns Hopkins Hospital from June, 1889, to January, 1894. Ann Surg (1894) 20: 497-555.

[26] Tanis PJ, Nieweg OE, Valdés Olmos RA, Rutgers EJT, Kroon BBR. History of sentinel node and validation of the technique. Breast Cancer Res (2001) 3: 109–12.

[27] Cochran AJ, Wen DR, Morton DL. Occult tumor cells in the lymph nodes of patients with pathological stage I malignant melanoma. An immunohistological study. Am J Surg Pathol (1988) 12: 612-18.

[28] Cochran AJ, Wen DR, Herschman JR. Occult melanoma in lymph nodes detected by antiserum to S-100 proteins. Int J Cancer (1984) 34: 159-63.

[29] Sherman AI, Ter-Pogossian M. Lymph-node concentration of radioactive colloidal gold following interstitial injection. Cancer (1953) 6: 1238–40.

[30] Strand SE, Persson BR. Quantitative lymphoscintigraphy I: Basic concepts for optimal uptake of radiocolloids in the parasternal lymph nodes of rabbits. J Nucl Med (1979) 20:1038-46.

[31] Jain R, Dandekar P, Patravale V. Diagnostic nanocarriers for sentinel lymph node imaging. J Control Release (2009) 138: 90-102.

[32] Phillips WT, Klipper R, Goins B. Novel method of greatly enhanced delivery of liposomes to lymph nodes. J Pharmacol Exp Ther (2000) 295: 309–13.

[33] Phillips WT, Klipper R, Goins B. Use of 99mTc-Labeled Liposomes Encapsulating Blue Dye for Identification of the Sentinel Lymph Node. J Nucl Med (2001) 42: 446-51.

[34] Koyama Y, Talanov VS, Bernardo M, Hama Y, Regino CAS, Brechbiel MW, Choyke PL, Kobayashi H. A dendrimer-based nanosized contrast agent dual-labeled for magnetic resonance and optical fluorescence imaging to localize the sentinel lymph node in mice. J Magn Reson Imaging (2007) 25: 866–71.

[35] Kim S, Lim YT, Soltesz EG, De Grand AM, Lee J, Nakayama A, Parker JA, Mihaljevic T, Laurence RG, Dor DM, Cohn LH, Bawendi MG, Frangioni JV. Near-infrared fluorescent type II quantum dots for sentinel lymph node mapping. Nat Biotechnol (2004) 22: 93–97.

[36] Ballou B. Quantum dot surfaces for use in vivo and in vitro. Curr Top Dev Biol (2005) 70: 103-20.

[37] Hultborn KA, Larsonn LG, Ragnhult I. The lymph drainage from the breast to the axillary and parasternal lymph nodes studied with the aid of colloidal Au 198. Acta Radiol (1955) 43: 52-63.

[38] Morton DL, Chan AD. The Concept of Sentinel Node Localization: How It Started. Semin Nucl Med (2000) 30: 04-10.

[39] Cabanas RM. An approach for the treatment of penile carcinoma. Cancer (1977) 39: 456-66.

[40] Eshima D, Fauconnier T, Eshima L, Thornback JR. Radiopharmaceuticals for Lymphoscintigraphy: Including Dosimetry and Radiation Considerations. Semin Nucl Med (2000) 30: 25-32.

[41] Bergqvist L, Strand SE, Persson B, Hafström L, Jönsson PE. Dosimetry in lymphoscintigraphy of Tc-99m antimony sulfide colloid. J Nucl Med (1982) 23: 698-705.

[42] Wilhelm AJ, Mijnhout GS, Franssen EJF. Radiopharmaceuticals in sentinel lymph-node detection – an overview. Eur J Nucl Med (1999) 26 (Suppl): S36–S42.

[43] Larson SM, Nelp WB. Radiopharmacology of a simplified technetium-99m-colloid preparation for photoscanning. J Nucl Med (1966) 7: 817-26.

[44] Eshima D, Eshima LA, Gotti NM, Herda SC, Algozine CA, Burns TG, Vansant JP, Alazraki NP, Taylor AT. Technetium-99m-Sulfur Colloid for Lymphoscintigraphy: Effects of Preparation Parameters. J Nucl Med (1996) 37: 1575-78.

[45] Bergqvist L, Strand SE, Persson BR. Particle sizing and biokinetics of interstitial lymphoscintigraphic agents. Semin Nucl Med (1983) 13: 9-19.

[46] Guerrero DQ, Allemann E, Fessi H, et al. Preparation techniques and mechanism of formation of biodegradable nanoparticles from preformed polymers. Drug Dev Ind Pharm (1998) 24: 1113.

[47] Jain RA, Rhodes CT, Railkar AM, Malick AW, Shah NH. Controlled release of drugs from injectable in situ formed biodegradable PLGA microspheres: effect of various formulation variables. Eur J Pharm Biopharm (2000) 50: 257–62.

[48] Spiers ID, Eyles JE, Baillie LWJ, Williamson ED, Alpar HO. Biodegradable microparticles with different release profiles: effect on the immune response after a single administration via intranasal and intramuscular routes. J Pharm Pharmacol (2000) 52: 1195–201.

[49] Danhier F, Ansorena E, Silva JM, Coco R, Breton AL, Préat V. PLGA-based nanoparticles: An overview of biomedical applications. J Control Release (2012) 161: 505-22.

[50] Herrman J, Bodmeier R. Biodegradable somatostatin acetate containing microspheres prepared by various aqueous and nonaqueous solvent evaporation techniques. Eur J Pharm Biopharm (1998) 45: 75–82.

[51] Tafaghodi M, Tabassi SAS, Jaafari MR, Zakavi SR, Momen-nejad M. Evaluation of the clearance characteristics of various microspheres in the human nose by gamma-scintigraphy. Int J Pharm (2004) 280: 125-35.

[52] Jovanović MS, Brborić J, Vladimirov S et al. Correlation between lipophilicity of the ligands and the hepatobiliary properties of the radiopharmaceuticals: approach to the development of new IDA derivatives. J Radioanal Nucl Ch (2000) 245: 555-60.

[53] Subramanian S, Dandekar P, Jain R, Pandey U, Samuel G, Hassan PA, Patravale V, Venkatesh M. Technetium-99m-labeled poly(DL-lactide-co-glycolide) nanoparticles as an alternative for sentinel lymph node imaging. Cancer Biother Radiopharm (2010) 25: 637-44.

[54] Vera DR, Wallace AM, Hoh CK, Mattrey RF. A synthetic macromolecule for sentinel node detection: 99mTc-DTPA-Mannosyl-Dextran. J Nucl Med (2001) 42: 951-59.

[55] Vera DR, Wallace AM, Hoh CK. [99mTc]–MAG3-Mannosyl-Dextran: a receptor-binding radiopharmaceutical for sentinel node detection. J Nucl Med (2001) 28: 493-98.

[56] Takagi K, Uehara T, Kaneko E, Nakayama M, Koizumi M, Endo K, Arano Y. 99mTc-labeled mannosyl-neoglycoalbumin for sentinel lymph node identification. Nucl Med Biol (2004) 31: 893-900.

[57] Jeong JM, Hong MK, Kim YJ, Lee J, Kang JH, Lee DS, Chung JK, Lee MC. Development of 99mTc-mannosyl human serum albumin (99mTc-MSA) as a novel receptor binding agent for sentinel lymph node imaging. Nucl Med Commun (2004) 12: 1211-17.

[58] Jiang HL, Kim YK, Arote R, Jere D, Quan JS, Yu JH et al. Mannosylated chitosan-graft-polyethylenimine as a gene carrier for Raw 264.7 cell targeting. Int J Pharm (2009) 375: 133-9.

[59] Alberto R, Schibli R, Egli A, Schubiger AP, Abram U, Kaden TA. A novel organometallic aqua complex of technetium for the labelling of biomolecules: Synthesis of [99mTc(OH2)3(CO)3]+ from [99mTcO4]- in aqueous solution and its reaction with a bifunctional ligand. J Am Chem Soc (1998) 120: 7987–8.

[60] Tsotakos T, Morais M, Correiac JDG, Santos I, Pelecanou M, Papadopoulos IM, Pirmettis I. New 99mTc(CO)3 mannosylated dextrans bearing S-derivatized cysteine chelator. Nucl Med Biol (2010) 37: 680.

[61] Morais M, Subramanian S, Pandey U, Samuel G, Venkatesh M, Martins M, Pereira S, Correia, JDG, Santos I. Mannosylated Dextran Derivatives Labeled with fac-[M(CO)3]+ (M = 99mTc, Re) for Specific Targeting of Sentinel Lymph Node. Mol Pharmaceutics (2011) 8: 609-20.

[62] Subramanian S, Pandey U, Papadopoulos M, Pirmettis I, Venkatesh M, Samuel G. Studies toward the biological efficacy of (99m)Tc-labeled dextran-cysteine-mannose ([(99m)Tc(CO)(3)]DCM20) for sentinel lymph node detection. Cancer Biother Radiopharm (2012) 27: 365-70.

[63] Poon RT, Fan ST, Tsang, FH, Wong J. Locoregional therapies for hepatocellular carcinoma: A critical review from the surgeon's perspective. Ann Surg (2002) 235: 466-86.

[64] Greten TF, Manns MP, Korangy F. Immunotherapy of hepatocellular carcinoma. J Hepatol (2006) 45: 868–78.

[65] Llovet JM, Burroughs A, Bruix J. Hepatocellular carcinoma. Lancet (2003) 362: 1907–17.

[66] Blum HE. Hepatocellular carcinoma: Therapy and prevention. World J Gastroentero (2005) 11: 7391-400.

[67] Huynh H. Molecularly targeted therapy in hepatocellular carcinoma. Biochem Pharmacol (2010) 80: 550–60.

[68] Bruix J, Boix L, Sala M, Llovet JM. Focus on hepatocellular carcinoma. Cancer Cell (2004) 5: 215–19.

[69] Barbara L, Benzi G, Gaiani S, Fusconi F, Zironi G, Siringo S, Rigamonti A, Barbara C, Grigioni W, Mazziotti A, Bolondi L. Natural history of small untreated hepatocellular carcinoma in cirrhosis: a multivariate analysis of prognostic factors of tumor growth rate and patient survival. Hepatology (1992) 16: 132–37.

[70] Kalva SP, Thabet A, Wicky S. Recent Advances in transarterial therapy of primary and secondary liver malignancies. RadioGraphics (2008) 28: 101–17.

[71] Sundram FX. Radionuclide therapy of hepatocellular carcinoma. Biomed Imag Interv J (2006) 2: e40.

[72] Greten TF, Papendorf F, Bleck JS, Kirchhoff T, Wohlberedt T, Kubicka S, Klempnauer J, Galanski M, Manns MP. Survival rate in patients with hepatocellular carcinoma: a retrospective analysis of 389 patients. Brit J Cancer (2005) 92: 1862–68.

[73] Bruix J, Sherman M, Llovet JM, Beaugrand M, Lencioni R, Burroughs AK, Christensen E, Pagliaro L, Colombo M, Rodes J. Clinical management of hepatocellular carcinoma. Conclusions of the Barcelona—2000 EASL conference. European Association for the Study of the Liver. J Hepatol (2001) 35: 421–30.

[74] Ibrahim SM, Lewandowski RJ, Sato KT, Gates VL, Kulik L, Mulcahy MF, Ryu RK, Omary RA, Salem R. Radioembolization for the treatment of unresectable hepatocellular carcinoma: A clinical review. World J Gastroentero (2008) 14: 1664-69.

[75] Salem R, Hunter RD. Yttrium-90 microspheres of the treatment of hepatocellular carcinoma: a review. Int J Radiat Oncol (2006) 66 (suppl): S83–S88.

[76] Sasson AR, Sigurdson ER. Surgical treatment of liver metastases. Semin Oncol (2002) 29: 107–18.

[77] Kennedy AS, Coldwell D, Nutting C, Murthy R, Wertman DE Jr., Loehr SP, Overton C, Meranze S, Niedzwiecki J, Sailer S. Resin 90 y-microsphere brachytherapy for unresectable colorectal liver metastases: modern USA experience. Int J Radiat Oncol (2006) 65: 412–25.

[78] Gerolami R, Cardoso J, Lewin M, Bralet MP, Sa Cunha A, Clement O, Brechot C, Tran PL. Evaluation of HSV-tk gene therapy in a rat model of chemically induced hepatocellular carcinoma by intratumoral and intrahepatic artery routes. Cancer Res (2000) 60: 993–1001.

[79] Semela D, Dufour JF. Angiogenesis and hepatocellular carcinoma. J Hepatol (2004) 41: 864–80.

[80] Kitada T, Seki S, Kawakita N, Kuroki T, Monna T. Telomere shortening in chronic liver diseases. Biochem Bioph Res Co (1995) 211: 33–39

[81] Satyanarayana A, Manns MP, Rudolph KL. Telomeres and telomerase: a dual role in hepatocarcinogenesis. Hepatology (2004) 40: 276-83.

[82] Lechel A, Manns MP, Rudolph KL. Telomeres and telomerase: new targets for the treatment of liver cirrhosis and hepatocellular carcinoma. J Hepatol (2004) 41: 491–97.

[83] Schulte-Hermann R, Bursch W, Grasl-Kraupp B, Millauer L, Ruttkay-Nedecky B. Apoptosis and multistage carcinogenesis in rat liver. Mutat res (1995) 333: 81-87

[84] Strand S, Hofmann WJ, Hug H, Müller M, Otto G, Strand D, Mariani SM, Stremmel W, Krammer PH, Galle PR. Lymphocyte apoptosis induced by CD95 (APO-1/Fas) ligand-expressing tumor cells–a mechanism of immune evasion? Nat Med (1996) 2: 1361–66.

[85] Rust C, Gores, GJ. Apoptosis and Liver Disease. Am J Med (2000) 108: 567-74.

[86] Muller M, Strand S, Hug H, Heinemann EM, Walczak H, Hofmann WJ, Stremmel W, Krammer PH, Galle PR. Drug-induced apoptosis in hepatoma cells is mediated by the CD95 (APO-1/Fas) receptor/ligand system, and involves activation of wild-type p53. J Clin Invest (1997) 99: 403–13.

[87] Sherman M, Klein A. AASLD single-topic research conference on hepatocellular carcinoma: Conference proceedings. Hepatology 2004;40:1465–1473.

[88] Shetty K, Timmins K, Brensinger C, Furth EE, Rattan S, Sun W, Rosen M, Soulen M, Shaked A, Reddy KR, Olthoff KM. Liver transplantation for hepatocellular carcinoma validation of present selection criteria in predicting outcome. Liver Transplant (2004) 10: 911–18.

[89] Cronin DC 2nd, Millis JM, Siegler M. Transplantation of liver grafts from living donors into adults – too much, too soon. New Engl J Med (2001) 344: 1633–37.

[90] Simonetti RG, Liberati A, Angiolini C, Pagliaro L. Treatment of hepatocellular carcinoma: a systematic review of randomized controlled trials. Ann Oncol (1997) 8: 117–36.

[91] Schwartz JD, Schwartz M, Mandeli J, Sung M. Neoadjuvant and adjuvant therapy for resectable hepatocellular carcinoma: review of the randomised clinical trials. Lancet Oncol (2002) 3: 593–603.

[92] Yuen MF, Poon RT, Lai CL, Fan ST, Lo CM, Wong KW, Wong WM, Wong BCY. A randomized placebo-controlled study of long-acting octreotide for the treatment of advanced hepatocellular carcinoma. Hepatology (2002) 36: 687–691

[93] Chow PK, Tai BC, Tan CK, Machin D, Win KM, Johnson PJ, Soo KC. High-dose tamoxifen in the treatment of inoperable hepatocellular carcinoma: A multicenter randomized controlled trial. Hepatology (2002) 36: 1221–1226.

[94] Yang TS, Lin YC, Chen JS, Wang HM, Wang CH. Phase II study of gemcitabine in patients with advanced hepatocellular carcinoma. Cancer (2000) 89: 750–56.

[95] Kawata S, Yamasaki E, Nagase T, Inui Y, Ito N, Matsuda Y, Inada M, Tamura S, Noda S, Imai Y, Matsuzawa Y. Effect of pravastatin on survival in patients with advanced hepatocellular carcinoma. A randomized controlled trial. Brit J Cancer (2001) 84: 886–91.

[96] Lencioni RA, Allgaier HP, Cioni D, Olschewski M, Deibert P, Crocetti L, Frings H, Laubenberger J, Zuber I, Blum HE, Bartolozzi C. Small hepatocellular carcinoma in cirrhosis: randomized comparison of radio-frequency thermal ablation versus percutaneous ethanol injection. Radiology (2003) 228: 235–40.

[97] Llovet JM, Bruix J. Systematic review of randomized trials for unresectable hepatocellular carcinoma: Chemoembolization improves survival. Hepatology (2003) 37: 429–42.

[98] Marelli L, Stigliano R, Triantos C, Senzolo M, Cholongitas E, Davies N, Tibballs J, Meyer T, Patch DW, Burroughs AK. Transarterial therapy for hepatocellular carcinoma: which technique is more effective? A systematic review of cohort and randomized studies. Cardiovasc Inter Rad (2007) 30: 6–25.

[99] Lewis AL, Dreher MR. Locoregional drug delivery using image-guided intra-arterial drug eluting bead therapy. J Control Release (2012) 161: 338–50.

[100] Lewandowski RJ, Geschwind JF, Liapi E, Salem R. Transcatheter intraarterial therapies: rationale and overview. Radiology (2011) 259: 641–57.

[101] Lewis AL. Drug eluting beads in the treatment of liver cancer, in: Drug–Device Combination Products Delivery Technologies and Applications, Lewis AL (Ed.), Woodhead Publishing Ltd, Cambridge (2010) 154–89.

[102] Salem R, Lewandowski RJ, Atassi B, Gordon SC, Gates VL, Barakat O, Sergie Z, Wong CY, Thurston KG. Treatment of unresectable hepatocellular carcinoma with use of 90Y microspheres (TheraSphere): safety, tumor response, and survival. J Vasc Interv Radiol (2005) 16: 1627-39.

[103] Subramanian S, Das T, Chakraborty S, Sarma HD, Banerjee S, Samuel G, Venkatesh M. Preparation of 177Lu-Labeled Oxine in Lipiodol as a Possible Agent for Therapy of Hepatocellular Carcinoma: A Preliminary Animal Study. Cancer Biother Radiopharm (2010) 25: 539-43.